AD-A185 723 ACTA AERODYNAMICA SINICA (SELECTED ARTICLES)(U) FOREIGN 1/2
TECHNOLOGY DIV WRIGHT-PATTERSON AFB OH 02 SEP 87
FTD-ID(RS)T-0116-87

UNCLASSIFIED F/G 20/4 NL

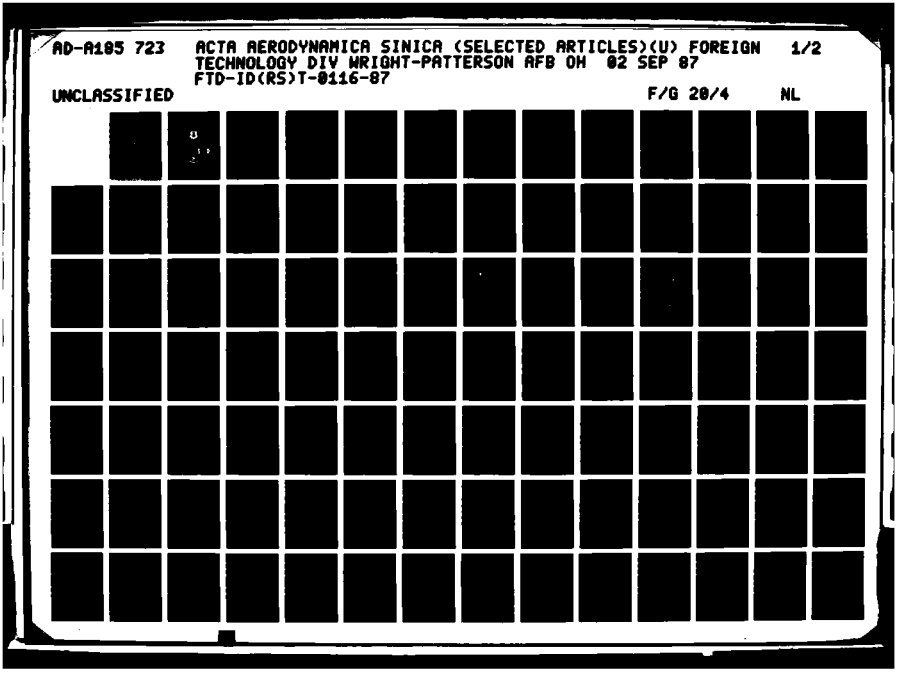

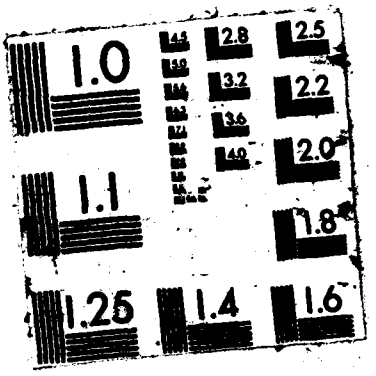
1.0
1.1
1.25
2.8
3.2
3.6
4.0
2.5
2.2
2.0
1.8
1.4
1.6

FTD-ID(RS)T-0116-87

FOREIGN TECHNOLOGY DIVISION

ACTA AERODYNAMICA SĪNICA

(Selected Articles)

Approved for public release;
Distribution unlimited.

HUMAN TRANSLATION

FTD-ID(RS)T-0116-87 2 September 1987

MICROFICHE NR: FTD-87-C-000698

ACTA AERODYNAMICA SINICA (Selected Articles)

English pages: 114

Source: Kongqidonglixue Xuebao, Vol. 4, Nr. 2, June 1986, pp. 140-192; 218-225

Country of origin: China
Translated by: SCITRAN
F33657-84-D-0165
Requester: FTD/TQTA

PREPARED BY:

TRANSLATION DIVISION
FOREIGN TECHNOLOGY DIVISION
WPAFB, OHIO.

Partial contents:

TABLE OF CONTENTS

(Chinese translations, China)

GRAPHICS DISCLAIMER

All figures, graphics, tables, equations, etc, merged into this translation were extracted from the best quality copy available.

SEMI-ANALYTICAL SEMI-NUMERICAL METHOD TO TREAT THE THREE-DIMENSIONAL STOKES FLOW

/140

Lin Shengtian Wu Wangyi

(Department of Mechanics, Beijing University)

SUMMARY This article makes use of the axially symmetrical Sampson flow body internal distribution method to numerically solve three dimensional Stokes flow problems. As far as the complicated integrals which appear in this method are concerned, we initially obtained systematic and simple results of succesive estimation type analysis. Because of this, the high accuracy of the method is guaranteed, and the method has the advantage of a small amount of required calculation. We carried out specific calculations for the three dimensional Stokes flow lateral prolate spheroid and Cassini oval flow bodies in a uniform oncoming flow. We obtained pressure distributions for object surfaces and drag coefficient values with very good convergence and accuracy. As an actual example of the Stokes flow for a three dimensional body, this article also calculated the Stokes flow for a three dimensional prolate ellipsoid in a uniform oncoming flow. Moreover, it obtained for the first time the corresponding drag coefficients and pressure distributions.

Creep flow for viscous, non-compressible flow bodies has always been a problem having basic significance and engaging people's interest. Following along with the products in the last twenty years of such fields as biological engineering and chemical engineering as well as with the development of the fields of science and technology, the problem of the Stokes flows around the viscous flow bodies surrounding any configuration of object has undergone rapid development. People have hoped to find a type of method which had

relatively broad applicability, as well as a relatively high degree of accuracy and a reasonable amount of calculation involved. Such people as Gluckman [1] selected for use a ring-form singularity point surface distribution method to handle unbounded Stokes flow movements for any convex shaped axially symmetrical body. Youngren and Acrivos [2] have brought forward the method of continuously distributing the Stokes flow body on the surface of the object in order to handle unbounded Stokes flow movements for three dimensional bodies. Both these two types of methods include numerical value integr ations. Because of this, the amount of calculation is relatively large. Most recently, such people as Wu Wangyi [3,4,5,6,7] have presented a new method which takes Sampson flow bodies and distributes them continuously on a certain selected line segment of the body internal axis of symmetry and on a certain selected central surface of the body interior. This successfully solved the problem of the Stokes winding flow around any body symmetrical around its long axis and around any body symmetrical around its side axis. This method achieved thoroughly ideal results. We calculated the axially symmetrical flow movements for such bodies as spheroids , flattened spheres, elongated Cassini oval bodies, flattened Cassini oval bodies, and long bodies with pointed tips. It goes without saying that these reflected the special characteristics of the bodies as a whole in terms of drag coefficients or localized pressure distributions which appear. All of these quantities possessed relatively good convergence results and relatively high

calculation accuracy. Therefore, this explains the fact that Sampson flow bodies present a type of fast, highly accurate numerical value method appropriate to axial points of singularity in order to solve for the Stokes flow movements for any configuration of axially symmetrical body

The test diagrams in this article generalize a method suggested in reference [3] for handling problems of three dimensional Stokes winding flows. We found the algebraic expressions for several collections of functions and several successive estimation equations in equations expressing the Sampson progression, and completed several totally different integrals in the coordinate directions. They were expressed in the form of analytic successive estimation formulae. Therefore, the success of the method was guaranteed. For the sake of the effectiveness of inspection methods, we did research into the three dimensional Stokes problem of a spheroid in a uniform oncoming flow from the side direction. This used very little in the way of position points and a small amount of calculation. We obtained quite good drag coefficients and pressure distribution values in agreement with precise solutions. This, therefore, confirmed the convergence characteristics and precision of this method in solving three dimensional problems. After this, we selected for use the same type of method and calculated the drag coefficient value for the lateral direction three dimensional winding flow for the Cassini oval body of rotation to act as a practical example of the treatment of the concave cavity portion of three dimensional flow movements. Finally, we did research on the Stokes flow movements of three dimensional ellipsoids, obtaining, for the first time, drag coefficient values and pressure distribution values for flows around three dimensional ellipsoid bodies in a uniform oncoming flow from any given direction.

I. Lateral Direction Stokes Winding Flows Around Bodies Symmetrical About the Long Axis

/141

Consider the Stokes flow (See Fig. 1) around the x axis of a body of rotation in a uniform oncoming flow along the direction of the z axis at a velocity U. Select $L, U, \mu U/L$, to respectively be the characteristic parameters for length, velocity and pressure. In this, L is a certain characteristic length of the body. μ is the dynamic viscosity coefficient of the flow body. Copying the method used in reference (3), on the line connecting the rate of curvature centers A and B, we, separately or in a continuous manner, position the Sampson flows along the direction of the z axis.

1. The Separated Line Distribution Method

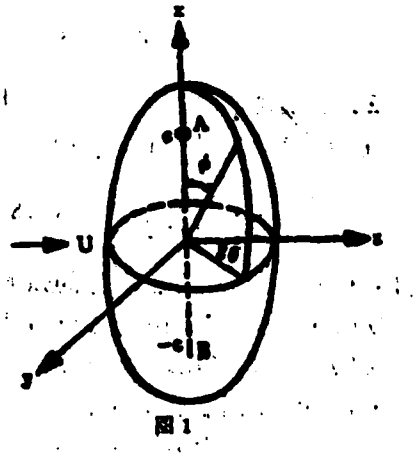

Fig. 1

On the basis of certain considerations, on the line segment AB, we select M different points. Their coordinates are $(0, \xi_j)$, $j=1, \cdots, M$. At these points, we position Sampson flows. After the disturbance fields produced by them are added to the uniform oncoming flow, it gives us

$$U(r,\xi_i)=\sum_{n=1}^{\infty}\sum_{i=1}^{M}[C_{ni}S_n(r,\xi_i)+D_{ni}T_n(r,\xi_i)] \tag{1.1}$$

In this

$$U=(v_x-1,v_y,v_z,p-p_\infty),\ S_n=\left(F_n^{(1)}(r_i,z),F_n^{(1)}(r_i,z)\frac{x-\xi_i}{R_i},F_n^{(1)}\frac{y}{R_i},0\right)$$

$$T_n=\left(F_n^{(2)}(r_i,z),F_n^{(2)}(r_i,z)\frac{x-\xi_i}{R_i},F_n^{(2)}\frac{y}{R_i},\frac{4n-3}{n}F_{n-1}^{(1)}(r_i,z)\right)$$

In this, r is a vector radius. $r_i=\sqrt{(x-\xi_i)^2+y^2+z^2}$; $R_i=\sqrt{(x-\xi_i)^2+y^2}$; v_x,v_y,v_z are respectively the projections of the velocity vectors on the x,y,z axes. p_∞ is the pressure. p is the pressure at an infinitely distant point. C_{ni}, D_{ni} are parameters awaiting determination. The equations expressing $F_n^{(i)}(i=1,2,5,6)$ are:

$$\begin{aligned}
&F_n^{(1)}(r,z)=r^{-(n+1)}p_n(\zeta)\\
&F_n^{(2)}(r,z)=r^{-(n-1)}[p_n(\zeta)+2\mathcal{J}_n(\zeta)]\\
&F_n^{(5)}(r,z)=(n+1)r^{-n}\frac{1}{R}\mathcal{J}_{n+1}(\zeta)\\
&F_n^{(6)}(r,z)=(n+1)r^{-(n-2)}\frac{1}{R}\mathcal{J}_{n+1}(\zeta)\\
&\qquad -2zr^{-(n-1)}\frac{1}{R}\mathcal{J}_n(\zeta)
\end{aligned} \tag{1.2}$$

At these positions $R=\sqrt{x^2+y^2}$, $r=\sqrt{R^2+z^2}$, $\zeta=z/r$. . P_n, $\mathcal{J}_n$ are respectively n order Legendre multi-term equations and n order-1/2 degree Gegenbauer multi-term equations.

Take a cross section at the quantity $N+1$ in the infinite progression in equation (1.1). After that, select points MN on the surface of the object. Make the viscous adhesion conditions at the points MN satisfactory. Obtain the equation for $2MN$ and determine the $2MN$ unknown parameters and and C_{n1}及D_{n1}, C_{n1}, D_{n1}. After this, substitute into equation (1.1) and obtain an equation approximately expressing velocity and pressure. The drag coefficient is /142

$$\lambda = \frac{\sum_{i=1}^{M} D_{n1}}{1.5LU} \tag{1.3}$$

2. Continuous Line Distribution Method

On AB, we continuously distribute the Sampson flow in the direction of the z axis. We obtain the equation expressing the flow field, which is:

$$U = \sum_{n=0}^{\infty} \int_{-d}^{d} [C_n(\xi) S_n(r,\xi) + D_n(\xi) T_n(r,\xi)] d\xi \tag{1.4}$$

In this, $C_n(\xi)$, $D_n(\xi)$ are strength distribution functions awaiting determination. ξ at points A, B equals d and $-d$. Line AB and divide it into M sections. In each section, the strength distribution function can be approximated by the use of an n order multi-term equation $(n=0, 1, \cdots)$. On the basis of the experiences in reference [5], the accuracy of approximations by second order, multi-term equations is high, and the amount of calculation involved is reasonable. Because of this, this article mainly makes use of parabolic approximation. Due to this fact, in each segment, we select the two end points and the midpoint to be the interpolation points. The strength distribution in each section is approximately replaced by the use of the second degree functions at each extrapolation point. Moreover, we take the cross section of the infinite series at the quantity $N+1$. Due to equation (1.4), it is possible to write:

$$U=\sum_{n=2}^{N+1}\sum_{i=1}^{M}\int_{d_{i_1}}^{d_{i_3}}[C_{ni}(\xi)S_n(r,\xi)+D_{ni}(\xi)T_n(r,\xi)]d\xi \tag{1.5}$$

In this

$$\begin{Bmatrix}C_{ni}(\xi)\\D_{ni}(\xi)\end{Bmatrix}=\sum_{m=1}^{3}N_{im}(\xi)\begin{Bmatrix}C_{n,2(i-1)+m}\\D_{n,2(i-1)+m}\end{Bmatrix} \tag{1.6}$$

Moreover,

$$N_{i1}=\frac{1}{H_2H_1}(\xi-d_{i2})(\xi-d_{i3}),\quad N_{i2}=\frac{1}{H_1H_2}(\xi-d_{i1})(\xi-d_{i3}),$$

$$N_{i3}=\frac{1}{H_2H_1}(\xi-d_{i1})(\xi-d_{i2})$$

$$H_1=d_{i1}-d_{i2},\quad H_2=d_{i3}-d_{i1},\quad H_3=d_{i2}-d_{i3}$$

Here, d_{i1}, d_{i2}, d_{i3} are respectively the coordinates for the two end points and the midpoint of each small section.

We take equation (1.6) and substitute it into equation (1.5). Moreover, we make the integral transformation $x-\xi=t$, . After going through the manipulations, we obtain

$$U=\sum_{n=2}^{N+1}\sum_{i=1}^{M}\sum_{k=1}^{3}[C_{n,2(i-1)+k}P_{n,i,k}+D_{n,2(i-1)+k}Q_{n,i,k}] \tag{1.7}$$

In this

$$P_{n,i,k}=(G^{(1)}_{n,i,k},\ G^{(2)}_{n,i,k},\ G^{(3)}_{n,i,k},\ 0)$$

$$Q_{n,i,k}=\left(G^{(2)}_{n,i,k},\ G^{(3)}_{n,i,k},\ G^{(4)}_{n,i,k},\ \frac{4n-3}{n}G^{(1)}_{n-1,i,k}\right)$$

$$G_{\cdot\cdot}^{(1)}{}_{i..k}=\sum_{l=1}^{2} q_{l..k}\left[f_{\cdot\cdot}^{(1)}{}_{i+l-1}(x-d_{i_1},y,z)-f_{\cdot\cdot}^{(1)}{}_{i+l-1}(x-d_{i_2},y,z)\right] \quad i=1,2$$

$$G_{\cdot\cdot}^{(1)}{}_{i..k}=\sum_{l=1}^{3} q_{l..k}\left[f_{\cdot\cdot}^{(1)}{}_{i+l}(x-d_{i_1},y,z)-f_{\cdot\cdot}^{(1)}{}_{i+l}(x-d_{i_2},y,z)\right] \quad i=3,4$$

$$G_{\cdot\cdot}^{(1)}{}_{i..k}=y\sum_{l=1}^{3} q_{l..k}\left[f_{\cdot\cdot}^{(1)}{}_{i+l-1}(x-d_{i_1},y,z)-f_{\cdot\cdot}^{(1)}{}_{i+l-1}(x-d_{i_2},y,z)\right] \quad i=5,6$$

$$q_{l..k}=\frac{(x-d_{i_1})(x-d_{i_2})(x-d_{i_3})}{x-d_{i_k}}\Delta_k$$

$$q_{l..k}=\{(x-d_{i_4})-[(x-d_{i_1})+(x-d_{i_2})+(x-d_{i_3})]\}\cdot\Delta_k$$

$$q_{l..k}=\Delta_k$$

$$\Delta_k=\frac{(-1)^{k-1}H_k}{H_1H_2H_3}$$

Moreover,

$$f_{\cdot\cdot}^{(k)}{}_{i}=\begin{cases}\int x^k F_{\cdot}^{(i)}\,dx & i=1,2 \quad k=0,1,2,\cdots\\ \int \frac{x^k}{R} F_{\cdot}^{(i)}\,dx & i=5,6 \quad n=1,2,3,\cdots\end{cases} \tag{1.8}$$

The success or failure of the current method is determined by the ability or inability to complete the integration in equation (1.8). It is particularly fortunate that we successfully went through a series of iterative approximation formulas and solved for an equation expressing the closed form of all integrals in (1.8).

First, we make use of the related equations

$$F_n^{(1)} = \frac{z}{R} F_n^{(1)} - \frac{n-1}{n} \frac{1}{R} F_{n-1}^{(1)}$$

$$F_n^{(2)} = \frac{z}{R}\left[(R^2+z^2)F_n^{(1)} - \frac{2z}{n} F_{n-1}^{(1)}\right] - \frac{n-3}{n} \frac{1}{R}(R^2+z^2)F_{n-1}^{(1)}$$

$$F_n^{(3)} = \frac{R}{n} F_{n-1}^{(1)}$$

$$F_n^{(4)} = \frac{1}{n} R(R^2+z^2)F_{n-1}^{(1)} \qquad (1.9)$$

$$F_n^{(5)} = (R^2+z^2)F_n^{(1)} - \frac{2z}{n} F_{n-1}^{(1)}$$

We obtain

$$f_{n,k}^{(k)} = -f_{n,k}^{(k+2)} + (y^2+z^2) f_{n,k}^{(k)} - \frac{2z}{n} f_{n-1,k}^{(k)} \qquad /144$$

$$f_{n,1}^{(k)} = z f_{n,1}^{(k)} - \frac{n-1}{n} f_{n-1,1}^{(k)} \qquad \begin{matrix} k=0,1,2,\cdots \\ n=1,2,3\cdots \end{matrix} \qquad (1.10)$$

$$f_{n,2}^{(k)} = z f_{n,2}^{(k)} - \frac{n-3}{n} f_{n-1,2}^{(k+2)} - \frac{n-3}{n}(y^2+z^2) f_{n-1,2}^{(k)}$$

The problem reduces to one of solving for an equation to express $f_{n,k}^{(k)}$

It is not difficult to derive the successive approximation $f_{n,k}^{(k)}$ formula shown below:

$$f_{n,k}^{(k)} = -\frac{x^{k-1}}{n} F_{n-1}^{(1)} + \frac{k-1}{n} z f_{n-1,k-1}^{(k-2)} - \frac{(k-1)(n-2)}{n(n-1)} f_{n-1,k-2}^{(k-2)} \qquad \begin{matrix} k=2,3,\cdots \\ n=2,3,\cdots \end{matrix} \qquad (1.11)$$

If one is able to solve for $f_{n,0}^{(k)}, f_{n,1}^{(k)}, f_{n,2}^{(k)}, f_{n,3}^{(k)}$, then, from equation (1.11), $f_{n,k}^{(k)}$ is entirely determined. It is easy to demonstrate that

a) $$f^{(1)}_{n,0} = -\frac{1}{n} F^{(1)}_{n-1} \quad n=1,2,\cdots \tag{1.12}$$

b) $$f^{(0)}_{n,0} = \frac{1}{nz(y^2+z^2)}\left[(n-1)(y^2+3z^2) f^{(0)}_{n-1,0} - 3(n-2) z f^{(0)}_{n-2,0} + \right.$$
$$\left. + (n-3) f^{(0)}_{n-3,0} - xR F^{(1)}_{n-1}\right]$$

$$f^{(0)}_{0,0} = -\frac{1}{y}\,\mathrm{tg}^{-1}\frac{xz}{yr},\quad f^{(0)}_{1,0} = \frac{1}{y^2+z^2}\,\frac{x}{r},\quad f^{(0)}_{2,0} = \frac{xz}{r(y^2+z^2)}\left[\frac{1}{y^2+z^2}+\frac{1}{2r^2}\right]$$
$$n \geq 3 \tag{1.13}$$

c) $$f^{(1)}_{k,0} = -\frac{x^{k-1}}{r} + (k-1) B_{k-2}$$

$$f^{(1)}_{1,0} = \frac{1}{y^2+z^2}\,\frac{x}{r},\quad f^{(1)}_{0,0} = \frac{1}{r} \tag{1.14}$$

d) $$f^{(1)}_{k,0} = -z B_{k-2} - y^2 f^{(1)}_{k-2,0}$$

$$f^{(0)}_{0,0} = -\frac{1}{y}\,\mathrm{tg}^{-1}\frac{xz}{ry},\quad f^{(1)}_{0,0} = \frac{1}{2}\ln\left(\frac{r+z}{r-z}\right) \tag{1.15}$$

In c) and d)

$$B_k = \int \frac{x^k}{r}\,dx,$$

From the successive approximation formula given below and the equations expressing B_0, B_1, one determines that

$$B_k = \frac{r}{k} x^{k-1} - \frac{k-1}{k}(y^2+z^2) B_{k-2},\quad k \geq 2 \tag{1.16}$$

$$B_0 = \ln(r+x),\quad B_1 = r$$

Arriving at this, and with the help of equations (1.10)-(1.15), it is very easy to derive all the integrals in equation (1.8).

In the equation expressing the physical quantities in formula (1.7), there are $2N(2M+1)$ unknown functions. In order to solve for them, let the velocity field at these points satisfy the non-slippage movement condition. Then, obtain the linear algebraic equation set of $2N(2M+1)$ order, which gives precise values for C_{ml}, D_{ml}. We make use of the method of solving for the inverse of C_{ml}, D_{ml} any type of matrix and solve for the numerical values in this set of equations. We, then, obtain C_{ml}, D_{ml}. After substituting into equation (1.7), we then obtain equations which approximately express velocity and pressure.

The formula for the drag coefficient is /145

$$\lambda = -\frac{2}{3LU}\sum_{j=1}^{N}\left[D_{1,2(j-1)+1}+4D_{1,2(j-1)+2}+D_{1,2(j-1)+3}\right](d_{j_2}-d_{j_1}) \qquad (1.17)$$

II. Lateral Stokes Flows Around Spheroids

In order to check the convergence characteristics and accuracy of the method discussed above, we first consider the unbounded Stokes flow movements in a lateral direction around the z axis of spheroid bodies of rotation and carry out a comparison of precise solutions.

In a rectangular coordinate system, the equation for spheroidal object surfaces is

$$x=a\cos\lambda,\ y=b\sin\lambda\sin\theta,\ z=b\sin\lambda\cos\theta$$

$$a\geq b,\ 0\leq\lambda\leq\pi,\ 0\leq\theta\leq 2\pi \quad \text{(See Fig. 1)}$$

In these problems, the precise solutions for object surface pressure distributions and drag coefficients are respectively [8]

$$\lambda = \frac{16}{3}e^3\left[2e+(3e^2-1)\ln\frac{1+e}{1-e}\right]^{-1}$$

$$\bar{p} = \frac{p-p_\infty}{\mu U/a} = -\frac{3\lambda}{2}\frac{z}{1-e^2x^2}$$

In this, $c=\sqrt{a^2-b^2}$ is the half focal distance, and $e=c/a$ is the eccentricity.

When the separated line distribution method is chosen for points of singularity, we select the long axis a as the characteristic length. $(c,0,0)$, $(-c,0,0)$ are the points A, B. Due to the fact that flows around the body are completely symmetrical about the plane $x=0$, the singularity point strength relating to the plane $x=0$ is also symmetrical. On the x axis, we select for use the bisection principle to position M points of singularity. When $M=1$, a point of singularity is positioned at the origin point. When $M\geqslant 2$, the position of the point of singularity on the x axis is

$$\xi_j=-\frac{c}{M-1}(j-1) \quad (j=1,\cdots,M).$$

When the continuous line distribution method is selected for use with the points of singularity, we take M and divide it into c equal sections. Moreover, we choose the interpolation value points to be the center points of the various sections. Because of this, we have

$$d_{j_1}=\frac{c}{M}(j-1),\quad d_{j_2}=\frac{c}{M}j,\quad d_j=\frac{d_{j_1}+d_{j_2}}{2} \quad (j=1,\cdots,M).$$

For the placement of points on the surface of spheroids, we make use of the polar angle, equal division principle. On the boundary line, $\lambda=\theta=\pi/2$, $\lambda=\theta=0$, . This possesses special importance. The reason for this is that it is precisely these which determine the spheroid projection area perpendicular to the direction of movement. When we do a detailed examination of the parameter matrix of the set of linear equations, we discover that the points of singularity are on these points. In order to overcome the

difficulties discussed above, we use four nearby points $\theta=\delta_1$, $(\pi/2)-\delta_2$; $\lambda=\delta_3$, $(\pi/2)-\delta_4$; which respectively take the place of $\theta=0,\pi/2;\lambda=0,\pi/2$.

Here $\delta_1,\delta_2,\delta_3,\delta_4$ are constants awaiting definition. Their selection must follow this type of principle; that is, that it is both necessary to avoid the influence of singularity and also necessary, as much as is possible, to control the windward surface of the object. In the calculations in this article, we choose 0.05 degrees or 0.1 degrees.

The results for drag coefficients which are obtained through the use of the calculation methods discussed above are set out in Table 1 and Table 2. Moreover, at the same time, these tables present a comparison of precise solutions for various data. It is possible to see that, in the few circumstances in which M, N do not match well with the position points, it is possible to obtain drag coefficient values which are quite satisfactory and which have good convergence characteristics and accuracy. In the dispersed singularity point distribution method, when the length to width ratio $b/a\leq 0.7$, the convergence characteristics and accuracy of drag coefficients are relatively good. It is possible to achieve four significant digits. However, when the width to length ratio is larger than 0.7, the convergence characteristics of drag coefficients turn bad. After the strength distribution function selects for use a division segment which approaches a parabola, the difficulties above are thoroughly resolved. In calculating the width to length ratio straight through from 0.9 to 0.01, the convergence characteristics and the accuracy of the results get better and better. Estimates for width to length ratios somewhat smaller than this show that this type of good convergence result will continue straight through as the process is continued.

/146

Table 1 and Table 3 present the pressure distributions on the surface of spheroids as calculated using all the methods discussed above. Moreover, at the same time, it presents a comparison of the precise values calculated for these materials. These results demonstrate that the results of calculations made using the parabolic section approximation method also possess relatively good accuracy as concerns such localized characteristic quantities as pressure distribution. Approximate and precise calculations for pressure agree with each other to 4 or 5 significant digits.

1 长球的阻力系数 M=9 δ=0.1°					2 长球表面的压力分布 b/a=0.9 M=9 N=10				
N	LN	b/a=0.9	b/a=0.8	b/a=0.7	I	x	z	p	p(准确解)
8	48	0.93972	0.8787	0.8170	1	0.9848	0.1264	-0.2697	-0.2697
10	60	0.93972	0.8788	0.8170	2	0.8660	0.3641	-0.7390	-0.7388
3 准确解		0.93972	0.8788	0.8170	3	0.9848	0.0483	-0.1031	-0.1030
LN=2MN/3					4	0.8660	0.1391	-0.2822	-0.2822

Table 1 The Separated Line Distribution Method 1. Spheroid Drag Coefficient 2. Pressure Distribution on the Surface of Spheroids 3. Precise Solutions

N	LN	b/a=0.9	b/a=0.7	b/a=0.5	b/a=0.3	b/a=0.1
4	8	0.93972	0.816989	0.689436	0.551740	0.381153
6	12	0.93972	0.816984	0.689450	0.551737	0.381153
1 准确解		0.93972	0.816984	0.689450	0.551737	0.381153
N	LN	b/a=0.09	b/a=0.07	b/a=0.05	b/a=0.03	b/a=0.01
3	6	0.370022	0.345995	0.318256	0.283692	0.229951
4	8	0.370055	0.345995	0.318256	0.283692	0.229951
准确解		0.370055	0.345995	0.318256	0.283692	0.229951

Table 2 Spheroid Drag Coefficients (Continuous Line Distribution Method) 1. Precise Solutions

	b/a=0.74		M=1	N=6		b/a=0.1		M=1	N=6
I	x	z	p	p(准确解)	I	x	z	p	p(准确解)
1	0.9230	0.2832	-1.0638	-1.0638	1	0.7818	0.0623	-9.02785	-9.02786
2	0.7071	0.5293	-1.5593	-1.5593	2	0.6235	0.0782	-7.20647	-7.20647
3	0.3827	0.9237	-1.6883	-1.6884	3	0.2225	0.0975	-5.86125	-5.86126
4	0.0017	0.7400	-1.7064	-1.7064	4	0.0748	0.0936	-0.02763	-0.02762
5	0.9230	0.0005	-1.8838×10^{-3}	-1.8567×10^{-3}	5	0.9010	0.00005	-2.2047×10^{-3}	-2.2048×10^{-3}
6	0.7071	0.0009	-2.7218×10^{-3}	-2.7215×10^{-3}	6	0.7818	0.00011	-1.57566×10^{-3}	-1.57566×10^{-3}
7	0.3827	0.0012	-2.9467×10^{-3}	-2.9468×10^{-3}	7	0.4330	0.00016	-1.10498×10^{-3}	-1.10497×10^{-3}
8	0.0017	0.0013	-2.9782×10^{-3}	-2.9782×10^{-3}	8	0.0017	0.00018	-9.9787×10^{-3}	-9.9786×10^{-3}

Table 3 Pressure Distribution on Spheroid Surfaces (Continuous Line Distribution Method) 1. Precise Solution

The sample calculations above explain the fact that the parabolic line segment approximation method offers a type of method for handling three dimensional Stokes flow problems which not only has the advantages of fast convergence, high accuracy, and savings on time, but is also not limited by width to length ratiios. In the continuous line distribution method calculations below, parabolic segment approximation is always used. /147

		阻力系数					2表面上压力分布 λ=1.1 M=12 N=6				
M	N	λ=1.1	λ=1.16	λ=1.3	λ=2.0	λ=7.0	I	X	Y	Z	P
1	4	0.8468	0.9234	0.8684			1	1.376	0.0005	0.3140	-0.328
1	8				0.734	0.607	2	1.418	0.0015	0.0020	-0.0017
1	8	0.8468	0.9234	0.8684	0.734	0.607	3	0.834	1.046	0.0018	-0.0016

Table 4. Cassini Oval Body 1. Drag Coefficient 2. Surface Pressure Distribution

b/a=0.9		N.MY=12			b/a=0.8		N.MY=12		
M	c/a=1.0	c/a=0.9	c/a=0.8	c/a=0.7	M	c/a=0.9	c/a=0.8	c/a=0.7	c/a=0.6
3	0.8587	0.9397	0.9200	0.887	3	0.899	0.8788	0.8592	0.839
4	0.8587	0.9387	0.9200	0.887	4	0.899	0.8788	0.8592	0.839

b/a=0.7	M=1			
N.MY	c/a=0.8	c/a=0.7	c/a=0.6	c/a=0.5	c/a=0.4
40	0.837	0.8170	0.7975	0.7788	0.761
48	0.837	0.8170	0.7975	0.7788	0.761

Table 5 Three Dimensional Ellipsoid Drag Cofficients $1.^{*MY}$ is the point separation number in the direction of separation on the central surface.

III. The Three Dimensional Stokes Flows of Rotating Cassini Oval Bodies

In the section above, we went through the Stokes flow for a spheroid in a lateral uniform oncoming flow and looked at the convergence characteristics and the accuracy of three dimensional flow movements as determined by the Sampson singularity point distribution method. The results were entirely satisfactory. This section will go a step further in selecting the methods discussed above in order to determine the Stokes flow in a uniform oncoming flow from the z direction around any given form of rotation body in the x direction. We choose the Cassini oval body of rotation to be an example. When the parameters are not the same, the Cassini oval body presents many types of forms. There are completely convex ones. There are partially convex ones. And, there are partially concave ones. This is very useful for the increased applicability of inspection methods.

The equation for a Cassini body of rotation in the x direction, in a three dimensional rectangular coordinate system, is

$$x=\rho\cos\phi,\ y=\rho\sin\phi\sin\theta,\ z=\rho\sin\phi\cos\theta$$

$$\rho=c^2\cos 2\phi+\sqrt{a^4-c^4\sin^2 2\phi}\quad (a>c>0)$$

In this, ρ, ϕ are respectively vector radii and polar angles in a polar coordinate system. c is the focal length. a is some constant. $b=\sqrt{a^2-c^2}$ is the coordinate for the point of intersection between the oval body and the R axis (see Fig. 2). /148

Take b to be the characteristic length. Diagrams of the meridian surfaces of the Cassini oval bodies when $c=0.8,\ 2.5,\ 50$ are shown in Fig. 3. $c=0.8$ corresponds to a fully convex form. $c=2.5$ has a slightly concave section. $c=50$ has a very deep concave dip section. Obviously, the larger c is the more severe is the concave dip. We first select $\lambda=\rho_{max}/\rho_{min}=\sqrt{1+2c^2}$ to be the parameter. Then, we consider the several situations where $\lambda=1.1,\ 1.15,\ 1.3,\ 2.0,\ 7.0$. We position a point of singularity at $(-c,c)$, and respectively make use of the separation line distribution method and the parabola line segment approximation to carry out calculations. The singularity point placement and the handling of the position points are the same as in the case of spheroids.

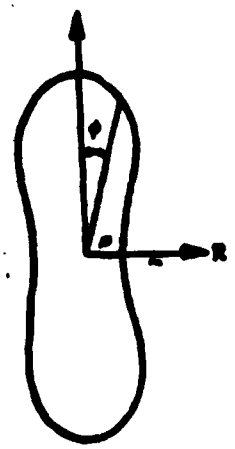

Fig. 2

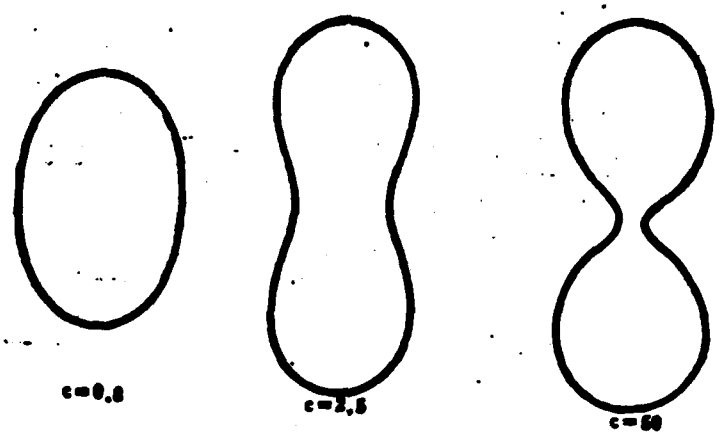

Fig. 3

IV. Stokes Flows Around Three Dimensional Ellipsoids in Uniform Oncoming Flows

Concerning the Stokes flows around an ellipsoid in a uniform oncoming flow from a certain direction, it is possible to solve respectively for the oncoming flow around the ellipsoid in the directions of the three coordinate axes . Not to lose universality, it is possible only to consider the flow around an ellipsoid in a uniform oncoming flow in the z direction. We position a Sampson flow on the central plane in the body perpendicular to the oncoming flow (take the focal length to be half the axis of the ellipse). Make the points of singularity in the x direction (or y direction) distribute continuously. Moreover, we use separate distribution in the z direction. Because of this, it is possible to make use of formulae (1.1) and (1.5)-(1.6) from the first section. The position points on the surface of objects all make use of the principle of the equal division of polar angles. In making use of the methods described in the two sections above, we avoided the singularity of the linear equation set parameter matrix. /149

The results obtained from calculations for drag coefficients are presented in Table 5. The calculation results show that, within a certain range of width to length ratios, segments in a certain direction approximate parabolas. In another direction, we selected for use the separation approximation Sampson singularity point surface distribution method. This was sufficient to obtain drag coefficient values of over three significant digits. This, therefore, explains the applicability of the Sampson singularity point iterative addition method in handling problems involving the Stokes flows around three dimensional bodies.

REFERENCES

[1] Gluckman, M. M., Weinbaum, S and Pfeffer R., *J. Fluid Mech.*, 55 (1972), 677-709.

[2] Youngren, G. K and Acrivos, *J. Fluid Mech.* 69 (1975), 377-403.

[3] Wu Wangyi; Chinese Science, A ed. 2 (1984) , 145-156

[4] Wu Wangyi, He Qing; AppliedMathematics and Mechanics, 6, (1981) 793-800

[5] Wu Wangyi, Wang Shaohua; Mechanics Bulletin, 5, (1984) 443-458

[6] Wu Wangyi, Zhu Min; Mechanics Bulletin; Awaiting publication.

[7] Zhu Min, Wu Wangyi; Applied Mathematics and Mechanics; 10, 1985

[8] A. T. Chwang and T. Y. T. Wu, *J. Fluid Mech.* 67 (1975), 787-815.

THE SEMI-ANALYTIC SEMI-NUMERICAL METHOD TO TREAT THE THREE-DIMENSION STOKES FLOW

Lin Shengtian Wu Wangyi
(Department of Mechanics, Beijing University)

Abstract

This paper deals with the numerical solutions of the three-dimension Stokes flow by means of the axisymmetric Sampsonlets distribution method whithin the body. The systematical and simple formulas are obtained for the first time to evaluate the complex integrals emerged in this paper. This leads to the advantages of proposed method, high accuracy and small amount of the computational work. The three-dimension Stokes flow for the prolate spheroid and the revolutional Cassini oval passed by uniform flow in the side direction are calculated. The good convergence properties the high accuracy of the results for the drag factor and the pressure distribution are demonstrated. Finally in this paper the three-dimension Stokes flow passed an ellipsoid are considered and the corresponding drag factor and the pressure distribution are presented.

A NEW TECHNIQUE OF NUMERICAL CONFORMAL MAPPING AND ITS APPLICATIONS

/150

Huang Mingke

(Nanjing Aeronautical Institute)

SUMMARY This article develops a type of systematic, linear numerical value conformal method, which makes it possible to take the exterior area of a given curved, multi-sided form containing several angular points and do a linear, conformal mapping of it as the exterior area of a unit circle. Due to the fact that, in this method, use is made of the FFT technique, computational speed is very fast. This type of method can be used in calculating two-dimensional, noncompressible flows around a given body, as well as in figuring the apparent mass coefficient of two-dimensional bodies, producing the orthogonal, conformal, body-attached coordinate grid required in limited difference calculations. Results with calculations from several types of exterior forms show that, on the grid surface pro duced, the machine time required is an order of magnitude smaller than that for the Thompson method, and the orthoganality of the grid is preserved everywhere. Besides this, in quite a few problems, the governing equation on the transformation plane is particularly simple.

I. Introduction

In the last ten years, the technology of producing coordinate grids that adhere to surfaces has rapidly developed. This has overcome the difficulties of handling curve boundary conditions in limited difference methods. The use of equations for elliptical forms to produce grids, as developed by Thompson [1], is relatively good and flexible. However, the expenditures of time involved are relatively great. If this method is used in calculations for supersonic flow speeds, the time occupied in the production of the grid and the time used in the calculation of the flow field can be of the same order of magnitude. Object-adhering coordinate grids produced for conformal mapping have several advantages. They preserve orthogonality. In potential flow problems outside of shock wave areas, in areas where one often gets abrupt changes in flow movements (such as the vicinities of the forward and rear edges of airfoils) one obtains denser grid patterns. Besides this, the governing equations for many problems, in the conformal mapping calculation planes, have particularly simple forms. Because of this, it is widely used for calculations in transonic potential flows [2,3] and other flow movement problems.

Conformal mapping methods were used very early to handle non-compressible flows around given airfoils [4]. In the 1970's FFT [13] was developed as the basic method for fast, conformal mapping [5,6], which causes an order of magnitude increase in the speed of calculations. If the exterior form included several points of angularity, we generally chose for use a series analytic transformation to eliminate the angular points [7,8]. After this, we carried out a transformation of the smooth boundary. Recently, Davis (9), also taking Schwarz-Christoffel transformations as a basis developed a type of capability to handle the conformal mapping of curved edge exterior forms containing angular points. The conformal mapping which is used by Jameson [2] also takes FFT techniques as a basis. In this, it is possible to take any airfoil and map it as a unit circle. The rear edge of the airfoil is equivalent to an angular point. This article will take the latter type of method and generalize it to include any curved, multi-sided form containing many points of angularity. The method developed is not only capable of being used to produce coordinate grids adhering to bodies. It is also capable of being used to calculate incompressible flows. It can also be used to calculate apparent mass coefficients. It is the foundation for calculating the aerodynamic derivatives for guided missiles and aircraft [10-12].

II. Conformal Mapping Methods

The problem is to take the exterior of a certain curved, multi-sided form (Fig. 1) on physical plane Z and map it confromally as the exterior of a unit circle on complex plane σ. We assume that the transformation derivative can be expressed as /151

$$\frac{dZ}{d\sigma} = \left\{ \sum_{i=1}^{M} \left(1 - \frac{e^{-i\theta_i}}{\sigma} \right)^{1-\frac{\alpha_i}{\pi}} \right\} \exp \sum_{n=0}^{N} \frac{c_n}{\sigma^n} \qquad (1)$$

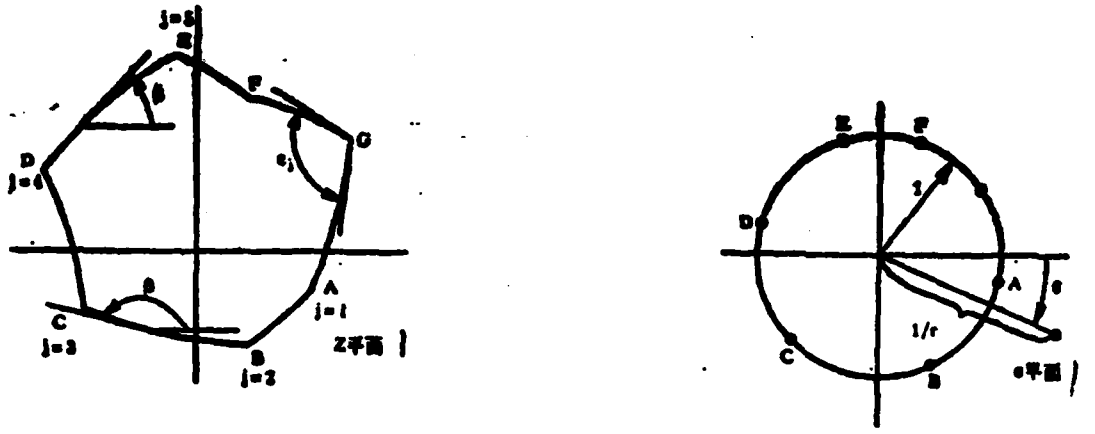

Fig. 1 Physical Plane z and Transformation Plane σ 1. Plane

In the equation, the large brackets enclose the Schwarz-Christoffei factor. This is used to cause the rate of slope of the lines of intersection to be discontinuous at the points of angularity. M is the number of points of angularity. ε_j is the included angle at the j. th point of angularity. $e^{-i\theta_j}$ is the corresponding complex coordinate for points of angularity on the σ plane. They are on the unit circle. θ_j is unknown before the fact. $c_n = a_n - i b_n$ is an unknown complex parameter. The number of quantities in the expansion formula N must be chosen to be adequately large.

Take equation (1) and expand it in an infinitely distance neighborhood. In order to make the transformation have a single value (that is, the closed exterior form mapping being a closed exterior form), in the expansion of the equation, it is necessary not to include the quantity $1/\sigma$. Because of this, the value of parameter c_1 must necessarily be

$$c_1 = \sum_{j=1}^{M} \left(1 - \frac{\varepsilon_j}{\pi}\right) e^{-i\theta_j} \tag{2}$$

Making use of this equation, the expansion formula can be written as

$$\frac{dZ}{d\sigma} = \exp(c_0)\left\{1+\frac{1}{\sigma^2}\left[c_1-\frac{c_1^2}{2}-\sum_{j=1}^{M}\frac{\left(1-\frac{\varepsilon_j}{\pi}\right)\frac{\varepsilon_j}{\pi}}{2}e^{-ik\theta_j}+\right.\right.$$

$$\left.\left.+\sum_{j=1}^{M-1}\sum_{k=j+1}^{M}\left(1-\frac{\varepsilon_k}{\pi}\right)\left(1-\frac{\varepsilon_j}{\pi}\right)e^{-ik(\theta_k+\theta_j)}\right]+O\left(\frac{1}{\sigma^3}\right)\right\} \tag{3}$$

In order to determine the complex parameter c_n, on the unit circle $\sigma=e^{-i\theta}$. Because of this, $d\sigma=-ie^{-i\theta}d\theta$. Correspondingly, $dZ=e^{i\beta}ds$. Here, s is the arc length calculated in a counterclockwise direction. β is the angle of slope of the tangent or intercept line (Fig. 1). We take these equations and substitiute them into formula (1). We take the logarithm and separate the real and imaginary sections, obtaining a precise definition of the formulas for a_n and b_n.

$$\log\left(\frac{1}{e^{c_0}}\frac{ds}{d\theta}\right)-\sum_{j=1}^{M}\left(1-\frac{\varepsilon_j}{\pi}\right)\log\left|2\sin\frac{\theta-\theta_j}{2}\right|=\sum_{n=1}^{\infty}(a_n\cos n\theta+b_n\sin n\theta) \tag{4}$$

$$\left(\beta+\theta-\frac{3}{2}\pi\right)\sum_{j=1}^{M}\left(1-\frac{\varepsilon_j}{\pi}\right)\frac{(\theta-\theta_j)+2\pi H(\theta_j-\theta)-\pi}{2} \tag{5}$$

/152

$$=-b_0+\sum_{n=1}^{N}(a_n\sin n\theta-b_n\cos n\theta)$$

In this, $H(\theta_j-\theta)$ is the unit step function. When $\theta>\theta_j$ take the value to be zero. When $\theta<\theta_j$ take the value to be 1.

As far as the exterior form given on the Z plane is concerned, β acts as a function of s. $\beta(s)$ is already known. We take the circumference of the unit circle on the σ plane ($\theta=0$ to 2π) and divide it into J equal sections. The iterative substitution procedure for determining the parameters a_n and b_n is given below:

1. Assume that the point division location value s is already known; that is, assume the functional relationship $s(\theta)$. For example, in the initial approximation, it is possible to assume this to be a linear relationship. For the function $s(\theta)$, we use interpolation values for values of θ determined for points of angularity, that is, θ_j, $j=1, 2, \cdots, M$.

2. From the already known values of (s) and s(θ). , the left side of equation (5) becomes the already known function of θ. It is possible to expand it as a Fourier series, specifying $a_0, \cdots, a_N$ and $b_0, b_1, \cdots, b_N$. Due to the fact that the exterior form has points of angularity, the function $\beta(\theta)$, therefore, is discontinuous at the points of angularity. It is possible to demonstrate that the second term of the left side of equation (5) will produce a corresponding discontinuity at the points of angulariity. This causes the difference in the second term of the left side to be 2π the periodic discontinuity function of θ. Because of this, the right side of this type of equation is a Fourier series with good convergence.

3. We take the values determined for a_0 and b_0 and substitute them into the right side of equation (4). In this, a_1 and b_1 are calculated according to formula (2). Reconciling this to the Fourier series, we get

$$\frac{1}{e^{i\theta}} \frac{ds}{d\theta} = f(\theta) \tag{6}$$

In this, the value of $f(\theta)$ at the equally spaced point θ_1 on the circumference of the unit circle is already known. We again make use of numerical value integration methods to obtain a new function relationship where s functions as θ

$$s = e^{i\theta} \int_0^{\theta} f(\theta)\, d\theta \tag{7}$$

Due to the fact that the overall length of the circumference of the exterior form, s_w, on the plane Z is already known, it is, therefore, necessary

$$s_w = e^{i\theta} \int_0^{2\pi} f(\theta) d\theta \tag{8}$$

From this equation, we make a precise solution for $a_{0,0}$.

It is necessary to point out that, when making a numerical value integration of formula (7), if the domain of integration $[\theta_i, \theta_{i+1}]$ includes in itself a point of angularity θ_i, then, $\theta_i<\theta_i<\theta_{i+1}$.

According to equation (4), the singularity of $f(\theta)$ in the vicinity of θ_i is $f(\theta)\sim|\theta-\theta_i|^{\mu}$. In this $\mu=1-\varepsilon_i/\pi$. When $\pi<\varepsilon_i<2\pi$, although it is an infinitely large singularity, it is still possible to integrate it. Now, let us assume that, in the small segement (θ_i, θ_i) $f(\theta)$ may possibly approximate the expression

$$f(\theta)=f(\theta_i)(\theta_i-\theta)^{\mu}/(\theta_i-\theta_i)^{\mu}$$

Using an analytic method of integration, it is possible to find

$$\int_{\theta_i}^{\theta_i} f(\theta)d\theta=f(\theta_i)(\theta_i-\theta_i)\Big/\left(2-\frac{\varepsilon_i}{\pi}\right)$$

The same type of method leads to the integral of the area (θ_i, θ_{i+1}).

Because of this, /153

$$\int_{\theta_i}^{\theta_{i+1}} f(\theta)d\theta=\int_{\theta_i}^{\theta_i}+\int_{\theta_i}^{\theta_{i+1}}=\frac{f(\theta_i)(\theta_i-\theta_i)+f(\theta_{i+1})(\theta_{i+1}-\theta_i)}{\left(2-\frac{\varepsilon_i}{\pi}\right)}$$

This equation makes clear the fact that, when $\varepsilon_i=2\pi$, it cannot be integrated. Because of this, this method is not able to handle this type of situation.

If $[\theta_i, \theta_{i+1}]$ does not contain a point of angularity or $\varepsilon_i<\pi$, for a point of angularity, then, using a simple, ladder type formula we obtain

$$\int_{\theta_i}^{\theta_{i+1}} f(\theta)d\theta=\frac{1}{2}[f(\theta_i)+f(\theta_{i+1})](\theta_{i+1}-\theta_i)$$

4. Take the newly determined $s(\theta)$ and, using a low relaxation, orthogonal relationship $s(\theta)$, assumed in the first step, repeat the first to the third steps in cycles of iterative substitution. Continue this until the difference between $s(\theta)$ as determined in two neighboring iterative substitutions is within the nominal range for permissible differences. In the process described above, it is necessary several times to take the already known function and expand it to a Fourier series as well as taking the already known Fourier series and reconciling them. FFT techniques are very effective techniques when used in carrying out these operations [13]. When using FFT, the point separation or scanning number J must be chosen as a whole number power of 2, that is $J = 2^4=16, 2^5=32, 2^6=64, 2^7=128$, and so on. The N chosen in equation (1) is $N=J/2$. . The example calculation which was done demonstrates that the iterative convergence discussed above is fast. In the case of airfoils, 6-7 iterative substitutions is sufficient. In relatively difficult problems, the relaxation factor in step 4 can be chosen as 0.5 or smaller.

III. Orthogonal Conformal Grid Creation Methods

In the previous sections, we have already taken the mapping of the exterior portion of objects on the Z plane to be exterior portions of the unit circle on plane σ. Due to the fact that the exterior domain is infinitely large, we use the transformation $r=1/\sigma=re^{-i\theta}$ take the mapping of the exterior portion of the unit circle plane σ to be within the unit circle plane r. At this time, an infinitely distant point corresponds to the center of the circle. Within the unit circle plane r, in the direction r, we make use of the interval as Δr (it is also possible for the intervals to be unequal). Concentric circles at this interval as well as lines radiating in the θ direction at interval $\Delta\theta$ creates an orthogonal grid (Fig. 2). This type of grid takes the mapping to be an orthogonal, conformal coordinate grid adhering to the object on its surface plane. In order to determine the grid points of the

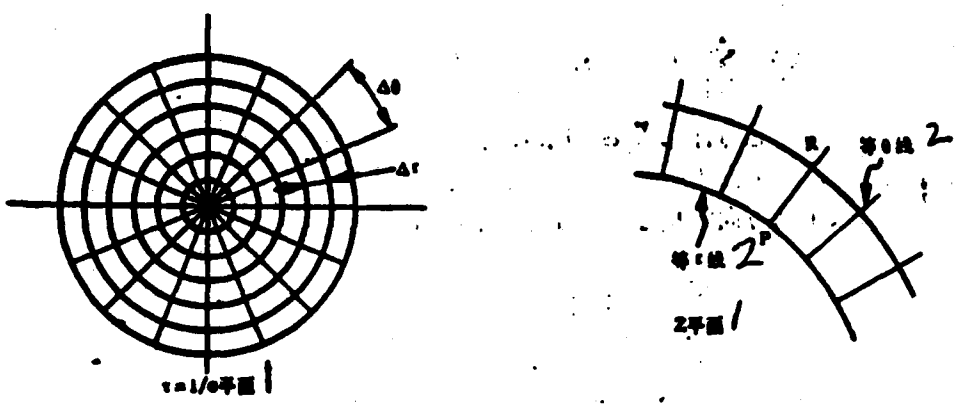

Fig. 2 Diagram of Grid Formation 1. Plane 2. th Line

coordinates, we first determine the transformation modulus H, on the τ plane,

$$H=\left|\frac{dZ}{d\tau}\right|=\left|\frac{dZ}{d\sigma}\right|\left|\frac{d\sigma}{d\tau}\right|=\frac{1}{r^2}\left|\frac{dZ}{d\sigma}\right| \tag{9}$$

In formula (1), let $\sigma=e^{-i\theta}/r$, . Take the logarithm. Then, if we take its real component, we obtain /154

$$\log\left|\frac{dZ}{d\sigma}\right|=\sum_{i=1}^{N}\frac{1}{2}\left(1-\frac{e_i}{\pi}\right)\log\{[1-r\cos(\theta-\theta_i)]^2+r^2\sin^2(\theta-\theta_i)\}+ \tag{10}$$

$$+\sum_{n=0}^{N}r^n(a_n\cos n\theta+b_n\sin n\theta)$$

The triangular series on the right side of the equation still uses FFT technology for reconciliation or summation. From this, we find grid point positions $|dZ/d\sigma$ and H values.

This is due to the fact that the transformation modulus H is the ratio between the grid step length at a location on the Z plane and the grid step length of the corresponding point on the τ plane. If we have already found, on the τ plane, the k th concentric circle $r=k\Delta r$, the corresponding curve on the physical plane Z as well as the positions of the grid points on it, then, due to the orthogonal grid, it is possible, from the grid points, to draw a perpendicular line toward the outside (for example, point P) (Fig. 2). If we take $PR=H\Delta r$, then, it is possible to obtain the grid point R on a line defined by r ($(r=(k+1)\Delta r)$) below. Because of this, the orthogonal conformal grid on the Z plane is able to be gradually created toward the outside along a perpendicular direction beginning from the surface of the plane. It is necessary to point out that, during the creation process discussed above, the radial direction step length Δr must not be chosen too large.

IV. Calculation of Apparent Mass Parameter

In order to cause the derivative of the mapping equation to be one at an infinitely distant point, we introduce $\zeta=\exp(c_0)\sigma$, and substitute it into equation (2). After integrating, we obtain

$$Z=\zeta+\sum_{n=1}^{\infty}\frac{A_n}{\zeta^n} \tag{11}$$

In this

$$A_1=-\exp(2c_0)\left[c_1-\frac{c_1^2}{2}-\sum_{i=1}^{N}\frac{\left(1-\frac{\varepsilon_i}{\pi}\right)\left(\frac{\varepsilon_i}{\pi}\right)}{2}e^{-i\theta_i}+\right.$$
$$\left.+\sum_{i=1}^{N-1}\sum_{k=i+1}^{N}\left(1-\frac{\varepsilon_k}{\pi}\right)\left(1-\frac{\varepsilon_i}{\pi}\right)e^{-i(\theta_k+\theta_i)}\right] \tag{12}$$

The other parameters $A_2, A_3, \cdots$ can also be calculated, however, it is very difficult to express them as simple analytic equations. The exterior form mapping of the exterior plane is a circle in plane ζ. Its radius is $R_0=\exp(c_0)$. According to the definition apparent mass coefficient in reference [10] as well as its symbols and calculation formulas, the calculation formulas for the translation of apparent mass coefficients in the direction of the horizontal axis as well as in the direction of the vertical axis are

$$\left.\begin{aligned} m_{11} &= 2\pi\rho\left[R_1^2 - \frac{S_c}{2\pi} - Re(A_1)\right] \\ m_{12} &= m_{21} = -2\pi\rho\, Im(A_1) \\ m_{22} &= 2\pi\rho\left[R_1^2 - \frac{S_c}{2\pi} + Re(A_1)\right] \end{aligned}\right\} \qquad (13)$$

In these equations, ρ is flow body density. S_c is the area of the exterior form of the Z plane. Re and Im are the symbols for the real and imaginary parts. Calculations of the apparent mass parameters m_{12}, m_{22} as well as m_{11} corresponding to rotations are relatively difficult. It is necessary to make full use of the parameters developed in formula (11). /155

V. Sample Calculation

Example 1: Semicircle with radius 1. Fig. 3 is β following changes in the arc length s. During the calculations, the scanning or spacing number of the unit circle on the plane τ is taken as 64($\Delta\theta = 2\pi/64$)

The radial direction scanning number is taken as 10($\Delta r = 0.1$)

In this example, the iterative substitution relaxation factor is taken as 0.5 (if it is taken as 0.8, one does not get convergence.) After 13 rounds of iterative substitution, the accuracy obtained is close to that for two iterative substitutions, and the maximum deviation of the scanning arc length is smaller than 0.0005. A comparison of the calculated results for apparent mass and precise solutions appears in Table I. Fig. 4 is the orthogonal, conformal grid which is produced (what is shown in the Fig. is based on only 32 points mapped per cycle). Fig. 5 is the pressure strength parameter C_p distribution for noncompressible, horizontal winding flows and agrees with the results of Davis [9].

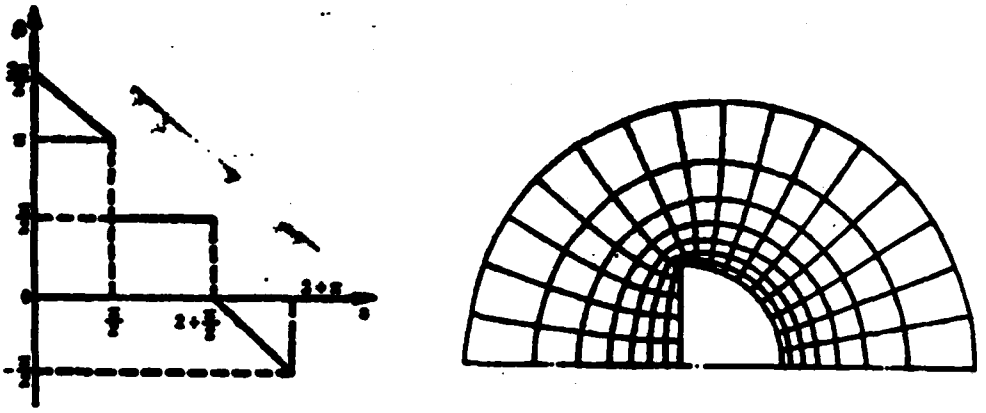

Fig. 3 Changes in the Semicircular Shape, Tangential Slope Angle θ According to Arc Length

Fig. 4 Orthogonal, Conformal Grid of Semicircular Outer Section Area

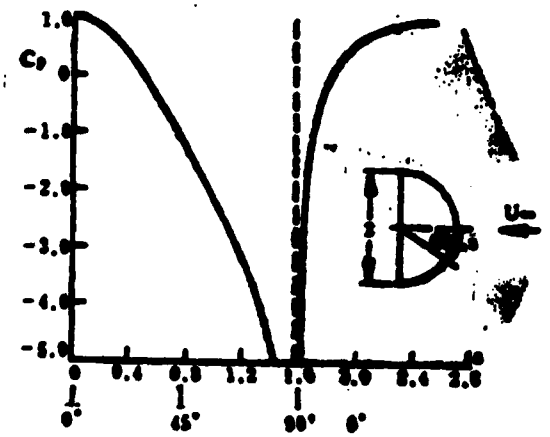

Fig. 5 Semicircular Shape Noncompressible Potential Flow Surface Pressure Strength Distribution

Example 2: Equilateral triangle of height 1. For the calculation, choose $\Delta\theta=2\pi/64$, $\Delta r=0.1$; . Choose the iterative substitution relaxation factor as 0.3. 15 iterative substitutions reaches the mandated accuracy. The results of calculations of apparent mass are seen in Table I. In the case of an equilateral triangle, the apparent mass coefficients for any given direction are all equal. The minute difference between m_{11} and m_{22} calculated in this example is caused by calculation error. Fig. 6 is the orthogonal /156

	单位半径的半圆		高度为1的正三角形	
	本 文 2	精解(文[11]) 3	本 文 1	精解(文[10,11]) 5
$\frac{m_{11}}{2\pi\rho}$	0.5314	$\frac{19}{36}=0.5278$	0.1471	$\frac{0.651}{2}\left(\frac{2}{3}\right)^2=0.1453$
$\frac{m_{12}}{2\pi\rho}$	0.1579	$\frac{17}{108}=0.1574$	0.1164	0.1453
$\frac{m_{13}}{2\pi\rho}$	0		0	0

Table I 1. Semicircle of Unit Radius 2. This Article 3. Precise Solution (Reference [11]) 4. Right Triangle of Height 1 5. Precise Solution (Reference [10,11])

conformal grid produced. Fig. 7 is the pressure strength distribution for noncompressible horizontal winding flows.

Example 3: A wing-fuselage composite assembly cross section surface. The half wing deployment equals 2. The round fuselage radius is 1. This example contains 6 points of angularity. Two interior angles are zero. Four interior angles are $3\pi/2$. . For these calculations, choose $J=128$; . Choose the relaxation factor as 0.15. Fig. 8 is a comparison of the calculated pressure strength distribution (C_p) for horizontal noncompressible winding flows and the results of precise solutions. From this figure one can see that, when equidistant points on the unit circle of plane σ are projected on the

physical plane, in the vicinity of points of angularity at which the interior angle is greater than π , the points are usually very thin, influencing the accuracy of calculations.

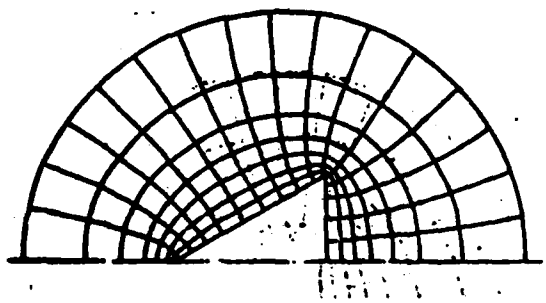

Fig. 6 Orthogonal, Conformal Grid for Equilateral Triangle Form

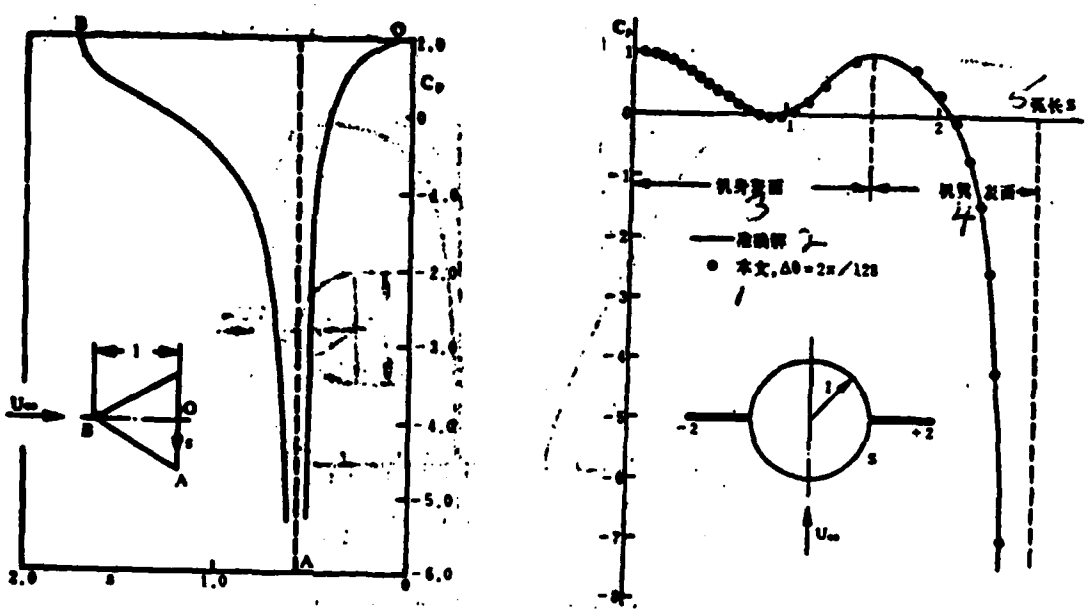

Fig. 7 Noncompressible Potential Flow Pressure Strength Distribution Around Equilateral Triangle Shape

Fig. 8 Noncompressible Potential Flow Pressure Strength Distribution Around Wing-Fuselage Composite Body Cross Section 1. This Article 2. Precise Solution 3. Fuselage Surface 4. Wing Surface 5. Arc Length

Example 4: GA (W)-1 supercritical airfoil. We have already done specialized work in calculating the low speed pressure strength distribution for a given airfoil and have composed a calculation program. These airfoils contain only one point of angularity. In /157
equation (1), if c_1 is taken to be an appropriate value (see reference [2]), it is possible to take the rear edge non-closed airfoil mapping to be a closed unit circle. Fig. 9 is a comparison between the surface pressure strength distribution calculated when the angle into the wind is $\alpha=4.17°$ and experimental values for it. When doing calculations, one circumference of the airfoil is taken as 128 points, that is, $\Delta\theta=2\pi/128$. 6 iterative substitutions reach the required accuracy. The whole process, on the IBM 4341 machine, takes only three seconds of CPU time. Discrepancies between calculations and experimental results are mainly due to the fact that, in calculations, there is no consideration of the effects of viscous boundary layers. We have also compiled a program to produce orthogonal, conformal coordinate grids which conform to objects such as a given airfoil. On the IBM 4341 machine, producing a 64x16 grid only required three seconds of CPU time.

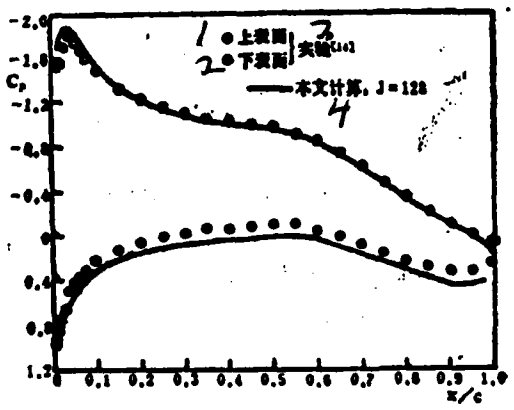

Fig. 9 GA (W)-1 Airfoil Low Speed Pressure Strength Distribution ($\alpha=4.17°$)
1. Upper Surface 2. Lower Surface 3. Experiment 4. This Article's Calculations

REFERENCES

[1] Thompson, J. F. etc., *J. of Computional Physics*, 15 (1974) 299-319.
[2] Jameson, A., Symposium Transsonicum II (1975).
[3] 黄明恪, 空气动力学学报, 2 (1984).
[4] Theodorsen, T., NACA Rept. No. 411 (1932).
[5] Ives, D. C., AIAA Paper 75-842 (1975).
[6] Halsey, N. D., *AIAA J.* 17, 12 (1979) 1281-1288.
[7] Arlinger, B., Lecture Notes in Physics 141 (1980).
[8] Moretti, G., Numerical/Laboratory Computer Methods in Fluid Mechanics (1976).
[9] Davis, R. T., AIAA Paper 79-1463 (1979).
[10] Nielsen, J. N., Missile Aerodynamics, McGraw-Hill, (1960).
[11] Huang, M. -K., and Chow, C. -Y., *J. of Aircraft*, 20, 9 (1983) 810-816.
[12] Huang, M. -K., ASME *J. of Applied Mechanics*, 49, 3 (1982) 470-475.
[13] E. O. 布赖姆, 快速富里叶变换, 上海科学技术出版社, (1979).
[14] McGbee, R. J. etc., NASA TN-D 7428 (1973).

[3] Huang Mingke; Acta Aerodynamica Sinica, 2 (1984)
[13] E.O. Blaymin (spelling uncertain); "High Speed Fourier Transforms"; Shanghai Scientific and Technical Press, (1979)

A NEW TECHNIQUE OF NUMERICAL CONFORMAL MAPPING AND ITS APPLICATIONS

Huang Mingke

(Nanjing Aeronautical Institute)

Abstract

A systematic method of numerical conformal mapping is developed in this paper to map the exterior of an arbitrary 2-D body having several discontinuities of surface slop onto the exterior of a unit circle. The use of the FFT technique makes the execution of the computation very fast. The method developed can be applied to the computation of incompressible flow past an arbitrary 2-D body, to that of the apparent mass coefficients of the cross-sections, and to the generation of the orthogonal, conformal grid used in finite difference method. Several examples presented show that the present method has an order faster in computation of the grid generation than that of the usual Thompson's method, and that the grid generated has the orthogonality everywhere. The another superiority is that, for many problems, the governing equation usually takes the especially simple form on the mapping plane.

NUMERICAL SOLUTION OF TRANSONIC SMALL DISTURBANCE PRESSURE EQUATIONS USING A MIXED DIFFERENCE METHOD

/159

Wang Lixia Luo Shijun

(Northwestern Polytechnical University)

SUMMARY This article presents a numerical value method for directly solving the transonic steady state small perturbation pressure equation

$$\left(1-M_{\infty}^{2}-\frac{\gamma+1}{V_{\infty}}M_{\infty}^{2}u\right)u_{xx}+u_{yy}-\frac{\gamma+1}{V_{\infty}}M_{\infty}^{2}u_{y}^{2}=0$$

As far as research into interference problems with various tunnel walls are concerned, compared to traditional velocity potential equations, the use of pressure equations to be the governing equations for solving transonic flow fields, with the boundary conditions of Dirichlet form, makes it easier to handle these problems. Moreover, taking pressure as the variable to be solved for, it is possible to reduce accumulated error and increase the accuracy of the calculations.

This article chooses for use a mixed difference method [8] to solve pressure equations through numerical value testing methods, solving the appropriate difference forms, and iterative substitution linearization methods. Convergence solutions with these methods, when compared to the solutions obtained by taking velocity potential equations as the governing equations, give results which compare relatively well. This, therefore, demonstrates the feasibility of the methods in this article.

Finally, this article presents typical sample calculations for applying the methods of this article to calculating tunnel wall interference during transonic wind tunnel tests of airfoils and the calculating of pressure distribution for the exterior forms of certain airfoils.

In recent years, the theory of self-correcting wind tunnels and various types of methods for the correction of interference, which have been developed, present quite an optimistic outlook for the solving of tunnel wall interference problems. Among these, there are quite a few methods which require the use of pressure distributions which are measured on the surface of wings and in the vicinity of tunnel walls in order to calculate the boundary conditions for flow fields inside wind tunnels [1-7]. This type of problem usually only involves model surfaces and flow field pressure distributions. The methods which have been used in the past [2,5-7], always start by taking the empirically measured pressure boundary condtions and using them for potential velocity. After that, they did numerical value solutions for velocity potential equations. Then, they turned back around and took the solutions for velocity potential and turned them into pressures. In this way, on the one hand, they handled the complexity of the procedures for boundary conditions, and, on the other, in the two stage pressure-velocity potential-pressure transformation process, they inevitablly added cumulative error. With reference to the particular characteristics of these types of problems, if it is possible to directly solve equations using pressure as a variable, changing the boundary conditions to Dirichlet boundary conditions, then, it is possible to overcome the drawbacks discussed above. Because of this, this article, in dealing with small transonic perturbations, derives small perturbation pressure equations. These equations, in transonic ranges, have the same forms as are found in small perturbation velocity potential equations. They can also have mixed forms. These two, in their mathematical natures, have certain points in common. However, because of the appearance of the term u_x, the pressure equations are slightly more complicated than the velocity potential equations. Moreover, the conversion characteristics and stability characteristics of numerical value solutions to pressure equations are also more difficult to rigorously demonstrate mathematically. Because of this, this article makes use of numerical value tests to research the actual calculation methods used in mixed difference methods [8] for solving pressure equations, and we have initially obtained satisfactory results

II. Transonic Steady State Small Perturbation Pressure Equations /160

The binary transonic small perturbation velocity potential equation is:

$$\left(1-M_\infty^2-\frac{\gamma+1}{V_\infty}M_\infty^2\phi_x\right)\phi_{xx}+\phi_{yy}=0 \qquad (1)$$

In this, M_∞ represents the mach number of pertubation gas flows which have not yet passed through. V_∞ stands for the velocity of the perturbation gas flows before they pass through. ϕ stands for the small perturbation velocity potential. γ stands for the heat adiabatic index of the atmosphere.

Take (1) and solve for x and let $u=\phi_x$. Then, the equation which satisfies the partial perturbation velocity u in the x direction is:

$$\left(1-M_\infty^2-\frac{\gamma+1}{V_\infty}M_\infty^2 u\right)u_x+u_y-\frac{\gamma+1}{V_\infty}M_\infty^2 u^2=0 \qquad (2)$$

If we take note of the relationship between the small perturbation pressure parameter C_p and u :

$$C_p=-\frac{2u}{V_\infty} \qquad (3)$$

then, as soon as we know u , we can conversely solve for C_p . Because of this, this article takes equation (2) and calls it the transonic small perturbation pressure equation.

III. Boundary Conditions

1. Boundary Conditions for the Calculation of Flow Fields Inside Wind Tunnels

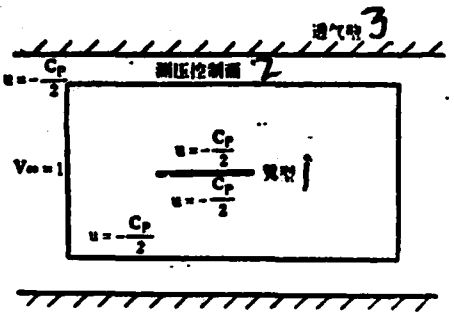

Fig. 1 Boundary Conditions for Calculations of Flow Fields Inside Wind Tunnels 1. Airfoil 2. Side Pressure Control Surface 3. Gas Permeable Wall

As Fig. 1 shows, when calculating flow fields inside wind tunnels, it is possible to select the calculated domain to be the rectangular area shown in the Fig. The boundary conditions of the wing surface are taken directly from wing surface pressure distributions measured by experiment, that is,

$$\frac{u}{V_\infty} = -\frac{C_p}{2} \tag{4}$$

We select the exterior boundaries of pressure measurement control surfaces close to the top and bottom walls of the wind tunnels. We still use the experimentally measured pressure distributions to be the boundary conditions. If, during wind tunnel experiments, static pressure holes are opened to measure pressure on the side walls of the upper and lower flows of the test section, then, the boundary conditions for the upper and lower flows can be directly taken as experimental pressure distributions. If wind tunnel structure is a

limiting factor, and there is no way to make experimental measurements of the pressure distribution on the boundaries of the upper and lower flows, then, the boundary conditions for the upper and lower flows of the wind tunnels can be approximated by making use of the already known conditions at the four corner points of the area of calculation to combine them into a multi-term expression and obtain the required values [9]. In this way, the boundary conditions for all the calculations of flow fields inside wind tunnels are Dirichlet boundary conditions.

2. Boundary Conditions for Calculations of Free Flow Fields

As is shown in Fig. 2, wing surface boundary conditions for the calculation of free flow flow fields are taken from experimental pressure distributions or already given pressure distributions. /161

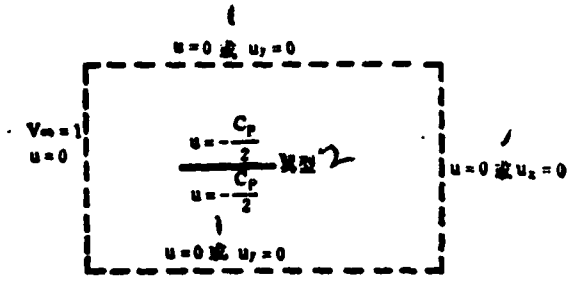

Fig. 2 Boundary Conditions from Calculations of Free Flow Flow Fields 1. Or 2. Airfoil

As far as the boundary conditions of distant fields are concerned, from the basic physical nature of the problem, it is possible to know that at an infinitely distant point $u \equiv 0$. If, during calculations, the distant field boundaries are selected sufficiently far from the model, it is possible to take the boundary conditions for an infinitely far point and make an adequate approximation of the boundary line [10]. During the calculations in this article, we selected the upper and lower flow distant field boundaries at a distance 10-15 times the chord length of the model. When considering the special point from which transonic horizontal disturbances propagate, the upper and lower areas should be even farther from the airfoil at approximately 20-25 times the chord length.

IV. Mixed Difference Forms

This article makes use of non-equidistant difference forms. The second order derivative in the y direction makes use of the central difference

$$u_{yy\,i,j}=2\,\frac{\Delta y_{j-1}u_{i,j+1}-(\Delta y_{j-1}+\Delta y_j)\,u_{i,j}+\Delta y_j u_{i,j-1}}{\Delta y_{j-1}\,\Delta y_j\,(\Delta y_{j-1}+\Delta y_j)} \tag{5}$$

The derivative in the x direction must depend on the velocity **discriminant** for that point

$$1-M^2=1-M_\infty^2-\frac{\gamma+1}{V_\infty}M_\infty^2 u \tag{6}$$

to determine its form.

When $(1-M^2)>0$, u_x and u_{xx} select for use the central difference

$$u_{x\,i,j}=\frac{u_{i+1,j}-u_{i-1,j}}{\Delta x_{i-1}+\Delta x_i} \tag{7}$$

$$u_{xx\,i,j}=2\,\frac{\Delta x_{i-1}u_{i+1,j}-(\Delta x_{i-1}+\Delta x_i)u_{i,j}+\Delta x_i u_{i-1,j}}{\Delta x_{i-1}\,\Delta x_i(\Delta x_{i-1}+\Delta x_i)} \tag{8}$$

When $(1-M^2)<0$, u_x and u_{xx} adopts for use the difference on one side of the upper flow

$$u_{x\,i,j}=\frac{u_{i,j}-u_{i-1,j}}{\Delta x_{i-2}+\Delta x_{i-1}} \tag{9}$$

$$u_{xx\,i,j}=2\,\frac{\Delta x_{i-2}u_{i,j}-(\Delta x_{i-2}+\Delta x_{i-1})u_{i-1,j}+\Delta x_{i-1}u_{i-2,j}}{\Delta x_{i-2}\,\Delta x_{i-1}(\Delta x_{i-2}+\Delta x_{i-1})} \tag{10}$$

When $(1-M^2)=0$, , the equation degenerates. However, the u_x term still adopts for use the central difference form (7).

This article, in its treatment of shock wave points, selects for use a "shock wave capturing method." According to a special characteristic of the pressure equation velocity discriminant (6), when $(1-M^2)_{i,j}<0$ and $(1-M^2)_{i,j}>0$, a shock wave step develops between two points. Choosing the points (i, j) as shock wave points, reference [9] carried out numerical value tests of three types of forms. It was discovered that taking shock wave points and comparing them to entering subsonic velocity points is appropriate.

V. The Linear Relaxation Iterative Substitution Solution Method /162

In turn, at the point (i, j), according to the form of the equation for that point, we select differing difference forms and substitute in equation (2). At the same time, we take the boundary conditions and insert them into the difference equations. Because of this, it is possible to obtain a set of high order non-linear algebraic equations relating to u. This article uses a linear relaxation iterative substitution method of solution, choosing the line of relaxation along the y direction.

According to the numerical value tests carried out in reference [9], if it is desired to make the calculations for subsonic and supersonic flow movements all converge, then, the term u_x^2 must be used in the calculation of the earlier field, that is,

$$u_{x\,i,j}^2=\begin{cases}\left(\dfrac{u_{i,j}^{(k+1)}-u_{i-1,j}^{(k+1)}}{\Delta x_{i-1}+\Delta x_i}\right)^2 & (1-M^2)_{i,j}\geqslant 0\\ \left(\dfrac{u_{i,j}^{(k+1)}-u_{i-1,j}^{(k+1)}}{\Delta x_{i-1}+\Delta x_{i-1}}\right)^2 & (1-M^2)_{i,j}<0\end{cases} \tag{11}$$

If we use the newest values in the calculations, it will lead to divergence in the calculation of supercritical flow movements.

This article makes use of the previous field value to calculate velocity discriminants [6]. The parameter for the term adopts the use of earlier field values in calculations. The remainder all make use of the newest values in calculations. After rearrangement, one finally obtains a one by three diagonal matrix

$$a_i u_{i,j-1} + b_i u_{i,j} + c_i u_{i,j+1} = d_i \qquad (12)$$

Equation (12) uses a "pursuit" type of method for its solution. Each time calculations are done, they begin by choosing a zero initial flow field. In order to speed up convergence as well as improving the stability of convergence, this article makes use of relaxation calculations. The selection of relaxation factors, on the basis of the calculation experience in reference [9], can make use of superrelaxation in the case of purely subsonic critical flow movements. As far as supercritical flow movements are concerned, the use of superrelaxation makes it easy to cause divergence in calculations. The adoption of a low relaxation is relatively more appropriate. When $M_\infty \geq 0.9$ one should adopt super low relaxation factors (for example, $\omega_1 = \omega_2 = 0.3$). Only then is one able to guarantee stable convergence in numerical value solutions.

VI. Calculation Tests

In order to test the feasibility of the methods discussed above, this article used a velocity potential method sample calculation to carry out comparative calculations with reference [5] and reference [6]. Table 3 shows the calculated results of pressure distribution in this article and in reference [5] for the point on an airfoil $y/c = 0.11$

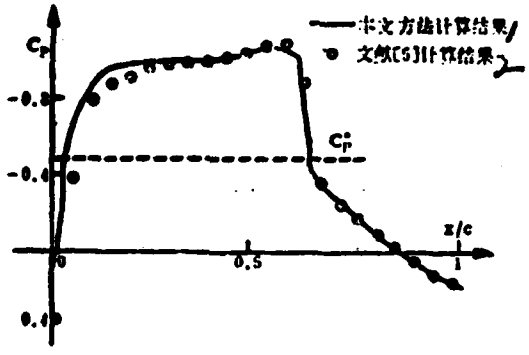

Fig. 3 Pressure Distribution for the Point $y/c=0.11$ on the Airfoil ($M_\infty=0.784, \alpha=2°56'$) 1. Calculated Results With This Article's Metod 2. Calculated Results from Raference [5]

/163

The airfoil is a supercritical airfoil, $M_\infty=0.784, \alpha=2°56'$. In the Fig., the results for this article are obtained by solving small perturbation velocity potential equations on the basis of interior and exterior boundary conditions from test pressure distributions.

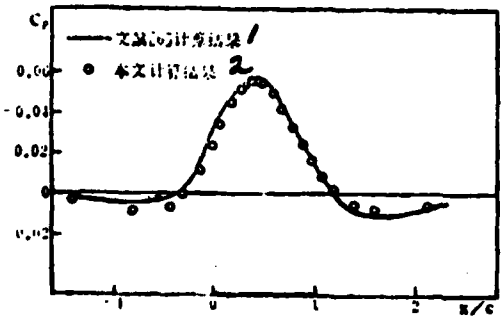

Fig. 4 Calculated Free Flow Pressure Distribution At Point $y/c=1.05$ ($M_\infty=0.72, \alpha=0$) 1. Results Calculated in Reference [6] 2. Results Calculated in This Article

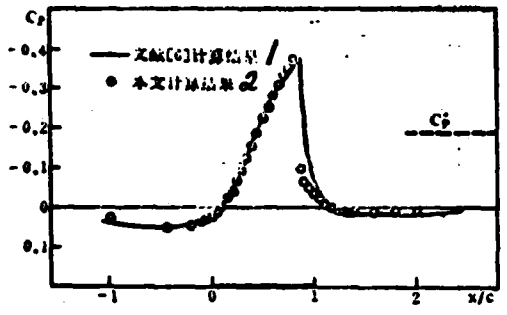

Fig. 5 Calculated Free Flow Pressure Distributions At Point $y/c=1.05$
1. Calculated Results from Reference [6] 2 Calculated Results from This Article ($M_\infty=0.9, \alpha=0°$)

Fig. 4 and Fig. 5 present the curves comparing the calculated results at the point $y/c=1.05$ for the pressure distribution of free flow flow fields, obtained with the wing surface pressure distribution as inner and outer boundary conditions using the NACA 0012 airfoil in reference [6], $\alpha=0°$, $M_\infty=0.72$ and 0.9 . From Fig. 3-5 it is possible to see that the results calculated in this article and in [5] and [6] agree relatively well. This, therefore, demonstrates that the convergence solution achieved with the method in this article is reliable.

In order to check out a step further the convergence speed of the calculation method in this article, this article ran a comparison of the convergence speeds of the mixed difference method for solving pressure equations [9] and for solving velocity potential equations for large disturbances in the x direction [6]. Due to the fact the factors actually influencing iterative substitution convergence speed are very numerous-including such factors as the grid, the initial field, the accuracy of convergence, and the actual boundary conditions-it is only possible to carry out a rough comparison of the two. The results of this are shown in Table 1.

项目 / 方法 (3) (2)	M_∞	网格 (6)	$\varepsilon = Max\lvert\Delta u^{(n)}\rvert$ 或 $\varepsilon = Max\lvert\frac{\Delta\phi^{(n)}}{\Delta\phi^{(1)}}\rvert$	迭代次数 (7)	机时(s) (8) (西门子7760) (9)
求解压力方程[9] (4)	0.72	98×23	5×10^{-4}	352	540
	0.85		10^{-4}	139	196
	0.9		4×10^{-5}	200	280
求解 方向大扰动速势方程[6] (5)	0.72	39×23	10^{-4}	393	327
	0.85		10^{-4}	1162	799
	0.9		0.2×10^{-4}	887	620

Table 1 Comparison of Convergence Speeds in Numerical Value Solutions for Pressure Distribution Equations and Velocity Potential Equations (The Airfoil Used Is NACA 0012, $\alpha=0°$) 2. Item 3. Method 4. Solution of Pressure Equation [9] 5. Solution of Velocity Potential Equation [6] for Large Disturbances in the * Direction 6. Grid 7. Number of Iterative Substitutions 8. Time 9. Siemens

From the Table it is possible to see that, when the method in this article and the method in reference [6] are compared, the method in this article shows relatively faster iterative substitution convergence and uses relatively less time. /164

VII. Typical Sample Calculations for Aspects of Applications

When the author of this article did research on the problems of tunnel wall interference in transonic airfoil wind tunnels, he produced the concept of using a mixed difference method to directly solve equation (2). After awaiting numerical value tests of its stability and convergence characteristics, he then turned the tables and used it for calculations of tunnel wall interference and in the calculation of difficult problems involving solving for airfoil configurations for already known pressure distributions. Its basic principles and details can be seen in reference [9]. Typical sample calculations can be seen in Fig. 6-9.

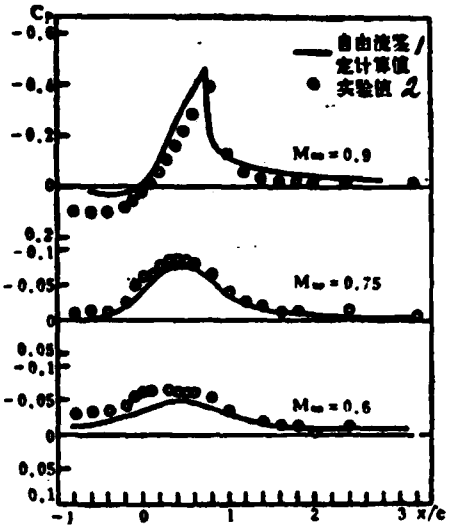

Fig. 6 Evaluation of Calculated Pressure Distributions on Control Surfaces $(y/c=1.05)$ NACA 0012, $\alpha=0°$, $\sigma=2\%$ 1. Free Flow Evaluation, Calculated Values 2. Test Values

Fig. 6 presents a comparison of the calculated pressure distribution and the empirical pressure distribution in an evaluation of free flow in this article. This comparison is made for a NACA 0012 airfoil in a situation where $M=0.6, 0.75, 0.9$; $\alpha=0°$, and the open-closed ratio $\sigma=2\%$. Because of this, it is possible to make a definite determination of the size and nature of the amount of tunnel wall interference. In the Fig., the distance from the control surface to the model is $y/c=1.05$.

Fig. 7-8 respectively show the pressure distribution when we use the circular arc given in [11] for $M=0.707$ and 0.817, $\alpha=0°$ followed by the results of a solving back for the geometrical configuration of the airfoil.

Fig. 9 shows the airfoil configurations designed from the pressure distributions which came out of this article for the NACA 0012 airfoil presented in [6], when $M=0.85$, $\alpha=0°$. From Fig. 7-9 one can see that the airfoil configurations calculated in this article match up quite well when compared with precisely determined airfoil configurations.

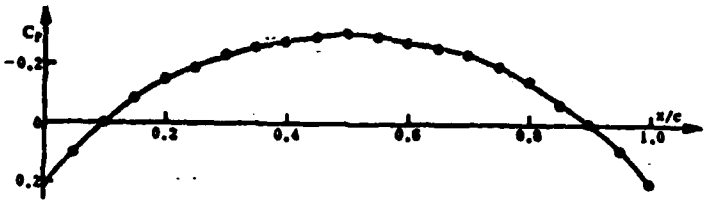

Fig. 7(a) Experimentally Determined Pressure Distribution on Airfoil Surface (11) ($M_\infty = 0.707$, $\alpha = 0°$)

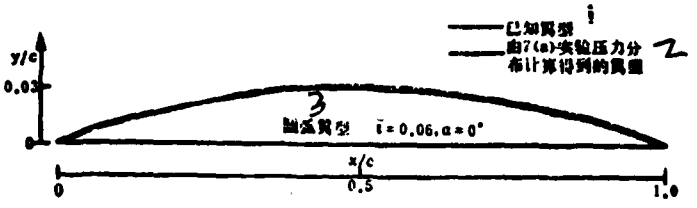

Fig. 7(b) Airfoil Configuration Calculated from Empirical Pressure Disribution 1. Already Known Airfoil 2. Airfoil Obtained from Calculations of the Experimentally Measured Pressure Distributions in 7(a) 3. Circular Arc Airfoil

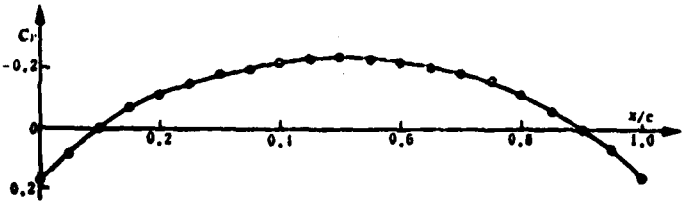

Fig. 8(a) Experimentally Determined Pressure Distribution on Airfoil Surface (11) ($M_\infty = 0.817$, $\alpha = 0°$)

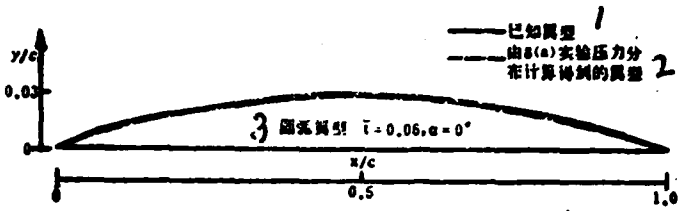

Fig. 8(b) Airfoil Configuration Calculated from Experimentally Determined Pressures 1. Already Known Airfoil 2. Airfoil Obtained by Calculations from the Experimentally Determined Pressure Distribution in 8(a) 3. Circular Arc Airfoil

VIII. Conclusion

The preliminary research which this article has done on numerical value calculation methods for transonic small disturbance pressure equations has already demonstrated that, on condition that an appropriate difference form is selected, as well as an appropriate iterative substitution method and relaxation parameter, the use of a mixed difference method to solve equation (2) produces convergence and that its convergence solutions are reliable.

While satisfying the assumed condition of small disturbances, this method handles tunnel wall interference problems with pressure distribution boundary conditions. The method in this article handles boundary conditions with ease, converges quickly, and has such advantages as saving machine time. Moreover, the solutions which are derived for flow field pressure distributions can also directly act as the basis for comparing definite tunnel wall disturbances, avoiding transformations, being both simple and direct. Besides this, the method in this article is used in designing airfoil configurations

from given pressure distributions. It has also obtained relatively satisfactory preliminary results.

Research into the calculation methods and applications of small disturbance pressure equations has still just begun. There are still a good many questions awaiting in-depth research and solution.

/166

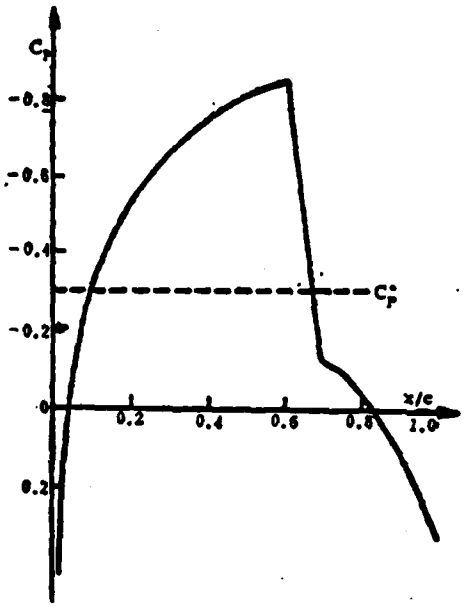

Fig. 9(a) NACA 0012 Airfoil Pressure Distribution (6) $M_\infty = 0.85$, $\alpha = 0°$

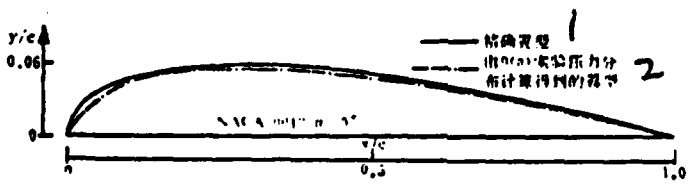

Fig. 9(b) Airfoil Configurations Calculated from Given Pressure Distribution 1. Exact Airfoil 2. Airfoil Obtained from Calculations of Experimentally Determined Pressure Distributions 9(a)

REFERENCES

[1] Kemp, W. B. Jr., AIAA 9th Aerodynamic Testing conference (1976), 31-38.
[2] Kemp, W. B. Jr., NASA CP 2045 (1978), 473-486.
[3] Mokry, M., Peake, D. J. and Bowker, A. J., NAE Aeronautical Rept. LR-575 (1974).
[4] Stahara, S. S., *AIAA J.* 18 (1980), 63-71.
[5] Kemp, W. B. Jr., NASA TM 81819 (1980).
[6] 刘学定，西工大硕士学位毕业论文 (1983)。
[7] 刘学定，罗时钧，空气动力学学报，3 (1984)，35—41。
[8] 罗时钧等，《跨音速定常势流的混合差分法》，北京，国防工业出版社 (1979)。
[9] 王利霞，西工大硕士学位毕业论文 (1984)。
[10] 罗时钧，西工大科技资料，SHJ 8029 (1980)。
[11] Knechtel, E. D., NASA TND-15 (1959).

[6] Liu Xueding; Northwestern Polytechnical University; M.S. Dissertation (1983)
[7] Liu Xueding; Luo Shijun; Acta Aerodynamica Sinica, 3, (1984), 35-41
[8] Luo Shijun, et.al.; "Transonic Steady State Potential Flow Mixed Difference Method" ,Beijing, National Defense and Industry Publishing House, (1979)
[9] Wang Lixia; Northwestern Polytechnical University, M.S. Thesis, (1984)
[10] Luo Shijun; Northwestern Polytechnical University Scientific and Technical Materials, SHJ 8029 (1980)

NUMERICAL SOLUTION OF TRANSONIC SMALL DISTURBANCE PRESSURE EQUATION USI NG A MIXED DIFFERENCE NETHOD

Wang Lixia Luo Shijun

(Northwestern Polytechnical University)

Abstract

A transonic small disturbance pressure equation (i. e. TSDP equation)

$$\left(1-M_\infty^2-\frac{\gamma+1}{V_\infty}M_\infty^2 u\right)u_{xx}+u_{yy}-\frac{\gamma+1}{V_\infty}M_\infty^2 u_x^2=0$$

is proposed for computing transonic flow fields in wind tunnel or free streams.

The mixed difference method is used to calculating TSDP equation. Numerical experimentation indicates that the use of suitable difference schemes and relaxation technique yields converged solutions to TSDP equation. Comparisons show that TSDP solutions agree well with those of transonic small disturbance potential equation. Application of the procedure to assessing transonic wind tunnel interference and designing airfoil from the given pressure distribution are illustrated.

INCOMPRESSIBLE THEORY OF THE INTERACTION BETWEEN MOVING BODIES AND VORTICITY FIELD -THE GENERATION OF VORTICITY BY BODY SURFACES AND ITS DISSIPATION

/168

Wu Jiezhi

(Chinese Aeronautical Establishment)

SUMMARY Using the point of view of vortical dynamics, we have taken a new look at the mutual effects of moving bodies and fluids, and we have obtained an even deeper understanding of this classic, fundamental problem. This article does research on the effects of bodies on vorticity fields and gives a generalized theory of the production of vorticity on the surface of objects as well as for its dissipation in fluids. It also presents two types of vorticity sources on the surface of objects-the total and the local-and analyses the effects of each of the sources.

I. Introduction

One of the fundamental problems of fluid dynamics is the mutual effects of moving bodies and fluids. This includes both the aspect of the effects of bodies on fluids and the aspect of the counter-reactions of fluids to bodies. The traditional route for handling this problem is through a Navier-Stokes equation analysis of the mutual relationships between the velocity field $\vec{v}$ and forces received by the surface of the objects. However, this process alone is not able to exhaust the knowledge relating to the mutual effects of fluids and moving bodies. In order to check out a new path, we looked at the considerations below.

The special point with fluids is that stress tensors are not directly related to either velocity fields or velocity gradient fields $\nabla\vec{v}$.

As is universally known, $\nabla\vec{v}$ can be uniquely analysed into a vorticity field $\vec{\omega}=\nabla\times\vec{v}$, , an expansion field $\theta=\nabla\cdot\vec{v}$, and a irrotational non-diffusion field. For real fluids, vorticity fields are restrained by the object surface viscosity conditions, and completely irrotational non-diffusion fields are almost non-existent. [1] [3] Because of this, the process of moving bodies affecting fluids is actually the process of objects producing vorticity fields and expansion fields. Conversely, the situation of forces being received by objects is also not the same velocity field itself. It is very closely related to the two derived fields of vorticity and expansion. Because of this, it is possible to predict that directly researching the mutual effects of these two derived fields and objects will enrich and deepen the knowledge we obtain through the use of the traditional method forming a second generation of theory on the mutual effects of fluids and bodies.

As far as non-compressible fluids are concerned, there is only a single vorticity field. The unique mechanism of bodies transfering energy to non-compressible fluids is none other than the production of vorticity through adhesion boundaries. Because of this, the reaction of fluids to bodies is also none other than the effects of the already produced vorticity on the bodies. The object of this research is, on the basis of this type of simple typical situation, to set up a general theory of the mutual interactions of vorticity fields and moving bodies.

This research is composed of two parts. These respectively consider the two sides of the mutual effects discussed above. Part I (the main text) sets up a general theory for the production of vorticity from any given movement over any given surface as well as for its dissipation in the fluid. The leader in this kind of research is Lighthill [3]. Recently, because of the fact that research concerning separation flows and vortical movements has been extensivly developed, he has also come in for renewed attention (Reference [4] in several reports from the 1985 AIAA Conference on Shear Flow Control.) This article develops the ideas of Lighthill into a finished form giving a scalar expression for vorticity sources. This enables us to make a comprehensive and systematic solution for the mechanism producing vorticity. These results have actually provided several new theoretical foundations for the processes controlling shear layers on the surface of objects and their separation. /169

II. A General Formula for the Strength of Vorticity Sources

When the forces penetrating the bodies are strong, we take the vortical dynamics equation for compressible fluids and integrate the fluid volume V_1. Moreover, we set up, except for the object surface ∂B_1, $\vec{\omega}=0$, on the fluid boundary. It is possible to demonstrate that

$$\frac{d}{dt}\int_{V_1}\vec{\omega}\,dV=-\nu\oint_{\partial B_1}\vec{n}\cdot\nabla\vec{\omega}\,dV \qquad (1)$$

$\vec{n}$ is normal to the outside of the surface of the object. Because of this, ∂B is a unique vorticity source. Moreover,

$$\vec{\sigma} = -\nu \vec{n} \cdot \nabla \vec{\omega}$$

is the amount of vorticity produced in a unit time for a unit surface; that is, the vorticity source strength as first introduced by Lighthill [3]. In the case of a two dimensional flat plate with movement of uniform speed, through a simple proof, reference [3] actually gives us:

$$\vec{\sigma} = -\frac{1}{\rho} \vec{n} \times \nabla p \quad \text{on } \partial B \tag{2}$$

Now, we generalize these results to the effects of any given movement on any given curved surface and derive a general formula pulling together the mutual relationships between $\vec{\sigma}$, p and the surface friction $\vec{\tau}$. We often need normal gradients and tangential gradients. In order to provide these, it is best to introduce the dynamic coordinate framework (5), which is often used on the curv in differential geometry. The vector radius for any point on S from the fixed origin point can be written as $\vec{r}(\xi^1, \xi^2), \xi^\alpha (\alpha = 1, 2)$ and is a parameter. Moreover,

$$\vec{r}_\alpha = \frac{\partial \vec{r}}{\partial \xi^\alpha} \qquad (\vec{r}_1 \times \vec{r}_2 \neq 0)$$

that is, the two basic stress vectors for S the point in question on the tangential plane π. It is also possible, from $\vec{r}^\beta \cdot \vec{r}_\alpha = \delta^\beta_\alpha$ to introduce the basic contravariant vector $\vec{r}^\alpha$ as well as the measuring tensor $g_{\alpha\beta} = \vec{r}_\alpha \cdot \vec{r}_\beta$, or $g^{\alpha\beta} = \vec{r}^\alpha \cdot \vec{r}^\beta$. Let the determinant of $g_{\alpha\beta}$ be the unit normal vector of g_α, the unit normal vector $\vec{n}$ of S is then

$$\vec{n} = \frac{1}{\sqrt{g}} (\vec{r}_1 \times \vec{r}_2) = \sqrt{g} (\vec{r}^1 \times \vec{r}^2)$$

Fig. 1

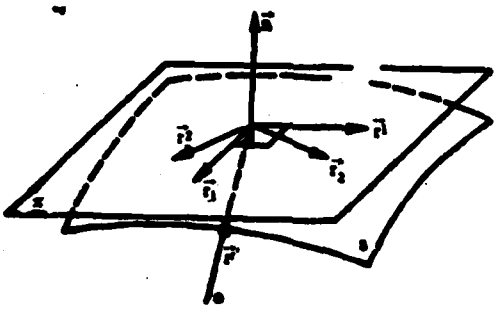

Therefore, $\{\vec{r}_i\}=(\vec{r}_1, \vec{r}_2, \vec{n})$ and $\{\vec{r}^i\}=(\vec{r}^1, \vec{r}^2, \vec{n})$ respectively form the three dimensional stress and contravariant right hand dynamic coordinate frame $(i=1, 2, 3)$, on S as is shown in Fig. 1. It is obvious that the determinant of the corresponding three dimensional measurement tensor $g_{ij}(i, j=1,2,3)$ is still g. If we set up s as the variable along $\vec{n}$, then, it is obvious that the normal derivatives of $\vec{r}_\alpha$ and $\vec{n}$ are $\vec{r}_{\alpha,3}=0$, $\vec{n}_{,3}=0$.

Their tangential derivatives from Gauss formulas and Weingarten formulas are

$$\begin{cases} \vec{r}_{\alpha,\beta}=\Gamma^{\lambda}_{\alpha\beta}\vec{r}_\lambda+b_{\alpha\beta}\vec{n}, & \vec{r}^{\alpha}_{,\beta}=-\Gamma^{\alpha}_{\beta\lambda}\vec{r}^{\lambda}+b^{\alpha}_{\beta}\vec{n} \\ \vec{n}_{,\beta}=-b^{\alpha}_{\beta}\vec{r}_\alpha=-b_{\alpha\beta}\vec{r}^{\alpha} \end{cases} \tag{3}$$

In these results, $\Gamma^{\lambda}_{\alpha\beta}=\Gamma^{\lambda}_{\beta\alpha}$ and is the two dimensional second type Christofell symbol on S. $b_{\alpha\beta}=b_{\beta\alpha}=-\vec{r}_{\alpha,\beta}\cdot\nabla\vec{n}\cdot\vec{r}_\beta$ is the S second basic equation parameter. Here and below, we see repeated examples of the customary practices of differential geometry such as taking basic vectors and writing them into calculation formulas. We will frequently take a certain vector $\vec{f}$ and operation ∇ and resolve them into vector projections in the normal direction on the tangent plane π. At this time, we write /170

$$\vec{f}=\vec{f}_\alpha+\vec{f}_n, \quad \vec{f}_\alpha=f^\alpha\vec{r}_\alpha, \quad \vec{f}_n=\vec{n}f_n=\vec{n}f^n$$
$$\nabla(\cdot)=\nabla_\alpha(\cdot)+\vec{n}(\cdot)_{,3}=\vec{r}^{\alpha}(\cdot)_{,\alpha}+\vec{n}(\cdot)_{,3}$$

Besides this, let

$$E^{\alpha\beta}=\frac{1}{\sqrt{g}}\varepsilon^{\alpha\beta}, \quad E_{\alpha\beta}=\sqrt{g}\,\varepsilon_{\alpha\beta}$$

This is a component of a third order totally skew matrix. Here, ε_{ijk} contains the familiar three index symbols. We then have

$$\vec{n} \times \vec{f} = E^{ijk} f_j \vec{r}_k ,$$

Through the use of this equation and (3), it is possible to verify the identity

$$\vec{n} \times (\vec{f} \cdot \nabla \vec{n} - \vec{f} \nabla \cdot \vec{n}) = -(\vec{n} \times \vec{f}) \cdot \nabla \vec{n} \qquad (4)$$

It is now possible to derive a general expression for $\vec{\sigma}$. First of all, solve for the normal gradient of $\vec{\omega}$ on any given curved surface S in the fluid. After that, change it to a form suitable for use on the surface of the object ∂B . Set the viscous stress on S to be $\vec{t}$. We have

$$\vec{t} = \mu(\Delta \tilde{\vec{v}} + \nabla \vec{v}) \cdot \vec{n} \qquad (5)$$

$\nabla \tilde{\vec{v}}$ is the transpositon of $\Delta \vec{v}$, and it is easy to prove that

$$\vec{t} = \mu(\vec{\omega} \times \vec{n} + \vec{A})$$

In this

$$\vec{A} = 2\nabla \vec{v} \cdot \vec{n} \qquad (6)$$

See reference [6] (According to reference [6] $\vec{A}$ is $2\tilde{\nabla}\vec{v} \cdot \vec{n}$. There seems to be an error.) After that, we note

$$\vec{B} = \mu \vec{\omega} \times \vec{n} = \vec{t} - \mu \vec{A} \qquad (7)$$

We have

$$\mu\vec{\omega}_{,}=\vec{n}\times\vec{B}=\vec{n}\times(\vec{i}-\mu\vec{A}) \quad (8)$$

Because of the fact that $\vec{n}_{,3}=0$, , we obtain

$$\mu\vec{\omega}_{,3}=\vec{n}\times\vec{B}_{,3}+\mu\vec{n}\,\omega^{3}_{,3}$$

In this, on the basis of $\nabla\cdot\vec{\omega}=0$, we have

$$\omega^{3}_{,3}=-\frac{1}{\sqrt{g}}(\sqrt{g}\,\omega^{\alpha})_{,\alpha}=-\nabla_{\alpha}\cdot\vec{\omega}_{\alpha} \quad (9)$$

Therefore, from (8), we obtain

$$\mu\vec{n}\,\omega^{3}_{,3}=\vec{n}[\vec{n}\cdot(\nabla\times\vec{B})]$$

Here, we make use of $\nabla_{\alpha}\times\vec{n}=-b_{\alpha\beta}\vec{r}^{\,\beta}\times\vec{r}^{\,\beta}=0$.

Due to the fact that the normal derivative of $\vec{B}$ breaks off during the period when it penetrates ∂B , it is necessary to make some additional changes to $\vec{n}\times\vec{B}_{,3}$. From (8) we have

$$\mu\nabla\times\vec{\omega}_{\alpha}=\vec{B}\cdot\nabla\vec{n}-\vec{B}_{,3}+\vec{n}\nabla\cdot\vec{B}-\vec{B}\nabla\cdot\vec{n}$$

Therefore, by the use of identity (4), it is possible to obtain /171

$$\vec{n}\times\vec{B}_{,3}=-\mu\vec{n}\times(\nabla\times\vec{\omega})+\mu\vec{n}\times(\nabla\times\vec{\omega}_{,3})-(\vec{n}\times\vec{B})\cdot\nabla\vec{n}$$

In this, it is possible to show that

$$\vec{n}\times(\nabla\times\vec{\omega}_{,3})=\nabla_{\alpha}\omega_{,}$$

Besides this, the Navier-Stokes equation gives us

$$-\mu\vec{n}\times(\nabla\times\vec{\omega})=\vec{n}\times\left(\nabla p+\rho\frac{d\vec{v}}{dt}\right)$$

By combining the results above, we obtain $\mu\vec{\omega}$ for any given curve on S.

$$\mu\vec{\omega}_{,3}=\vec{n}\times\left(\nabla p+\rho\frac{d\vec{v}}{dt}\right)-(\vec{n}\times\vec{B})\cdot\nabla\vec{n}+\vec{n}[\vec{n}\cdot(\nabla\times\vec{B})]+\mu\nabla_{,}\omega, \qquad (10)$$

Here, we have already avoided any interruptions in normal gradients on ∂B.

Now, we take S to be the object surface ∂B_0. On it, the velocity at any point is

$$\vec{v}=\vec{U}(t)+\vec{\Omega}(t)\times\vec{r}' \qquad (11)$$

$\vec{U}$ is the translation. $\vec{\Omega}$ is angular velocity. These are only functions of t. $\vec{r}'=\vec{r}-\vec{r}_0$ is the vector radius which corresponds to the instantaneous center of rotation. $\vec{r}_0$ is the vector radius for that instantaneous center in a fixed coordinate system. Because of the fact that $\vec{r}_0=\vec{r}_0(t)$, $\vec{r}'_0=\vec{r}_{00}$. On the basis of adhesion conditions, (11) is nothing other than the fluid point ∂B mass velocity. If we take (11) and substitute it in (6), we obtain

$$\vec{A}=2\vec{r}'\cdot[\vec{\Omega}\cdot(\vec{r}_0\times\vec{n})] \quad \text{on} \quad \partial B$$

Therefore, $\vec{A}=\vec{A}_0$, and, it is possible to obtain

$$\vec{n}\times\vec{A}=-2\vec{\Omega}_0 \qquad (12a)$$

This also gives

$$\vec{A}=\vec{n}\times(\vec{A}\times\vec{n})=2\vec{n}\times\vec{\Omega}_0 \qquad (12b)$$

Therefore

$$\nabla\times\vec{A}=2(\vec{\Omega}_0\cdot\nabla\vec{n}-\vec{\Omega}_0\nabla\cdot\vec{n}),\ \vec{n}\cdot(\nabla\times\vec{A})=0$$

In another respect, we have

$$\nabla_s \omega_1 = 2\nabla_s(\vec{\Omega}\cdot\vec{n}) = -2b_{ss}\Omega' \vec{\tau}^s = 2\vec{\Omega}_s \cdot \nabla\vec{n}$$

In this way, if we take (7) and substitute it into the right side of (10), it is possible to discover that the term $\vec{A}$ along with $\mu\nabla_s\omega_1$ disappear together. Therefore, if we take $\vec{r}$ on the surface of the object and write it as $\vec{r}_s$, we obtain a general expression for $\vec{\sigma}$

$$\vec{\sigma} = \frac{1}{\rho}\{-\vec{n}\times\nabla p + (\vec{n}\times\vec{\tau})\cdot\nabla\vec{n} - \vec{n}[\vec{n}\cdot(\nabla\times\vec{\tau})]\} - \vec{n}\times\frac{d\vec{v}}{dt} \tag{13}$$

In this, $d\vec{v}/dt$ is easy to obtain from (11).

Particularly in the case of two dimensional flows, we have

$$\vec{\sigma} = -\vec{n}\times\left(\frac{1}{\rho}\nabla p + \frac{d\vec{v}}{dt}\right) \tag{14}$$

Reference [4] has already used (14) to discuss the mechanism for the production of vorticity in two dimensional smooth flow on flat plates for different acceleration movements. Reference [7] makes use of (14) and a simplified point vortex system model to make a generalized discussion concerning non-steady state separation in two dimensional uniform flows. It also makes definitive solutions for a series of experimental results concerning non-steady state shear layer control.

In another regard, when $\mu\to 0$, due to the fact that $\vec{\tau}\to 0$, even in the case of three dimensional flow, we still have equation (14). Lighthill [3] has already pointed out that, at this time, it is not $\vec{\sigma}\to 0$, but, it is $|\vec{\omega}_n|\to\infty$, ∂B. The vorticity is concentrated in the unbounded thin layer and is not dispersed toward the interior of the fluid. Here, one should remember that the right side of (14) comes from the viscosity term of the NS equation and adhesion conditions. Reference [4] only determines, on the basis of the surface form for (14), that the source of $\vec{\sigma}$ is non-viscous. This thesis is not sound. /172

The derivation of (13) is used in movement equations and viscosity conditons. It is also unobtrusively used in the continuity equation $\nabla\cdot\vec{v}=0$. Due to the fact that the distribution of $p,\vec{\tau}$ on ∂B is not known, (12) is not the formula for calculating $\vec{\sigma}$, but is the expression which relates the distributions of $\vec{\sigma}$ and $p,\vec{\tau}$ as well as accelerations on the surface of the object. Attention should be paid to the assumption that $\vec{n}$ can be differentiated. Because of this, it is required that the surface of the object be everywhere smooth.

III. The Mechanism Producing Vorticity on the Surface of Objects

From (13) one can clearly see that, on the surface of objects, there are two types of vorticity sources:

(I) Stress Sources

These types of sources exist for any movement on any curved surface. For certain types of classical body forms, they have special characteristics which can also be called local sources. These are also composed of three parts.

1. Tangential Source $\vec{\sigma}_{,,}=-(1/\rho)\,\vec{n}\times\nabla p$

This type of source has already been discussed in references [3], [4], and [7]. Just as is pointed out in [7], if it is possible to ignore the pressure gradient which is caused by boundary layer displacment thickness on flat plates by semi-limitless smooth flows of uniform velocity, then, it is only in the vicinity of the forward edge stationary point that $\vec{\sigma}_{,,}\neq 0$.

2. Tangential Source $\vec{\sigma}_{,,}=(1/\rho)(\vec{n}\times\tau)\cdot\nabla\vec{n}$

This is an effect of object surface curvature and the three dimensional coupling of $\vec{\tau}$. From (5) and (12b), it is also possible to write this as

$$\vec{\sigma}_{,,}=\nu(\vec{\omega}_{,}-2\vec{\Omega}_{,})\cdot\nabla\vec{n} \tag{15}$$

Because of this, except for rotation of the body, at the point $\vec{\omega}\cdot\nabla\vec{n}\neq 0$, the $\vec{\omega}$ which the object surface already has will bring about the uninterrupted production of new vorticity in fluids. On sharp edges where $\nabla\vec{n}$ is extremely large, $\vec{\sigma}_{n}$ is very important. At such points, $\vec{\sigma}_{n}$ is also very large. These two together determine the form of free vortical layers on sharp edges. Discussion below points out that σ_{n} determines the effects of friction forces on the object surface as a whole.

3. Normal Source $\vec{\sigma}_{n}=\vec{n}\,\sigma_{n}=-(\vec{n}/\rho)[\vec{n}\cdot(\nabla\times\vec{\tau})]$

From (9), it is also possible to write this as

$$\vec{\sigma}_{n}=\nu\nabla_{n}\cdot\vec{\omega}_{n} \tag{16}$$

Because of this, σ_{n} appears in rotational areas of the two dimensional vector field $\vec{\tau}$ on the object surface or in areas of dissipation in the $\vec{\omega}_{n}$ field. For example, various areas on the rotating object. In the case of non-rotating objects, the discussion below applies.

(II) Acceleration Sources

When objects make non-inertial movements, on the one hand, it will influence the $p,\vec{\tau}$ distribution and alter the stress source. (15) presents an example of this. On the other hand, it also produces the tangential source $-\vec{n}\times d\vec{v}/dt$, which depends only on movements as affected by surface geometry. This is recorded as $\vec{\sigma}_{a}$. From (11) we have

$$\vec{\sigma}_{a}=-\vec{n}\times\{\dot{\vec{U}}+\dot{\vec{\Omega}}\times\vec{r}'+\vec{\Omega}\times\vec{U}'+\vec{\Omega}\times(\vec{\Omega}\times\vec{r}')\} \tag{17}$$

In two dimensions

$$\vec{\sigma}_{a}=-\vec{n}\times\dot{\vec{U}}-\dot{\vec{\Omega}}(\vec{n}\cdot\vec{r}')-\vec{\Omega}(\vec{n}\cdot\vec{U})+(\vec{n}\times\vec{r}')\Omega^{2} \tag{18}$$

The simplest example is simple translation acceleration movements [4]. Consider another type of example of the two dimensional oscillation of wing edges as shown in Fig. 2. Using (18) and the symbols in the Fig. it is easy to demonstrate that, on the top and bottom surfaces, one has

$$\vec{\sigma}_{AA} = \vec{e}_1 r\Omega^2, \vec{e}_1 = \vec{n} \times \vec{e}_{11}, r = |\vec{r}|$$

Note that this effect has no relationship to the direction of rotation. Moreover, on the trailing edge, (AB surface), one then has

$$\vec{\sigma}_{AA} = \vec{e}_1 c\dot{\Omega}$$

c is the chord length.

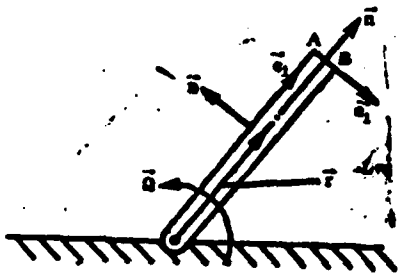

Fig. 2 Two Dimensional Oscillating Wing Edges or Flaps

It should be pointed out that surface vorticity $\vec{\omega}$ and vorticity sources are two different concepts. According to Taylor's development of this, $\vec{\sigma}$ only applies to vorticity in the interior of designated fluids. This is in agreement with equation (1). On the other hand, from (8) and (12b) we have

$$\vec{\omega} = \frac{1}{\mu} \vec{n} \times \vec{\tau} + 2\vec{\Omega} \quad (\text{on } \partial B) \tag{19a}$$

or

$$\vec{\tau} = \mu(\vec{\omega} - 2\vec{\Omega}) \times \vec{n} \tag{19b}$$

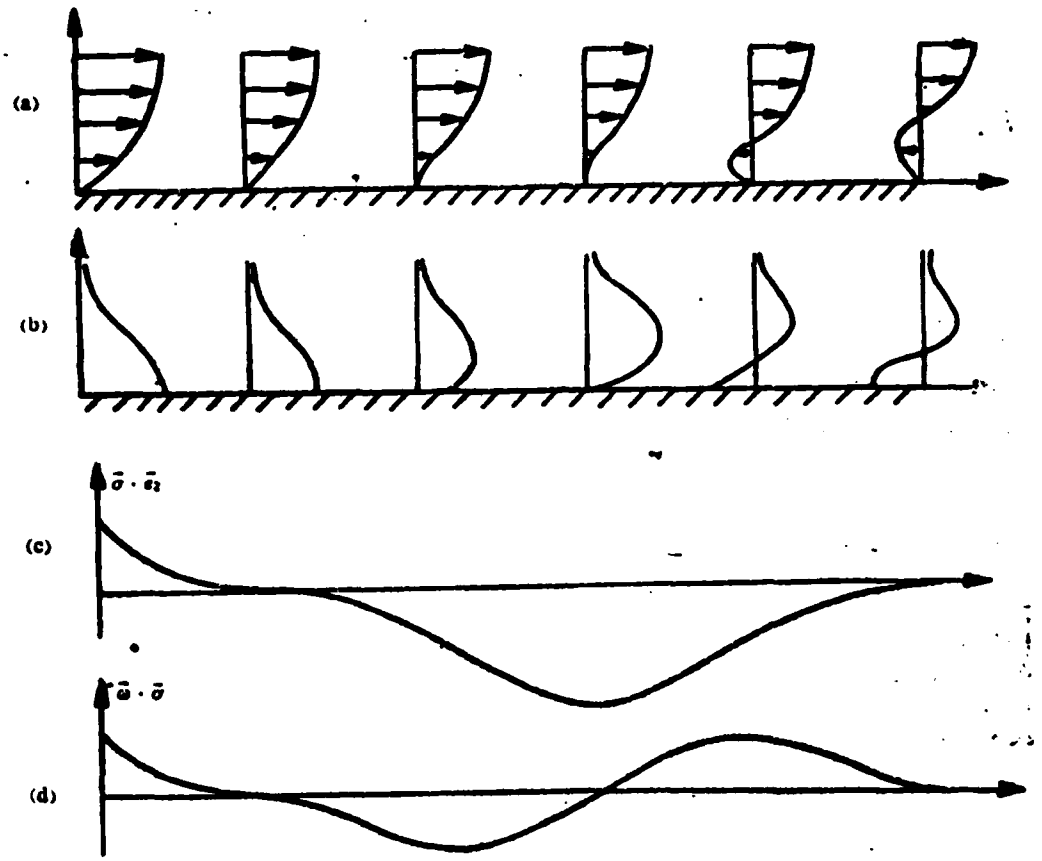

Fig. 3 Velocity Forms, Vorticity Forms, and Vorticity Sources (a) Velocity Forms (b) Vorticity Forms (c) Vector Vorticity Source Distribution (d) Scalar Vorticity Source Distribution /174

Because of this, object surface $\vec{\omega}$ is directly determined by $\dot{r}$ and $\dot{\Omega}$.

Moreover, it is not produced by $\vec{v}$. Particularly, in the case of the two dimensional encircling flows when $\vec{\Omega} = 0$, at times when the coordinate system is fixed to the surface of objects, one has

$$\vec{\omega} = \vec{n} \times \dot{v}_{\infty}$$

Moreover

$$\vec{\sigma} = \nu \vec{n} \times (\nabla \times \vec{\omega}) = -\nu \vec{n} \times \vec{v}_{,n}$$

Because of this, $\vec{\omega}$ and $\vec{\sigma}$ are respectively as shown by the velocity forms and the rates of slope and curvature on the surface of objects in Fig. 3.

If a body, beginning at instant t_0, begins to move in a fluid which was originally stationary, stress sources and acceleration sources will both begin to come into play. $\vec{\sigma}_{,n}$ in particular, during the process of initial movement, will start to exert an effect over the whole surface of the object. When the object transitions to movements of uniform speed at time t_1, one has $\vec{\sigma}_{,n} \equiv 0$ for $t \geq t_1$.

It is only the remaining local sources $\dot{\sigma}_{,n}, \dot{\sigma}_{,t}$ and σ, which continue, on portions of the object surface, to send vorticity toward the interior of the fluid. The amount which is sent is closely related to the $\vec{\omega}$ distribution on the surface involved. Because of this, global acceleration sources and localized stress sources have very different natures.

IV. Dissipation of Scalar Sources and Vorticity in Fluids

Fig. 3 shows that, when $\dot{\omega}$ and $\dot{\sigma}$ on the surface of the object are opposed to each other, the velocity form becomes concave. This foretells the coming of flow separation. Because of this, the relationship between the directions of $\vec{\omega}$ and $\vec{\sigma}$ are an important basis for the determination of separation. In order to do this, it is necessary to consider the scalar source $\dot{\omega} \cdot \dot{\sigma} = -(1/2)\nu \vec{n} \cdot \nabla \omega^2$. This quantity makes it possible for us to distinguish sources and confluences. If we consider the situation in which the acceleration form is convex, $(\vec{\omega} \cdot \dot{\sigma} > 0)$ is called a source. Then, exists a situation in which $\vec{\omega} \cdot \vec{\sigma} < 0$ is a confluence. Therefore, the appearance of confluences and separation are closely related.

Taking the situation in which $\vec{\Omega} = 0$ as an example, if we make use of (13), (17), and (19b), we obtain

$$\vec{\omega} \cdot \vec{\sigma} = -\frac{1}{\rho} \vec{v}_{\perp} \cdot \nabla p + \nu \vec{\omega} \cdot \nabla \vec{n} \cdot \vec{\omega} - \vec{v}_{\perp} \cdot \dot{\vec{v}} \qquad (20)$$

The contribution from normal sources disappears. If we let $\vec{r} > 0$, then, obviously, the back pressure gradient and the acceleration movement both produce vorticity confluences. In particular, from (3) we have

$$\vec{\omega} \cdot \nabla \vec{n} \cdot \vec{\omega} = -b_{\alpha\beta} \omega^{\alpha} \omega^{\beta}$$

The second basic rearrangement of this on a curved surface [5(number unclear)] is

$$\varphi_i = b_{\alpha\beta} d\xi^{\alpha} d\xi^{\beta}$$

To look at it another way, because of the fact that the symbols in $\vec{\omega} \cdot \nabla \vec{n} \cdot \vec{\omega}$ are only related to the geometrical form of the surface of the object, this has potential usefulness for controling flow separation.

$$\Omega(t) = \int_{V_t} \frac{1}{2} \omega^2 dV$$

In the same way that the vector source $\vec{\sigma}$ functions in (1), scalar sources influence the characteristics of integration operations. This integration is called enstrophy. The scalar quantity Ω here should not be confused with the angular velocity of solid body rotation vector $\vec{\Omega}$ previously introduced. If we integrate after taking the dot product of $\vec{\omega}$ and vorticity dynamics equations, we obtain [8]

$$\frac{d\Omega}{dt} = \int_{V_t} (\vec{\omega} \cdot \mathbf{D} \cdot \vec{\omega} - \nu \nabla \vec{\omega} : \nabla \vec{\omega}) \, dV - \nu \oint_{S_t} \frac{1}{2} \vec{n} \cdot \nabla \omega^2 \, dS \qquad (21)$$

In this, $\mathbf{D}$ is the rate of strain tensor. $'$ represents a second order contraction of the tensor. The last term in equation (21) is the overall scalar source. In equation (21), $\vec{\omega}\cdot\mathbf{D}\cdot\vec{\omega}$ stands for the enstrophy density transformation created because of pulls and bending forces on vortex tubes. When two dimensional, this is zero. Putting this in an orthogonal curved coordinate system (x_1, x_2, x_3) causes, for any $(\dot{x}, t), x_i$ $\dot{\omega}$ to be always along the direction. Then, $\vec{\omega}\cdot\mathbf{D}\cdot\vec{\omega} = \omega^2 D_{ii}$. Because of this, the existence of the mean value $\bar{D}_{ii}(t) \equiv (1/2)\, D(t)$ causes us to obtain /175

$$\int_{V_t} \vec{\omega}\cdot\mathbf{D}\cdot\vec{\omega}\, dV = D(t)\Omega(t)$$

In another regard,

$$\Phi \equiv \nu \int_{V_t} \nabla\vec{\omega}\cdot\nabla\vec{\omega}\, dV \geqslant 0$$

This is the attenuation of vorticity fields caused due to viscosity dissipation. Because of this, we write the overall scalar source as Σ, and solve (21) for the enstrophy energy operational formula

$$\Omega(t) = e^{D(t)}\left\{\Omega(0) + \int_0^t [\Sigma(\tau) - \Phi(\tau)]e^{-D(\tau)}\, d\tau\right\} \qquad (22)$$

For two dimensional flow, we simplify and get

$$\Omega(t) = \Omega(0) + \int_0^t [\Sigma(\tau) - \Phi(\tau)]\, d\tau \qquad (23)$$

It is obvious that, in (22), the functions of index factors and of Σ, Φ are different. Only the latter reflects the creation and disappearance of $\Omega(t)$. There is a popular point of view which recognizes that viscosity will not cause vorticity to disappear but will simply cause it to be redistributed. This is incorrect. In actuality, if, at a certain instant, the moving body is taken out, then, it is plain to see from (23) that Ω will ultimately attenuate

to zero. Therefore, $\vec{\omega} \equiv 0$.

V. Conclusions

(I) Vorticity in noncompressible fluids is produced by object surfaces through adhesion conditions. It is diffused by viscosity and dissipated by it.

(II) On the surface of moving objects, there are two different types of vorticity sources. One type is an overall or global acceleration source related to movements and object surface geometry. The other type is the localized stress source. This includes tangential sources created by pressure gradients, tangential sources from object surface curvature and vorticity coupling, as well as normal sources of rotation areas in $\vec{r}$ vector fields. The latter two types of localized sources only appear in three dimensional flows. These localized source areas are areas of energy supply from which energy is transfered to fluids by objects in uniform motion

(III) Except for vorticity and vector sources, it is possible to introduce scalar sources as the effects of area sources and confluences. The existence of vorticity confluences is the first sign of flow separation. The effect of three dimensional curved object surfaces on scalar sources is actually determined only by the characteristics of object surface geometry and has potential usefulness in the control of flow separation.

REFERENCES

[1] Supino, G., *Rend. Lincei* (8)6 (1949), 615.

[2] Truesdell, C., *The Kinematics of Vorticity*, Indiana Univ. Press (1951).

[3] Lighthill, M. J., *Laminar Boundary Layers*, ed. by Rosenhead, L., Oxford (1963).

[4] Morton, B. R., *Geophys. Astrophys. Fluid Dyn.* 28 (1984), 277.

[5] 吴大任, 《微分几何讲义》, 人民教育出版社, (1981).

[5] Wu Daren; "Lectures on Differential Geometry"; Peoples Education Publishing House, (1981)

INCOMPRESSIBLE THEORY OF THE INTERACTION BETWEEN MOVING BODIES AND VORTICITY FIELD ——THE GENERATION OF VORTICITY BY BODY SURFACES AND ITS DISSIPATION

Wu Jiezhi

(Chinese Aeronautical Establishment)

Abstract

The interaction between moving bodies and fluids, a classical problem of fluid dynamics, is reexamined from the viewpoint of vorticity dynamics. In this way, we may gain some new insight into the mechanism of the interaction and can be led to a series of results which are of practical value. The present paper studies the action of a moving surface to vorticity field and gives a general incompressible theory of the generation of vorticity at the surface and its dissipation in the fluid. It is found that there are two types of vorticity sources, the global one depends only on the acceleration property of the surface geometry, while the local one exists in both accelerated and uniform motion, consisting of tangential sources from pressure gradient and a three-dimensional effect of the surface curvature, and a normal source due to the divergence of the two-dimensional vorticity on the surface.

A STRONG INVISCID-VISCOUS INTERACTION SOLUTION OF A PLANE TRANSONIC CASCADE FLOW

177

Chen Yunwen Shen Mengyu
(Qinghua University)

Zhang Yaoke
(Computing Center, Academica Sinica)

I. Introduction

In order to design transonic turbine wheel machinery for both high efficiency and high loads, in aerodynamic calculations, it is necessary to deal with the calculation of the influence of viscosity. When gas movements on the surface of turbine blades do not produce separation, or when areas of separation are very small, gas movements in the flow way can be divided into turbine blade surface and trailing edge lower flow thin viscous layer-separation layers and wake areas as well as non-viscous flow areas other than these. Because of this, it is possible to distinguish the flow movements in these two types of areas which should be solved for by the use of Euler equation sets and those which should be solved for with boundary layer equation sets. The mutual influences of inviscid and viscous flows become apparent through a system of iterative substitution calculations of inviscid flows and boundary layers. By carrying out inviscid calculations from given aerodynamic parameters and blade cascade geometric configurations, we obtain a flow movement parameter distribution for turbine blades and wake surfaces. This acts as input data for the initial calculation of boundary layers and wakes to obtain the exclusion thickness δ^* for boundary layers and wakes. Moreover, we take this geometric boundary of inviscid flow and carry out adjustments so that it becomes the flow boundary for the next inviscid calculations. This type of iterative substitution is repeatedly carried out, and it continues straight on until the complete body convergence conditions for the whole field are satisfied, and then it stops. The flow chart for these iterative substitutions is as shown in Fig. 1.

In these calculations, we make use of a time advance integration method for finite areas to calculate inviscid flow fields [1]. We make use of an integration relationship equation to solve for laminar flow and turbulent flow boundary layers as well as wakes [2,3]. We make use of empirical relationships to precisely determine the turning

173

point position [4]. After all the calculations converge, on the basis of [5], we carry out calculations of the mixing of gas flows after the cascade. From this, we obtain the loss coefficient for the blade cascade. Below, we give a more detailed description of the carrying out of the matters mentioned above. Finally, we give two sample calculations for the flow movements in transonic turbine wheel flat plane blade cascades.

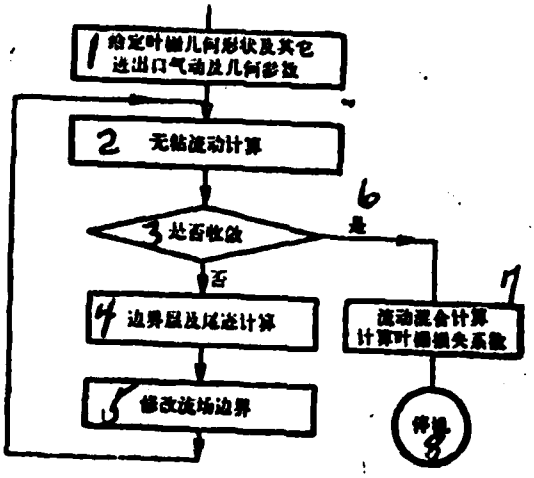

Fig. 1 1. Determining of the geometrical configuration of the blade cascade and other aerodynamic and geometrical parameters for intake and exhaust ports. 2. Inviscid flow calculations 3. Is there convergence or not? 4. Boundary layer and wake calculations 5. Alterations of flow field boundaries 6. Yes 7. Flow mixing calculations. Calculations of blade cascade loss coefficient 8. Machine stop

II. Inviscid Flow Calculations

If we assume constant specific heat in a perfect gas during adiabatic flow, we make use of a time advance method to solve for its steady state movements, and, at this time, the basic equation set for the planar movements can be taken to be:

$$\begin{cases} \dfrac{\partial \rho}{\partial t} + \dfrac{\partial \rho u}{\partial x} + \dfrac{\partial \rho v}{\partial y} = 0 & (2.1) \\ \dfrac{\partial \rho u}{\partial t} + \dfrac{\partial}{\partial x}(p + \rho u^2) + \dfrac{\partial}{\partial y}(\rho uv) = 0 & (2.2) \\ \dfrac{\partial \rho v}{\partial t} + \dfrac{\partial}{\partial x}(\rho uv) + \dfrac{\partial}{\partial y}(p + \rho v^2) = 0 & (2.3) \\ \dfrac{c_p}{R}\,\dfrac{p}{\rho} + \dfrac{1}{2}(u^2 + v^2) = H & (2.4) \end{cases}$$

Here, ρ, p are, respectively, the density and pressure of the gas; u, v are the velocity components of the gas along the x, y directions; c_p is the specific heat at fixed pressure. R is the gas constant. $H = c_p T$ is the overall heat content or enthalpy of the gas at the intake. As is shown in the Fig., ABCDEFGH is the area of calculation. $\overset{\frown}{GPF}$ and $\overset{\frown}{BSC}$ respectively the equivalent boundaries of the pressure surface and suction surface of the two phases shown near blades. The intake boundary AH and the exhaust boundary DE are parallel to the y axis. The parallelogram ABGH is the periodic flow field area in front of blades. The included angle between the straight lines AB and HG and the x axis are the intake flow angle β_1.

When making initial inviscid calculations, FE, CD are the directions along the estimated exhaust angle β_2. In later inviscid calculations, FE, CD are basically wake boundary lines solved for in initial wake calculations, and, in the process of calculations, continuously undergo adjustments.

In the x direction, it is possible to take equal distances (or unequal distances) and make contour lines roughly parallel to the y axis. In the flow path, it is possible to take equal distances (or unequal distances) and make lines giving a rough simulation of the flow. The points at which the contour lines or interval lines intersect with the flow simulation lines are, then, the grid points. The points of actual calculations are located between mutually adjacent grid points. This is represented in Fig. 3 with the symbol ·

We take the grid unit of two points between which there is a centrally located calculation point and form from it a unit of calculation. If we take the equations (2.1)-(2.3) after they have been made non-dimensional, and change the unit for these calculations to an integral form, it is possible to obtain: 179

$$\iint \frac{\partial \rho}{\partial t} dx\,dy + \oint (\rho u,\ \rho v)\cdot \hat{n}\, ds = 0 \qquad (2.5)$$

$$\iint \frac{\partial \rho u}{\partial t} dx\,dy + \oint (p+\rho u^{2},\ \rho uv)\cdot \hat{n}\, ds = 0 \qquad (2.6)$$

$$\iint \frac{\partial \rho v}{\partial t} dx\,dy + \oint (\rho uv,\ p+\rho v^{2})\cdot \hat{n}\, ds = 0 \qquad (2.7)$$

Here, $\hat{n}$ is an exterior normal line unit vector for the boundary of a calculation unit. According to Denton [6], the concept of setting

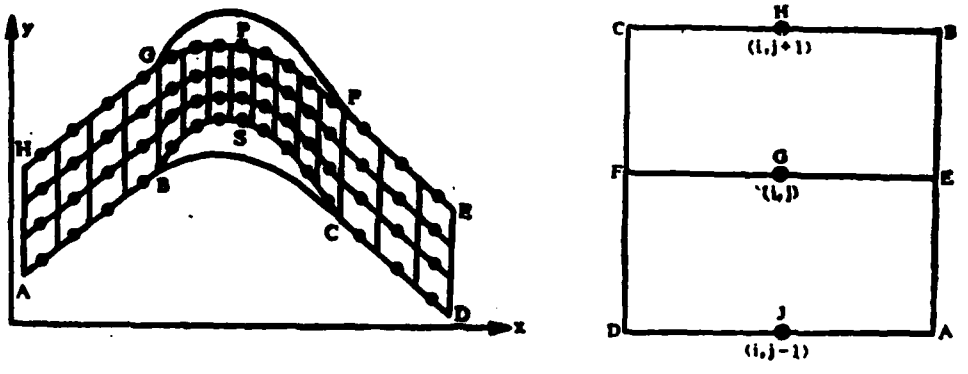

up a difference grid is that, carrying out a dispersion of (2.5)-(2.7), it is possible to obtain the apparent calculation form. From the flow parameters for the time increment n, it is possible to calculate the flow movement parameters for the time increment $n+1$. The form of its calculation expresses the equations refered to in [1] and [7].

The calculation boundary conditions are as shown below. The intake and exhaust boundaries AH and DE, when axial velocities are $0<u<c$ (c is the speed of sound), on AH , we are given p_*, T_* as well as the gas entry angle β_1. On DE , we are given the back pressure p_{2*} on blade surface $\widehat{BSC}$ as well the mutual intersection of the equivalent object surface boundaries and inviscid flow speeds on $\widehat{GPF}$.

On AB and HG , we select for use periodicity conditions for flow movements to act as conditions for determining solutions.

CD, FE

are wake boundary lines. Based on the exclusion functioning of wakes in inviscid flows (main flows) as well as the equivalence of gas static pressures along wake cross sections, it is, therefore, true during calculations, that, after each time increment, at corresponding points on CD and FE , the pressure takes its average value, in order to guarantee pressure equivalence at corresponding points. At the same time, on CD and FE , we eliminate the normal velocity component of gas flow in order to guarantee contact between flow movement velocities and wake boundaries. The positions of CD and FE are determined by moving the wake exclusion thickness on either side of the wake base line. When doing preliminary boundary layer calculations, we take the wake base line to be the flow line passing through the wake edge points. In the later iterative subsitution calculations, the curve passing through wake edge points and contacting the corresponding points on the two sides of the wake in the average direction of the gas flow is taken as the wake base line.

III. Boundary Layer and Wake Calculations

1. Laminar flow boundary layer calculatio ns.

We first select for use the Illingsworth-Stewartson transformation. We take the differential equation set for compressible laminar flow boundary layers on adiabatic object surfaces and transform them into the differential equation sets for non-compressible laminar flow boundary layers. After this, we make use of the single parameter Loitsianskii method to solve for its momentum integration relationships. Finally, through retransformation, one solves for and obtains the kinetic energy loss

thickness, the exclusion thickness, as well as the wall surface coefficient of friction (Refer to reference [2]) for compressible laminar flow boundary layers.

2. Determination of Turning Points

According to the nature of turning points, it is possible to divide them into natural turns and gas bubble turns. In these calculations, if gas bubble turns are produced, let us assume that the gas bubble length is zero. That is, let us recognize that laminar flow separation points are the starting points for turbulent flow boundary layers. If natural turnings are produced, we need make no assumptions about the length of the turning area. In the second situation, the boundary layer kinetic energy loss thickness after adopting the turning point does not change. The critical Reynolds number and boundary layer thickness ratios after turning points are gotten from empirical formulas [4].

3. Turbulent Flow Boundary Layer and Turbulent Flow Wake Calculations

In these calculations, we select for use the Lag-Entrainment integration relationship method of such people as Green [3] to calculate turbulent flow boundary layers and turbulent flow wakes. The Lag-Entrainment method of such people as Green, through the generalizations of such people as East [8], is used in the calculation of turbulent flow boundary layers in areas having small separations. At certain places before the separation points, the calculations turn toward an "inverse form", avoiding the appearance of a singularity in the original equation set at the separation point. At this time, the boundary layer exclusion thickness $\delta_1(x)$ is a given value. Moreover, the inviscid flow velocity $u_e(x)$ is a value awaiting determination. In the calculations, it is necessary to make (180)
continuous adjustments to the given $\delta_1(x)$, , causing the calculated values of $u_e(x)$ and $u_e(x)$ as obtained from inviscid flow calculations to coincide.

In the calculations, it appears that, in the case of certain transonic turbine blade cascades (such as sample calculation 1), the gases, while passing through the blades, receive an abrupt acceleration, leading, in the vicinity of the rear edge of the blades, to a change in flow parameters exceeding the appropriate ranges of the radial empirical formulas given by such people as Green. This makes it impossible to carry out the calculations. At this time, use is made of the Nash-McDonald method [9] which is introduced into the calculations after the reactions stop in order to carry them out. This overcomes the difficulties mentioned above.

IV. Iterative Substitution Calculations and Convergence Principles

1. First of all, we carry out time advance inviscid calculations for blade pathways of a given geometrical configuration. This leads directly to the convergence of the calculations, and the convergence principles are:

$$\text{(1)}\quad E_1=\max_{i,j}(|u^{n+1}_{i,j}-u^{n}_{i,j}|/\bar{V})<0.0002 \tag{4.1}$$

or

$$E_1=\frac{1}{N}\Sigma(|u^{n+1}_{i,j}-u^{n}_{i,j}|/\bar{V})<0.00005$$

Here

$$\bar{V}=\left[\frac{1}{N}\sum_{1}^{N}(u^2+v^2)^{n+1}_{i,j}\right]^{1/2}$$

N is the total number of calculation points. i, j represent the rank and file designations of the calculation points. The superscripts n and $n+1$ are the number of time increments.

2. From the results of inviscid calculations, one calculates the exclusion thicknesses of boundary layers and wakes Moreover, one carries out corrections of blades and wake boundaries. In order to improve the stability of calculations, one carries out, on boundary layer thicknesses, hyporelaxed iterative substitution:

$$\delta_i^{(n+1)} = \omega \delta_i^{(n+1)} + (1-\omega)\,\delta_i^{(n)}$$

ω is the relaxation parameter, $0<\omega<1$.

3. The results of the inviscid calculatiions above act as an initial calculation field. If one carries out a certain incremental inviscid calculation on the adjusted flow path, and one arrives at the overall iterative substitution convergence principles below, then the calculations stop. If not, then, the iterative substitution continues to progress.

The overall iterative substitution convergence principles are:

(1) The calculation errors between consecutive time increments in inviscid flow calculations are the same.-(4.1)

(2) The maximum error between two adjacent M number distributions on blade surfaces in inviscid calculations (also the input data for two adjacent boundary layer calculations) is

$$\mathrm{Max}_i |M_i^{(n+1)} - M_i^{(n)}| < 0.005$$

(3) The maximum difference value between the blade surface coordinate $y_{i,cal}$ in inviscid boundary calculations and the coordinates for the equivalent blade forms obtained in the same boundary layer calculation $y_{i,e}$ is

$$\mathrm{Max}_i |y_{i,cal} - y_{i,e}| / \text{cascade distance} < \varepsilon$$

The selection of the value of ε should be related to the precision which it is possible to achieve in the machining of blades. In the sample calculations, we select $\varepsilon = 0.0003$, which far exceeds the actual blade machining precision. 181

V. Calculations of Losses and Gas Exit Angles

After overall convergence of iterative substitution, according to the Stewart theory [5], other aerodynamic and geometrical parameters for the blade cascade as well as the boundary layer exclusion thickness for blade rear edge suction surfaces and pressure surfaces and their associated kinetic energy loss thickness are used to calculate blade cascade loss parameters and mixing effects of blade cascade lower flows as they impact on wakes and main flows. At the same time, on the basis of the direction of the wake base line after the convergence of the cal culations, it is possible to make precise determinations of numerical values for gas exit angles.

VI. Sample Calculations

Example one. This is a calculation of the middle section of a blade cascade in a 624 turbine. The principle aerodynamic parameters are as follows. Gas entry angle $\beta_1=50.4°$, . Overall entry presure $p_0=295987.3\ N/M^2$. Overall entry temperature $T_0=288\ K$, Back pressure $p_2=102730.3\ N/M^2$.

Example two. This is an RA turbine blade. Principle aerodynamic parameters are as follows. Gas entry angle $\beta_1=60°$, . Overall entry pressure $p_0=230300.3\ N/M^2$, . Overall entry temperature $T_0=288\ K$, . Back pressure $p_2=101292.8\ N/M^2$. .

The number of grid points for example caluclation number one and example calculation number two were respectively 41x11 and 71x11. After convergence of the inviscid calculations, we carried out boundary layer calculations and adjusted the inviscid calculation boundaries. After that, after inviscid calculations were carried out following each 50 time increments, one boundary layer calculation was carried out, and this continued right on until we arrived at overall convergence. Fig. 4 is the example calculation one blade surface non-dimensional pressure coefficient $\bar{p}=p/\rho^* a^{*2}$ -calculation results and experimental values (ρ^*, a^* are respectively the critical density and the critical sonic speed corresponding to entry gas flow parameters.) Fig. 5 is the M number distribution and experimental results for the sample calculation two blade surfaces. In this Fig., we also see presented the calculated results for inviscid flow.

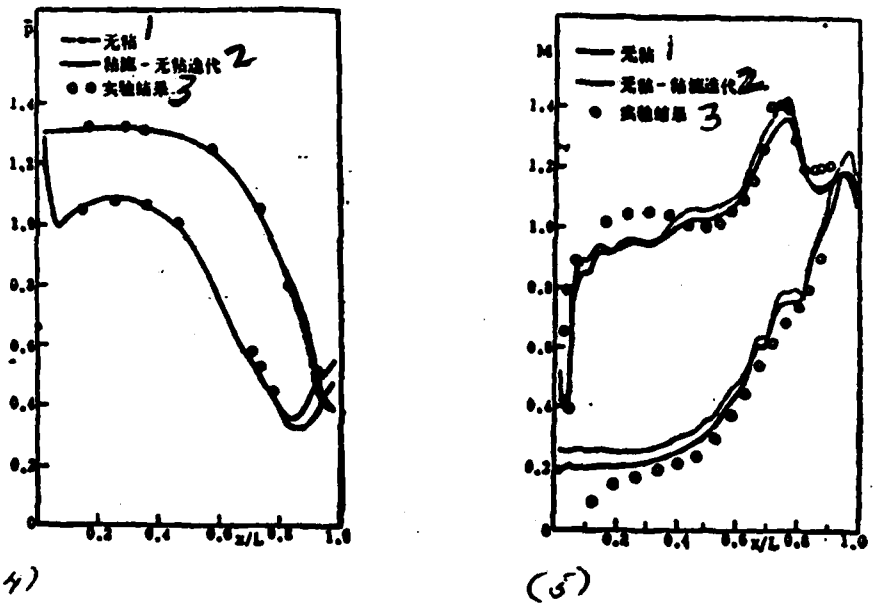

(4) (5)

Fig. 4 1. Inviscid 2. Viscous Flow-Inviscid Iterative Substitution 3. Experimental Results

Fig. 5 1. Inviscid 2. Viscous Flow-Inviscid Iterative Substitution 3. Experimental Results

The degree of correspondence between inviscid-viscous flow iterative substitution calculated results and experimental values is an obvious improvement over inviscid flow calculated results. Besides this, we also calculated the kinetic energy loss parameter. In the case of the 624 central blade cascade, its value was $\zeta = 0.04921$, . From the wake base line direction, we determined the gas exit angle to be $\beta_2 = -66.75°$, . These values are in relatively good agreement with the corresponding experimental values $\beta_2 = -67.4°$ (taken from [10]). In the case of the RA turbine blade cascade, the calculated example for ζ is 0.0248. . Because there are no experimental results, there is no way to make a comparison. 182

VII. Several Observations

1. Calculations demonstrate that the positions of wake boun-

daries and the specifying conditions for the wake boundaries have a very great effect on calculated results for blade surface aerodynamic parameters. We went through the process of carrying out test calculations on the 624 middle blade cascade for the two respective situations below. When the wake is fixed on the flow lines passing through the edge of the wake as obtained in initial inviscid calculations, as well as for the case where periodic boundary conditions are taken as the defining conditions for wake boundaries, the differences between blade surface pressure distributions and inviscid flow calculation results are extremely small.

2. Trailing edge thickness of blades has a very large influence on blade cascade loss coefficients. This is particularly true of blades which have relatively large trailing edge thicknesses. The error in loss parameters caused by errors in blade thicknesses will be much larger than the errors caused by calculation errors from boundary layer thicknesses. Because of this, when one carries out comparisons of calculated values and experimental results, it is necessary to carry out caluclations on the basis of the actual thicknesses of the experimental blade models used.

3. What this article describes is the initial results of our work. Looking from the standpoint of the calculation results in the preliminary work we have just done, and, using the inviscid-viscous flow iterative substitution method presented in this article, the degree of correspondence between the results obtained and experimental values is quite good. However, this work still waits for even more examples of calculations, including the carrying out of more sophisticated calculations and checks of flow movements on blades having small separation areas.

REFERENCES

[1] 张耀科，沈孟育，1985年全国科技应用软件学术会议报告。
[2] 张建迁，袁光华，陈允文，真实流体动力学(清华大学讲义)。
[3] Green, J. E., Weeks, D. J., Brooksman, J. W. F., A.R.C. R.& M. 3791 (1973).
[4] Singh, U. K., VKI Lecture Series 1980-8.
[5] Stewart, W. L., NACA TN 3515 (1955).
[6] Denton, J. D., A.R.C. R.& M. 3775 (1974).
[7] 张耀科，沈孟育，龚增锦，计算数学，4 (1978)。
[8] East, L. F., Smith, P. D., Merryman, P. J., R.A.E. T.R. 77046 (1977).
[9] 陈允文，中国工程热物理学报 5, 4 (1985)。
[10] 艾孝义，汽研027—80 (北京重型电机厂清河实验室实验报告)。

[1] Zhang Yaoke, Shen Mengyu; "1985 All China Conference Report on Software Techniques with Scientific and Technical Applications"
[2] Zhang Jieqian, Zhang Guanghua, Chen Yunwen; "Actual Fluid Dynamics" (Qinghua University Lecture)
[7] Zhang Yaoke, Shen Mengyu, Gong Zengjin; Computational Mathematics, 4 (1978)
[9] Chen Yunwen; China Engineering Thermal Physics Bulletin 5,4 (1985)
[10] Ai Xiaoyi; "Gas Research" 027-80 (Beijing Heavy Electric Generator Plant Qinghe Laboratory Experimental Bulletin)

A STRONG INVISCID-VISCOUS INTERACTION SOLUTION OF A PLANE TRANSONIC CASCADE FLOW

Chen Yunwen (*Qinghua University*) **Zhang Yaoke** (*Computing Center, Academia Sinica*) **Shen Mengyu** (*Qinghua University*)

Abstract

An inviscid-viscous interaction method has been developed to predict the blade-to-blade flow in plane turbine cascades. The interaction effect is taken into account by iteratively solving the inviscid and viscous flows. The inviscid flow is calculated by a finite area time-marching method. The viscous flow is calculated by the integral method, Loitsianskii's method for laminar boundary layer after performing Illingworth-Stewartson transformation and Green's lag-entrainment method for turbulent boundary layer and wake. A mixing calculation is carried out to determine the kinetic energy loss coefficient. The exit angle is determined by the base line of the wake predictions agree well with the test results for two transonic turbine cascades.

NUMERICAL CALCULATIONS OF INVISCID TRANSONIC FLOWS OVER WINGS

184

Chen Zuobin Yao Furu Zhang Yulun

(China Aerodynamic Research and Development Center)

SUMMARY This article introduces a type of numerical value method of calculation for non-viscous, steady state transonic flows around wings. It selects for use the full potential equation as mathematical model. Through the use of appropriate coordinate transformations, sweptback wings are changed to rectangular ones. Also, an unlimited physical domain is changed to a limited calculation domain. In the domain of calculations, use is made of the mixture-type limited difference form to discretize equations. The set of algebraic equations formed from difference equations is solved through linear relaxation iterative substitution. Successive refinements of the calculation grid make the calculations relatively economical.

I. Introduction

Wings are the aircraft's most important aerodynamic force components. The quality of their aerodynamic characteristics has an extremely great influence on the capabilities of the whole aircraft. Moreover, the development of research into the calculation of transonic flows around wings not only has significance for academic knowledge. It also has very great applied value.

The numerical value method presented in this article is the solution for transonic speed full potential equations in an orthogonal coordinate system. We first use shear transformations to change backswept wings into rectangular wings. After that, we use compression transformations to change an unlimited physical domain into a limited domain of calculation. In this way, on the one hand, we can make direct use of distant field boundary conditions and, on the other hand, it is also possible to get an automatic concentration of grid points in the vicinity of the wings and make a reasonable distribution of the grid points. The coordinates after the transformations are still orthogonal. The treatment of boundaries and relaxation scanning are directly observed. This article is a continuation and a development of the work in reference [1].

When the surfaces of objects satisfy precise boundary conditions, the actual method for handling them is similar to the wing surface boundary treatment in Carlson airfoil calculations [2]. In every cross section of wings, we take the perturbation speed potential analysis and expand it to the imaginary grid point simulation inside the wings in order to use it to set up difference equations for grid points close to the surface of objects. At points of subsonic speed, we select for use central difference forms. At points of supersonic speed, we select for use rotational difference forms as presented by Jameson [3]. This is done in order to guarantee that the difference forms will have accurate areas of dependence.

II. Basic Equations and Boundary Conditions

Under conditions where there are no strong shock waves and steady state, non-viscous compressible gas movements, it is possible to make an irrotational assumption, and satisfy the full potential equation:

$$(a^2-u^2)\varphi_{xx}+(a^2-v^2)\varphi_{yy}+(a^2-w^2)\varphi_{zz}-2uv\,\varphi_{xy}-2vw\,\varphi_{yz}-2uw\,\varphi_{xz}=0 \qquad (1)$$

In order to eliminate the singularity at an infinitely far point, we introduce the perturbation speed potential G

$$G=\varphi-x\cos\alpha-y\sin\alpha \qquad (2)$$

From velocity potential equation (1), it is possible to deduce that the perturbation speed potential G satisfies the equation below:

135

$$(a^2-u^2)G_{xx}+(a^2-v^2)G_{yy}+(a^2-w^2)G_{zz}-2uv\,G_{xy}-2uw\,G_{xz}-2vw\,G_{yz}=0 \qquad (3)$$

Velocity components are

$$\begin{cases} u=\varphi_x=\cos\alpha+G_x \\ v=\varphi_y=\sin\alpha+G_y \\ w=\varphi_z=G_z \end{cases} \tag{4}$$

The local speed of sound is

$$a^2=\frac{1}{M_\infty^2}+\frac{\gamma-1}{2}\left[1-(u^2+v^2+w^2)\right] \tag{5}$$

The pressure parameter C_p is

$$C_p=\frac{2}{\gamma M_\infty^2}\left\{\left[1+\frac{\gamma-1}{2}M_\infty^2(1-u^2-v^2-w^2)\right]^{\frac{\gamma}{\gamma-1}}-1\right\} \tag{6}$$

All the physical quantities in equations (1)-(6) are non-dimensionalized with the basic chord C_0 and the incoming flow velocity q_∞.

Object surface boundary conditons: velocity and object surfaces make mutual contact. Say that the upper and lower wing surface equations are

$$y=\begin{cases} y_\perp(x,z) & \text{upper surface} \\ y_\top(x,z) & \text{lower surface} \end{cases} \tag{7}$$

Then, the object surface boundary conditions can be represented as

$$\begin{cases} (\cos\alpha+G_x)\dfrac{\partial y^{\text{upper}}}{\partial x}-(\sin\alpha+G_y)+G_z\dfrac{\partial y^{\text{upper}}}{\partial z}=0 \\ (\cos\alpha+G_x)\dfrac{\partial y^{\text{lower}}}{\partial x}-(\sin\alpha+G_y)+G_z\dfrac{\partial y^{\text{lower}}}{\partial z}=0 \end{cases} \tag{8}$$

Vortical surface conditions: ignore the initiation of curling of wake vortical surfaces. Also, assume the wake vortical surface is congruent with the xoz coordinate surface. Then, on the wake vortical surface

$$\begin{cases} \varphi_s|_{s=0^+} = \varphi_s|_{s=0^-} \\ \varphi|_{s=0^+} - \varphi|_{s=0^-} = \Gamma(z) \end{cases} \tag{10}$$

Distant field boundary conditions:

$$G=0 \qquad (x=-\infty,\ y,z=\pm\infty) \tag{11}$$

$$G_{ss}+G_{nn}=0 \quad (x=+\infty) \tag{12}$$

Symmetry conditions: on the plane of symmetry $z=0$ conditions should satisfy

$$W=G_s=0$$

III. Coordinate Transformations

In order to make calculations convenient, we make a rational arrangement of the grid points, first transforming sweptback wings into rectangular wings. The actual transformatiion is as follows:

$$\begin{cases} X=(x-x_{LE}(z))/c(z)-0.5 \\ Y=y \\ Z=z \end{cases} \tag{14}$$

After that, we take a limitless physical domain and transform it into a limited domain of calculation. In this way, one is then able to directly use distant field boundary conditions. One first selects an appropriate transformation function, which is still able to make most of the grid points fall close to the surface of the wing. The actual transformation is as shown below: 136

In the x direction and the y direction

$$x=\begin{cases} -x_4+A_2\operatorname{tg}\left[\frac{\pi}{2}(\xi+\xi_4)\right]+A_1\operatorname{tg}\left[\frac{\pi}{2}(\xi+\xi_4)\right] & X\le -X_4 \\ \xi(a_1+b_1\xi^2) & -X_4\le X\le X_4 \\ x_4+A_2\operatorname{tg}\left[\frac{\pi}{2}(\xi-\xi_4)\right]+A_1\operatorname{tg}\left[\frac{\pi}{2}(\xi-\xi_4)\right] & X\ge X_4 \end{cases} \tag{15}$$

$$y=A_1\operatorname{tg}\left(\frac{\pi}{2}\eta\right) \tag{15}$$

The z direction transformation is similar to the x direction transformation. The transformation is seen in Fig. 1.

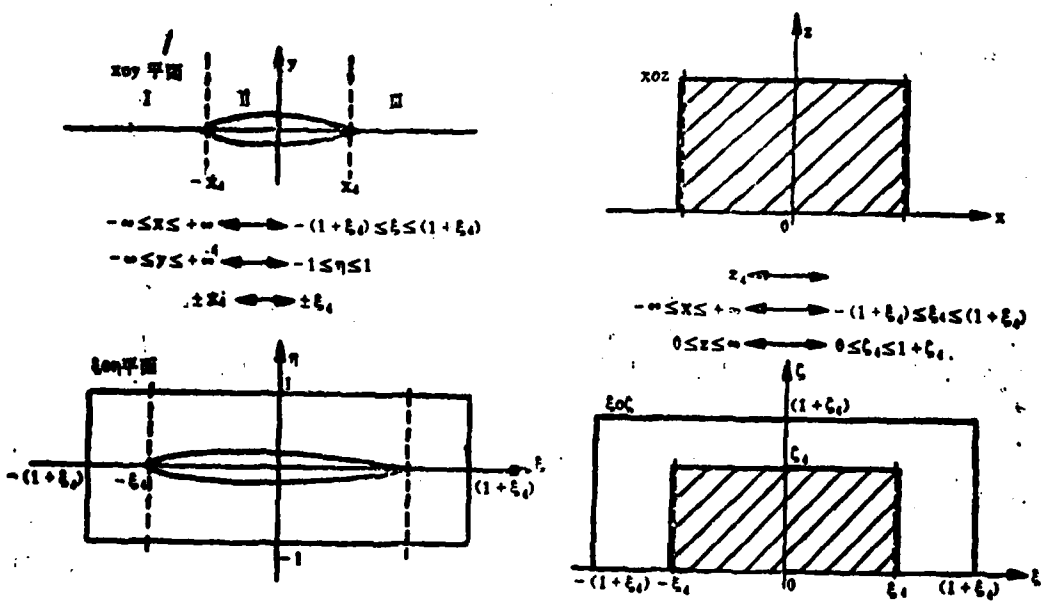

Fig. 1(a) The Relationship Between the Physical Coordinate System (X,Y,Z and the Calculation Coordinate System (ξ,η,ζ) 1. Plane

Fig. 1(b) The Relationship Between the Physical Coordinate System (X,Y,Z and the Calculation Coordinate System (ξ,η,ζ)

After the coordinate transformations, equation (3) becomes

$$\bar{A}f(fG_\xi)_\xi+\bar{B}g(gG_\eta)_\eta+\bar{C}h(hG_\zeta)_\zeta+\bar{D}fgG_{\xi\eta}+\bar{E}fhG_{\xi\zeta}+$$
$$+\bar{F}ghG_{\eta\zeta}+\bar{G}f(f_1fG_\xi)_\xi+\bar{H}fh(fG_\xi)_\zeta=0 \qquad (17)$$

The velocity components (4) become

$$\begin{cases} u=\cos\alpha+fG_\xi/c(z) \\ v=\sin\alpha+gG_\eta \\ w=f_1fG_\xi+hG_\zeta \end{cases} \qquad (18)$$

IV. Difference Forms

At points of subsonic speed, central difference forms are always selected for use. At points of supersonic speed, in order to produce a reasonable, man-made viscosity, and, to make the difference forms stable, we make use of localized velocity coordinate systems. Then,

$$\left(1-\frac{q^2}{a^2}\right)\varphi_{ss}+(\Delta\varphi-\varphi_{ss})=0 \qquad (19)$$

In the calculation coordinate system

$$\varphi_{ss}=\frac{1}{q^2}[A_1f(fG_\xi)_\xi+B_1g(gG_\eta)_\eta+C_1h(hG_\zeta)_\zeta+2D_1fgG_{\xi\eta}+$$
$$+E_1fhG_{\xi\zeta}+F_1ghG_{\eta\zeta}+G_1f(f_1fG_\xi)_\xi+R_1fh(f_1G_\xi)_\zeta]$$
$$\Delta\varphi=\frac{1}{c(z)}f(fG_\xi)_\xi+g(gG_\eta)_\eta+h(hG_\zeta)_\zeta+f_1fhG_{\xi\zeta}+$$
$$+f_1f(f_1fG_\xi)_\xi+fh(f_1G_\xi)_\zeta$$

AD-A185 723 ACTA AERODYNAMICA SINICA (SELECTED ARTICLES)(U) FOREIGN 2/2
TECHNOLOGY DIV WRIGHT-PATTERSON AFB OH 02 SEP 87
FTD-ID(RS)T-0116-87

UNCLASSIFIED F/G 20/4 NL

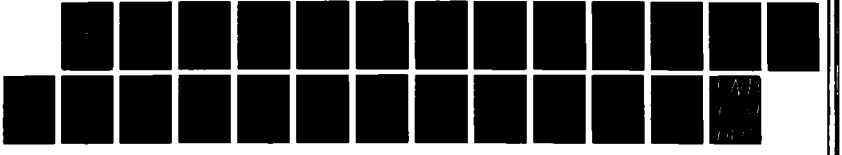

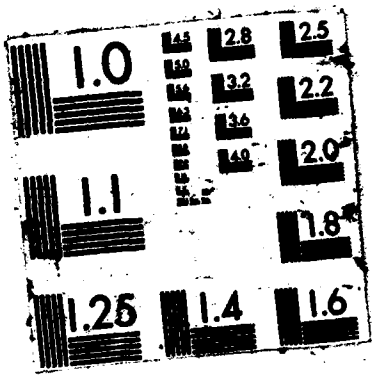
1.0
1.1
1.25
1.4
1.6
2.8
3.2
3.6
4.0
2.5
2.2
2.0
1.8

In order to cause the difference equations to have precise areas of dependence, at points of supersonic speed, we select for use a rotational difference formula [3]. That is, in the term $(\Delta\varphi-\varphi_{\alpha\alpha})$, the derivatives of the various terms use a central difference. In the term $\varphi_{\alpha\alpha}$ the various term derivatives use the headwind difference. The difference equation set is solved by the use of linear relaxation iterative substitution. The iterative substitution process can be seen as being the introduction of an artificial time coordinate term Δt,

Because of this, in the equations, except for $\varphi_{\alpha\alpha}$, $\varphi_{\alpha\alpha}$, we also added the terms $\varphi_{\alpha t}$, $\varphi_{\alpha t}$. Jameson makes use of the aggregate difference between the initial iterative substitution value and the last iterative substitution value. Let $\varphi_{\alpha t}$, $\varphi_{\alpha t}$ be implied in the difference formulae. Jameson has already pointed out that, in order to guarantee precise stability, it is sometimes necessary to add the term $\varphi_{\alpha t}$. This method is, in a real form, adding $\varphi_{\alpha t}$, $\varphi_{\alpha t}$ implied in $\varphi_{\alpha\alpha}$. Because of the fact that, when there is convergence, $\varphi_{\alpha t}$, $\varphi_{\alpha t}$ tends toward zero; therefore, in this way, there is no influence on the final results. The actual difference forms, when $v>0, \omega>0$, are exemplified by the various terms in $\varphi_{\alpha\alpha}$

$$(f\varphi_\xi)_\xi=[f_{i-\frac{1}{2}}(G_{i,j,k}-G_{i-1,j,k})-f_{i-\frac{1}{2}}(G_{i-1,j,k}-G_{i-2,j,k})]/\Delta\xi^2 \tag{22a}$$

$$(gG_\eta)_\eta=[g_{j-\frac{1}{2}}(G_{i,j,k}-G_{i,j-1,k})-g_{j-\frac{1}{2}}(G_{i,j-1,k}-G_{i,j-2,k})]/\Delta\eta^2 \tag{22b}$$

$$(hG_\zeta)_\zeta=[h_{k-\frac{1}{2}}(G_{i,j,k}-G_{i,j,k-1})-h_{k-\frac{1}{2}}(G_{i,j,k-1}-G_{i,j,k-2})]/\Delta\rho^2 \tag{22c}$$

$$G_{\xi\eta}=(G_{i,j,k}-G_{i,j-1,k}-G_{i-1,j,k}+G_{i-1,j-1,k})/(\Delta\xi\Delta\eta) \tag{22d}$$

$$G_{\eta\zeta}=(G_{i,j,k}-G_{i,j,k-1}-G_{i,j-1,k}+G_{i,j-1,k-1})/(\Delta\eta\,\Delta\zeta) \tag{22e}$$

$$G_{\xi\zeta}=(G_{i,j,k}-G_{i,j,k-1}-G_{i-1,j,k}+G_{i-1,j,k-1})/\Delta\xi\,\Delta\zeta) \tag{22f}$$

If we add the obvious form G_{tt}

$$-\varepsilon\Delta t\frac{f}{\Delta\xi}G_{tt}=-\varepsilon\Delta t\frac{f}{\Delta\xi\cdot q}(uf\,G_{\xi t}+vgG_{\eta t}+whG_{\zeta t})$$

$$=-\varepsilon\frac{f}{\Delta\xi\cdot q}\left[\frac{uf_{i-\frac{1}{2}}}{\Delta\xi}(G^*_{i,j,k}-G_{i,j,k}-G^*_{i-1,j,k}+G_{i-1,j,k})+\frac{vg_{j-\frac{1}{2}}}{\Delta\eta}(G^*_{i,j,k}-G_{i,j,k}-\right. \tag{23}$$

$$\left.-G^*_{i,j-1,k}+G_{i,j-1,k})+\frac{wh_{k-\frac{1}{2}}}{\Delta\zeta}(G^*_{i,j,k}-G_{i,j,k}-G^*_{i,j,k-1}+G_{i,j,k-1})\right].$$

In all situations, the velocity components u, v, w all use the old values of the central difference. If we take corresponding difference forms and substitute them into equations (17) and (19). In the η direction, we obtain the three diagonal algebraic equation set

$$A_i G_{i,j-1,k} + B_i G_{i,j,k} + C_i G_{i,j+1,k} = D_i \qquad (21)$$

We use follow up methods to solve this.

V. The Treatment of Boundary Conditions

The object surface condition (8) for the upper surface becomes

$$\left[\cos\alpha \frac{\partial V_{\perp}}{\partial x} + \left(\frac{\partial y_{\perp}}{\partial x}\frac{1}{c(z)} + f_1 \frac{\partial y_{\perp}}{\partial z}\right) f G_{i,j}\right] - (\sin\alpha + g_1 G_{i,j}) + h\frac{\partial y_{\perp}}{\partial z} G_{i,j} = 0 \qquad (25)$$

In the interior of each of the wing cross sections, we introduce the virtual grid points (i, j, k) (See Fig. 2).

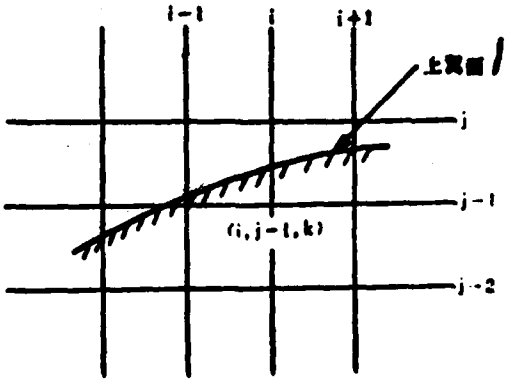

Fig. 2 The Relationship Between the Form of the Wing Cross Section and the Grid Network (Upper Surface) 1. Upper Surface

If we take $G_{\xi\delta}$, $G_{\eta\delta}$, $G_{\zeta\delta}$ and make a Taylor expansion on the virtual points

$$
\begin{aligned}
G_{\xi\delta} &= \frac{G_{i+1,j-1,k}-G_{i-1,j-1,k}}{2\Delta\xi} + \frac{(\eta_b-\eta_{j-1})}{2\Delta\xi\,\Delta\eta}(G_{i+1,j,k}-G_{i+1,j-1,k}-G_{i-1,j,k}+G_{i-1,j-1,k}) \\
G_{\eta\delta} &= \frac{3G_{i,j-1,k}-4G_{i,j,k}+G_{i,j+1,k}}{2\Delta\eta} + (\eta_b-\eta_{j-1})\frac{G_{i,j+1,k}-2G_{i,j,k}+G_{i,j-1,k}}{\Delta\eta^2} \\
G_{\zeta\delta} &= \frac{G_{i,j-1,k+1}-G_{i,j-1,k-1}}{2\Delta\zeta} + \frac{\eta_b-\eta_{j-1}}{2\Delta\eta\Delta\zeta}(G_{i,j,k+1}-G_{i,j-1,k+1}+G_{i,j,k-1}+G_{i,j-1,k-1})
\end{aligned}
\tag{26}
$$

If we then take the expansion form (26) and substitute it into (25), it is possible to obtain an expression for the perturbation velocity G potential at the virtual points. If flow movements at the points (i, j, k) are of supersonic speed, and, $v_{i,j,k}>0$, then, the value of $G_{i,j-1,k}$ is still required in the difference formula. At this time, $G_{i,j-1,k}$ is determined from linear extrapolation to be

$$G_{i,j-1,k}=-G_{i,j,k}+2G_{i,j-1,k} \tag{27}$$

The calculation of the perturbation velocity potential at the virtual points also involves the introduction of a relaxation process. First of all, we make use of the last iterative substitution value to 189
calculate the old value of $G_{i,j-1,k}$. After that, following the execution of a series of relaxation solutions, we make use of as many new values as possible and recalculate new values for $G_{i,j-1,k}$

Boundary conditions for the lower surface can be handled in the same way.

On the Trefftz plane, in the coordinate system (ξ,η,ζ), the Laplace equation becomes

$$\rho(\rho G_\eta)_\eta+h(hG_\zeta)_\zeta=0 \tag{28}$$

In areas of wake turbulence, the perturbation velocity potential G is not continuous,

$$G(\xi,+0,\zeta)-G(\xi,-0,\zeta)=\Gamma(\zeta) \quad (29)$$

VI. Result Analysis

We first make use of a rectangular wing and two sweptback wings (NACA 64A 010 and M6) to carry out transonic linear flow calculations. Fig. 3 and Fig. 4 show that the results of calculations for the two types of configurations of the NACA 0012 rectangular wing ($(M_\infty=0.75,\ \alpha=2^\circ$ and $M_\infty=0.85,$) when compared to the results of Jameson calculations, show precise matching of the position of the shock waves and a basic correspondence in pressure distribution.

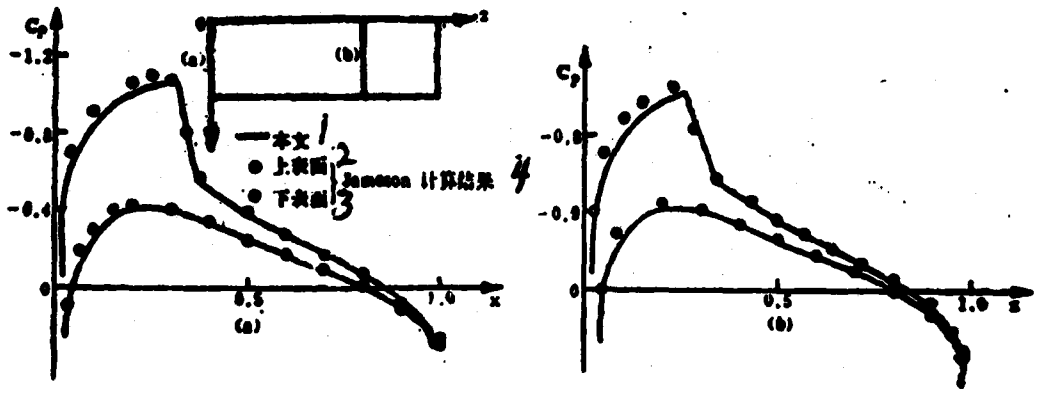

Fig. 3 Comparison of Pressure Distributions for NACA 0012 Rectangular Wing (λ =6) ($M_\infty=0.75,\alpha=2^\circ$) 1. This Article 2. Upper Surface 3. Lower Surface 4. Calculation Results

Fig. 5 shows that the NACA 64A 010 equal chord back swept wing (forward edge back sweep angle 30 degrees, expansion chord ratio 4.8). When the results of calculations under the conditions $M_\infty=$ $0.9,\alpha=1^\circ$ and the results of calculations with finite body integration methods as in reference [4] and Jameson are compared to each other, pressure distributions and shock wave locations are both in relatively good agreement.

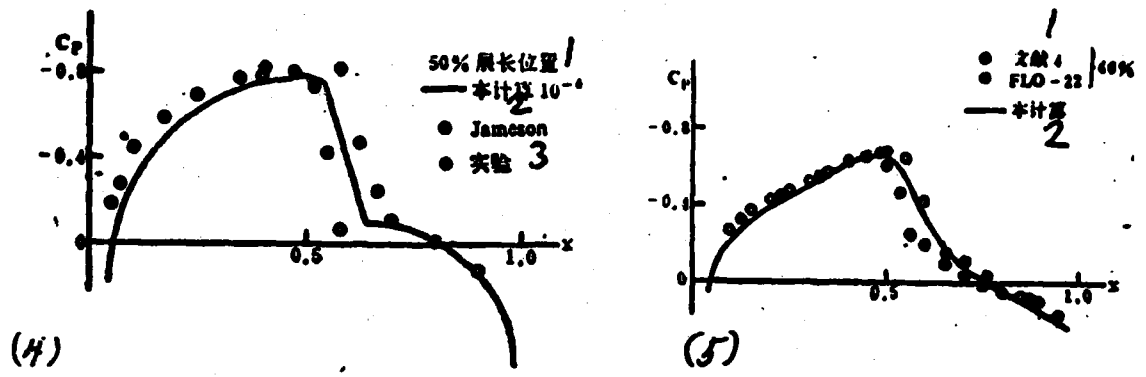

Fig. 4 Pressure Distribtution for NACA 0012 Rectangular Wing (Λ =0) ($(M_\infty=0.85, \alpha=0°)$) 1. Expansion Chord Position 2. Basic Calculation 3. Experiment

Fig. 5 Pressure Distribution on Surface of NACA 64 A 010 Back Swept Wing (λ = 4.8) ($(M_\infty=0.9, \alpha=1°)$) 1. Reference 4 2. Basic Calculation

190

Finally, we calculated the ONERAM 6 wing in the $M_\infty=0.84, \alpha=3.06°$ configuration. The front edge back sweep angle of the wing is 30 degrees. The taper ratio is 0.5624. The expanision chord ratio is 3.8. The solution for this has a double shock wave. It contains oblique shock waves of from transonic speeds to supersonic speeds following a main shock wave which is almost perpendicular to the oncoming flow. The two shock waves, in the vicinity of the wing tips, merge into a single shock wave.

Fig. 6 shows the pressure coefficient distributions for four different wing cross sections (0.163, 0.47, 0.614, 0.933). Moreover, it carries out a comparison for the calculated results-both experimental and Jameson-for adjacent cross sections. Looking at it as a whole, these results are fairly good. Except for the area of the forward edge on the top surface, there is entire agreement in pressure distributions and experimentation at other places. After an

adjustment in the second shock wave through comparison with the experimental results, we consider that there is no additional viscosity. Therefore, the second shock waves-before adjustment by comparison of the basic results with Jameson-are even more reasonable.

However, due to the fact that the grid which is employed in these calculations is relatively coarse (72x32x24)-it is particularly true that the grid points in the chord direction are rare-there is a flattening effect on the shock waves. In particular, the influence on the first shock wave passing from transonic to supersonic speeds is relatively large. This causes results which are dissimilar from Jameson (His grid was 192x24x32.), and, in the area of the forward edge, there is even better agreement with experimental values. On the basis of the currently existing calculation results for the two grids-the coarse (36x16x12) and the fine (72x32x24)-we estimate that a continued increase in the density of grid points in the chord direction will cause the pressure distribution and experimental results in the vicinity of the forward edges to agree very well.

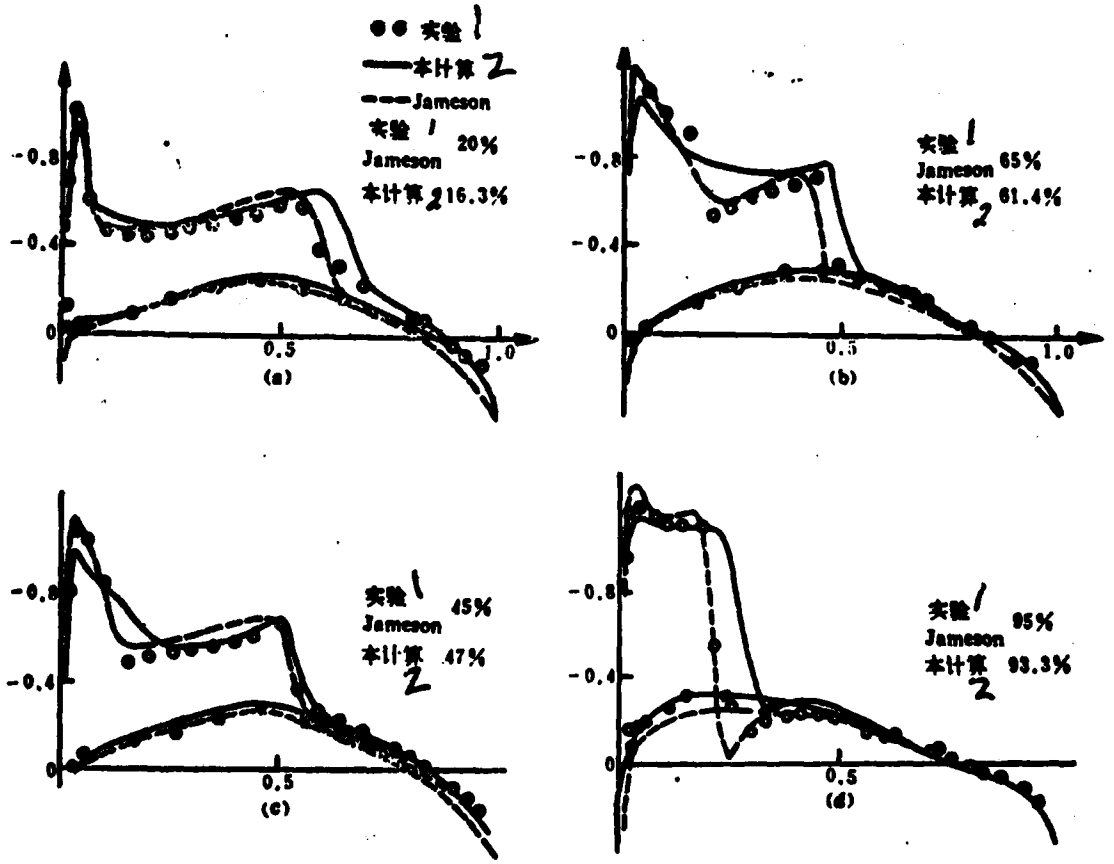

Fig. 6 ONERAM 6 Wing Pressure Coefficient Distribution Comparison (M_∞=0.84, α=3.06°) 1. Experiment 2. Original Calculation

The cross section surface of the root portion is difficult to calculate accurately. The Jameson method has made considerable improvement in this regard. Moreover, we have not yet seen its results demonstrated. The small perturbation method which was improved in reference [2] has yielded results. However, due to the fact that the equations which are employed in its use are not the same, it is only possible to see from Fig. 7 the coincidence in trend of the two. The Euler equations of Jameson solve for the pressure distributions at 99% of the cross section locations along the length of the development [3] (reference number unclear). At the same time, this reference provides experimental results. A comparison of the original calculation results and these results is shown in Fig. 8. It is obvious that the original results are even closer to experimental values.

191

The calculations demonstrate that, in calculations done in relatively dense grid systems, the mutual ratio between increment lengths Δx, Δy and the selection of the artificial viscosity coefficient ε have relatively large influences on the convergence characteristics and stability of the calculations. These calculations make use of adjustable values for ε and the relaxation constant ω, in order to increase the reliability of the calculations.

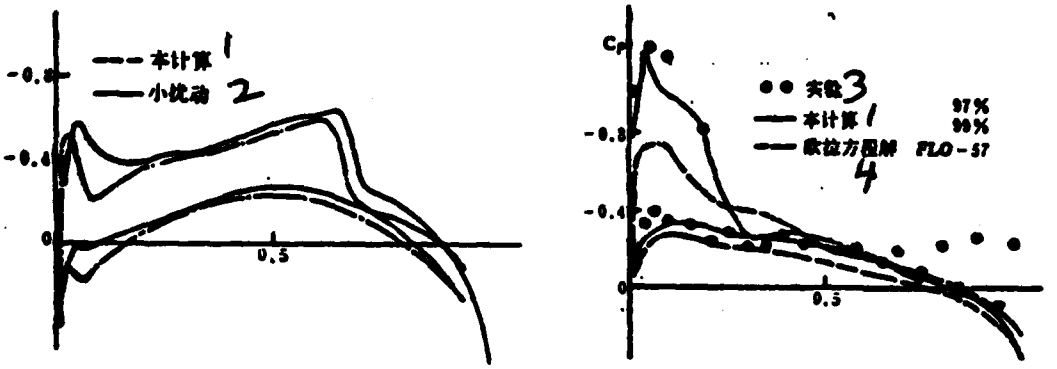

Fig. 7 Pressure Distribution on the Symmetrical Surface of the M6 Wing ($M_\infty = 0.84, \alpha = 3.06°$) 1. Original Calculations 2. Small Perturbation

Fig. 8 Pressure Distribution on M6 Wing Cross Section in the 0.99 Development Direction ($M = 0.84, \alpha = 3.06°$) 1. Original Calculation 3. Experiment 4. Euler Equation Solution

VII. Conclusion

The calculations which we currently have demonstrate that the method for handling the boundary conditions on the object surface of the flow around the Carlson two-dimensional airfoil is suitable, in principle, for the calculation of three-dimensional airfoils. At the same time, they also demonstrate that, in orthogonal coordinate systems, it is possible to obtain relatively accurate three-dimensional transonic flow solutions.

REFERENCES

[1] 姚福如, 机翼跨音速无粘流数值计算, 空气动力学学报, 3 (1982).

[2] Carlson, L.F., Transonic Airfoil Flow Field Analysis Using Curlesian Coordinates, CR 2577, NASA, Aug. 1975.

[3] Antony, Jameson, Iterative Solution of Transonic Flows over Airfoils and Wings, including flows at Mach 1, *Comm. Pure Appl. Math.*, Vol 27, (1974), 283-309.

[4] Sankar, N. L., Malone, J. B. and Tassa, Y., AIAA 81-1016 (1981).

[5] Antony Jameson, Caughey, D. A., AIAA Paper 77-635 (1977).

[1] Yao Furu; "Numerical Value Calculations of Inviscid, Transonic Flows Around Airfoils"; Acta Aerodynamica Sinica, 3, 1982

NUMERICAL CALCULATIONS OF INVISCID TRANSONIC FLOWS OVER WINGS

Chen Zuobin Yao Furu Zhang Yulun

(China Aerodynamic Research and Development Center)

Abstract

A numerical method for calculating steady inviscid transonic flows over wings is introduced in this paper. The fully potential equation is chosen as the mathematical model. The infinite physical domain is transformed to the finite computing domain and the swept wing is transformed to the rectangle wing, using proper mathematical transformation. The equation is discretized in computing domain using mixed finite scheme and the line relaxation method is used for solving the resulting nonlinear algebraic equation. Successively refining mesh makes the calculation very economic.

THE CALCULATION OF NON-STEADY STATE VISCOUS FLOWS BY N-S EQUATION AROUND JOUKOWSKY AIRFOILS HAVING ANGLE OF ATTACK

193

Du Dirong Li Jin

(Northwestern Polytechnical University)

SUMMARY This article makes use of N-S equations to calculate viscous flows around Joukowsky airfoils with angles of attack of 0 degrees and 42 degrees. The thickness of the symmetrical airfoil is 25.8%. The non-dimensional grid time intervals are $t=0$ to $t=10$.

The calculation results include: flow function distribution, wing surface pressure distribution, and lift coefficients as well as drag coefficients.

I. Introduction

When aircraft are flying with large angles of attack, one always has a considerable number of vortical flows and separati on flows created. The occurrence of the related steady state vortices and the development process as well as such questions as the aerodynamic characteristics of conditions with separation flows all require the doing of more advanced research and discussion. Because of the rapid development and broad applications of electronic computers, and only because of them, has it become gradually possible to do research on these problems and find solutions to them. [1,4-6]

This article intends to make use of N-S equations on the flow configurations when non-compressible gases flow around airfoils as well as on the processes of formation and development of vortices in order to carry out numerical value calculation research. We make direct use of difference methods to calculate the initial movements of Joukowsky airfoils starting from a static configuration and moving suddenly to constant velocity V. In numerical value calculation examples, the thickness corresponding to symmetrical airfoils is 25.8%; the angles of attack are 0 degrees and 42 degrees; and, the Reynolds number is 20. In these calculations, the non-dimensional grid time intervals are from $t=0$ to $t=10$, . The results of calculations include graph forms for flow movements, wing surface pressure distributions, and coefficients for lift and drag.

The general procedure for these calculations is as follows. We first make use of a Joukowsky transform to take the plane, physical surface of a flow movement (x, y) and transform it to plane (ξ, η). On plane (ξ, η), the wing surface becomes a unit circle. At the same time, on the (ξ, η) plane, we carry out a rotational transformation, causing the polar axis and the direction of the incoming flow to coincide in polar coordinate system (r, θ_1) after the transformation. In order to make the calculations simple, on the (r, θ_1) plane, we carry out an extension transformation: $r=e^{\rho}$. The purpose of this transformation is to make the uniform distribution difference grid on the plane (ρ, θ_1) able to correspond to the grid distribution, which is loose on the outside and dense on the inside, on the physical plane (x, y). At this time, the N-S equations and boundary conditions on plane (x, y) are gradually transformed onto the plane (ρ, θ_1) according to the principles described. In the calculations, we selected for use a non-conserved form of difference equation For time increment derivative, we selected for use the forward difference. For the space derivative, we chose to use a central difference. In handling the difference in boundary conditions, the space derivative makes use of a single side difference. Intercept error is $0(h)$. In numerical value calculations, the initial flow function value ψ_{in} is taken to be an inviscid potential flow solution. Concerning calculations of the difference equations obtained from the transfer of vorticity displacement equations, we made use of the time increment driven method. Concerning difference equations obtained from Poisson equations, we made use of the superrelaxation, iterative substitution method to carry out the calculatiions.

II. Coordinate Transformations and Formulae Derivation 134

In problems relating to two dimensional, viscous non-steady state, non-compressible flows, the N-S equation can be written as

$$\frac{\partial u}{\partial x}+\frac{\partial v}{\partial y}=0$$

$$\frac{\partial u}{\partial t}+u\frac{\partial u}{\partial x}+v\frac{\partial u}{\partial y}=-\frac{\partial p}{\partial x}+\frac{1}{Re}\nabla^2 u$$

$$\frac{\partial v}{\partial t}+u\frac{\partial v}{\partial x}+v\frac{\partial v}{\partial y}=-\frac{\partial p}{\partial y}+\frac{1}{Re}\nabla^2 v$$

We select for use the flow function Ψ and the vorticity ω to be the new variables. Then, the equations above become

$$\frac{\partial \omega}{\partial t}+v\cdot\nabla\omega=\frac{1}{Re}\nabla^2\omega$$

$$\nabla^2\Psi=-\omega$$

We choose to use a series of coordinate transforms to simplify the process of numerical value calculation. Moreover, we make use of the Joukowsky transform to take the airfoil and change it into a unit circle.

$$x=(\xi+\epsilon)\left(1+\frac{l^2}{(\xi+\epsilon)^2+\eta^2}\right)$$

$$y=\eta\left(1-\frac{l^2}{(\xi+\epsilon)^2+\eta^2}\right)$$

In the numerical example, we choose $l=0.8, \epsilon=0.2,$. At this time, on the plane (x, y) , the corresponding thickness of the Joukowsky airfoil is 25.8%, which is changed, on the (ξ, η) plane, into a unit circle.

The equations discussed above in which Ψ and ω were taken as new unknowns are changed to be:

$$\frac{\partial \omega}{\partial t}+H^2 v_1\cdot\nabla_1\omega=\frac{1}{Re}H^2\nabla_1^2\omega$$
$$H^2\nabla_1^2\Psi=-\omega$$

In the equations,

$$H^2=\left(\frac{\partial\xi}{\partial x}\right)^2+\left(\frac{\partial\xi}{\partial\eta}\right)^2,\qquad \nabla_1=\left\{\frac{\partial}{\partial\xi},\ \frac{\partial}{\partial\eta}\right\}$$
$$v_1=\{u_1, v_1\}=\left\{\frac{\partial\Psi}{\partial\eta},\ -\frac{\partial\Psi}{\partial\xi}\right\}$$

Moreover, on the basis of $\xi=r\cos\theta,\qquad \eta=r\sin\theta$

it is possible to obtain the equation form in polar coordinates, which is:

$$\frac{\partial\omega}{\partial t}+H^2\left(u_r\frac{\partial\omega}{\partial r}+u_\theta\frac{1}{r}\frac{\partial\omega}{\partial\theta}\right)=\frac{H^2}{Re}\left(\frac{\partial^2}{\partial r^2}+\frac{1}{r}\frac{\partial}{\partial r}+\frac{1}{r^2}\frac{\partial^2}{\partial\theta^2}\right),$$
$$H^2\left(\frac{\partial^2}{\partial r^2}+\frac{1}{r}\frac{\partial}{\partial r}+\frac{1}{r^2}\frac{\partial^2}{\partial\theta^2}\right)\Psi=0$$

When the angle of attack is not zero, we select for use on this a rotational transform $\theta_1=\theta-\alpha$ 195

Then, the form of the equation on the plane (r, θ_1) is:

$$\frac{\partial\omega}{\partial t}+H^2(r,\theta_1+\alpha)\left[u_r\frac{\partial\omega}{\partial r}+u_\theta\frac{1}{r}\frac{\partial\omega}{\partial\theta_1}\right]$$
$$=\frac{1}{Re}H^2\left[\frac{\partial^2\omega}{\partial r^2}+\frac{1}{r}\frac{\partial\omega}{\partial r}+\frac{1}{r^2}\frac{\partial^2\omega}{\partial\theta^2}\right]$$
$$H^2(r,\theta_1+\alpha)\left[\frac{\partial^2\Psi}{\partial r^2}+\frac{1}{r}\frac{\partial\Psi}{\partial r}+\frac{1}{r^2}\frac{\partial^2\Psi}{\partial\theta_1^2}\right]=-\omega$$

Making use of an extension transform $r=e^\rho$

Then, the form of the equations on the (ρ, θ_1) plane is

$$\frac{\partial \omega}{\partial t} + H^2(e^\rho, \theta_1 + a) \cdot e^{-2\rho}\left(\frac{\partial \Psi}{\partial \theta_1} \cdot \frac{\partial \omega}{\partial \rho} - \frac{\partial \Psi}{\partial \rho} \cdot \frac{\partial \omega}{\partial \theta_1}\right)$$
$$= \frac{1}{Re} H^2(e^\rho, \theta_1 + a) \cdot e^{-2\rho}\left(\frac{\partial^2 \omega}{\partial \rho^2} + \frac{\partial^2 \omega}{\partial \theta_1^2}\right)$$
$$H^2(e^\rho, \theta_1 + a) \cdot e^{-2\rho}\left(\frac{\partial^2 \Psi}{\partial \rho^2} + \frac{\partial^2 \Psi}{\partial \theta_1^2}\right) = -\omega$$

Again, we bring into play the variable transform

$$\Psi = e^\rho \sin \theta_1 + \Phi$$

Then, the equations change to become

$$\frac{\partial \omega}{\partial t} + H^2(e^\rho, \theta_1 + a) \cdot e^{-2\rho}\left[\left(\frac{\partial \Phi}{\partial \theta_1} \cdot \frac{\partial \omega}{\partial \rho} - \frac{\partial \Phi}{\partial \rho} \cdot \frac{\partial \omega}{\partial \theta_1}\right)\right.$$
$$\left. + e^\rho\left(\frac{\partial \omega}{\partial \rho} \cos \theta_1 - \frac{\partial \omega}{\partial \theta_1} \sin \theta_1\right)\right]$$
$$= \frac{1}{Re} \cdot H^2(e^\rho, \theta_1 + a) \cdot e^{-2\rho}\left(\frac{\partial^2 \omega}{\partial \rho^2} + \frac{\partial^2 \omega}{\partial \theta_1^2}\right)$$
$$H^2(e^\rho, \theta_1 + a) \cdot e^{-2\rho}\left(\frac{\partial^2 \Phi}{\partial \rho^2} + \frac{\partial^2 \Phi}{\partial \theta_1^2}\right) = -\omega$$

The formula for calculating wing surface pressure coefficients is as follows:

$$C_p(\theta_1) = \int_0^{\theta_1} \frac{\partial p}{\partial \theta_1} d\theta_1 - p(0) = \int_0^{\theta_1} \frac{1}{Re} \frac{\partial \omega}{\partial \rho} d\theta_1 - p(0)$$

The formulas for calculating the coefficients of lift and drag are as given below:

$$CDP = -\int_0^{2\pi} 2CP(\theta_1) y_1'(\theta_1) d\theta_1$$
$$CLP = \int_0^{2\pi} 2CP(\theta_1) x_1'(\theta_1) d\theta$$
$$CDF = \int_0^{2\pi} -\frac{2}{Re} \omega(\theta_1) x_1'(\theta_1) d\theta_1$$
$$CLF = -\int_0^{2\pi} \frac{2}{Re} \omega(\theta_1) y_1'(\theta_1) d\theta_1$$

In these formulas, $x_1=y\sin\alpha+x\cos\alpha, \quad y_1=y\cos\alpha-x\sin\alpha$

Here, the direction of the x_1 axis in the (x_1, y_1) coordinate system is parallel to the direction of the infinitely distant oncoming flow.

Besides this, the initial conditions and boundary conditions are as stated below:

$$\begin{array}{llll} t<0 & 0\le\theta\le 2\pi & 0\le\rho\le\infty & u=0,\ v=0 \\ t\ge 0 & 0\le\theta\le 2\pi & \rho=0 & u=0,\ v=0 \\ t\ge 0 & 0\le\theta\le 2\pi & \rho=\infty & \Psi=e^{t}\sin\theta_1, \text{ on } \Phi=0 \end{array}$$

III. Numerical Value Calculation Methods and Procedures

We choose the place at which $\rho=\rho_{max}$ to represent an infinitely distant boundary.

In domains on the calculation plane (ρ, θ_1), we lay out a rectangular coordinate grid with $0\le\rho\le\rho_{max}, \ 0\le\theta_1\le 2\pi$ the grid side length being h.

Finally, the difference equations which we get from the equations which we get by taking ω and Φ as variables are:

$$x=\frac{\partial(\Phi,\omega)}{\partial(\rho,\theta_1)}\Big|_{i,j}=\left(\frac{\Phi_{i+1,j}-\Phi_{i-1,j}}{2h}\right)\cdot\left(\frac{\omega_{i,j+1}-\omega_{i,j-1}}{2h}\right)-$$

$$-\left(\frac{\Phi_{i,j+1}-\Phi_{i,j-1}}{2h}\right)\cdot\left(\frac{\omega_{i+1,j}-\omega_{i-1,j}}{2h}\right)$$

$$y=\left(\frac{\partial\omega}{\partial\theta_1}\sin\theta_1-\frac{\partial\omega}{\partial\rho}\cos\theta_1\right)_{i,j}=\left(\frac{\omega_{i,j+1}-\omega_{i,j-1}}{2h}\right)\cdot\sin(j-1)h-$$

$$-\left(\frac{\omega_{i+1,j}-\omega_{i-1,j}}{2h}\right)\cdot\cos(j-1)h$$

$$X=\left(\frac{\partial^2\omega}{\partial\rho^2}+\frac{\partial^2\omega}{\partial\theta_1^2}\right)_{i,j}=\frac{\omega_{i+1,j}-2\omega_{i,j}+\omega_{i-1,j}}{h^2}+\frac{\omega_{i,j+1}-2\omega_{i,j}+\omega_{i,j-1}}{h^2}$$

$$\omega_{i,j}^{m+1}=\omega_{i,j}^{m}+\Delta t\cdot e^{-2(i-1)h}H_{i,j}^{1}\cdot\left(x+e^{(i-1)h}y+\frac{1}{Re}X\right)$$

Here

$$\rho=(i-1)\cdot h \qquad \theta_1=(j-1)\cdot h \qquad t=m\cdot\Delta t$$

At this time, the difference equation which corresponds to the Poisson equation in the equation set is

$$\Phi_{i,j}^{n+1} = (1-s)\Phi_{i,j}^{n} + \frac{s}{4}(\Phi_{i+1,j}^{n} + \Phi_{i-1,j}^{n+1} + \Phi_{i,j+1}^{n} + \Phi_{i,j-1}^{n+1} + \omega_{i,j}h^2 e^{2(i-1)}/H_{i,j}^{2})$$

In this equation, s is the relaxation factor, and the superscript n represents the n th iterative substitution.

In the division of the grid net, the radial direction is 45. The circumferance is 60. ρ_{max} is selected at the position where it is $3\pi/2$

The exterior boundary separation from the object surface has a chord length of approximately 33.34.

Numerical value calculation procedures are as shown below. 197

In calculating $H_{i,j}$, the given boundary placement conditions and wing surface conditions provide the initial values for $\Phi_{i,j}$ and $\omega_{i,j}$. Subsequently, we calculate the value of $\omega_{i,j}$ for wing surfaces. Again, we solve for the value of $\omega_{i,j}$ at the next instant, and, following that, we solve for the value of $\Phi_{i,j}$ at that same next instant. On the flow movement diagrams printed for the given instant, we also calculate the values for CP, CDP, CLP, CDF, CLF.

In order to obtain the required precise value, it is possible to obtain, from the calculated value of $\Phi_{i,j}$, a calculation for the value of $\omega_{i,j}$ on wing surfaces. Again, we do substitution calculations in order to facilitate the calculations for final flow diagrams and for aerodynamic coefficient values.

In the process of these calculations, one becomes involved in the question of the selection of initial values, the question of determining exterior boundary conditions for the lower flows, as well as being involved in the questions of grid size and coordinate convergence. Each of these questions requires separate consideration.

When doing calculations in flow problems concerning the patterns of viscous, non-compressible fluids as they pass objects after having been suddenly launched into motion, we make use of flow solutions for an ideal fluid (the amount of circulation is zero), and it is reasonable and workable to take these as initial values (because, at this time, the influence of viscosity has still not had an effect). On this foundation, the calculations as a whole go smoothly and well.

Because of this, to the extent that we are concerned with flow pattern problems in viscous gases with differing angles of attack, it is appropriate to select for use the corresponding potential flow solutions as initial values. In the case of the Joukowsky airfoil, potential solutions for angles of attack make it easy to solve for and analyze the solutions. As far as airfoils in general are concerned, there is normally no conventional or appropriate formula expressing the analyzed solution. In this case, it is possible, on the foundation of the relationship $\Phi_{ij}=\omega_{ij}=0$, to adopt a relaxation iterative substitution method to solve corresponding difference equations for Laplace equations. Moreover, the given circulation is zero. In this way, the initial values which are solved for are actually nothing more than numerical value approximations of potential flow solutions. Of course, when the angle of attack is zero, the problem is relatively simpler. This is particularly true of symmetrical airfoils. From the symmetrical characteristics of the flow movements on the upper and lower surfaces, it is possible to make a solution. However, in a situation where the angle of attack for the airfoil is set at zero, is usually also necessary to make use of the condition that the circulation is zero in order to calculate initial values.

Here, we take the wing surface boundary and designate it as the interior boundary of the calculation domain.

This closed curve is designated as the exterior $\rho=\rho_{max}$, $0\leq\theta<2\pi$ boundary of the domain of the calculations. Concerning the determination of the exterior boundary conditions in the lower flows, different theorists each have their own methods for doing the determination (see references [2] and [3]). We recognize that, in the situation in which the exterior boundaries of the domain of calculation are chosen relatively far away from wing surfaces, it is possible to make initial use of the free flow conditions as the exterior boundaries of the lower flows in order to carry out the calculations. Because of this, at this time, wake vortices have still not dragged out the exterior boundaries. When t reaches a specified numerical value of a certain size, then, wake vortices have already

reached the vicinity of the boundaries. At just the time that that happens, we consider opting for the use of relatively precise differential equation forms in order to specify the conditions for the exterior boundaries of the lower flows. In these calculations, one makes use of the conditions for the free incoming flow to be the exterior boundary conditions for the lower flows. The duration of the calculations only reaches to $t=10$. The perturbation on the airfoil from the influence of the incoming flow has still not reached-in the form of vortices-the exterior boundaries of the lower flows. Simplifying the calculations in this way, one sees the calculations for problems becoming easy and their solutions coming in a timely manner.

The selection of the size of the grid network is not only effected by the influence of the values of Re. It is also related to the thickness of the airfoil. In order to make an appropriate selection of the level of density of the-gradient, one should base it on the extent of the space invloved in the changes which occur in the flow movements.

This article makes use of the standard of absolute convergence, that is, when the absolute value of the difference between two adjacent iterative substitution values of Φ_{ij} on grid points is $|\Phi^{n+1}_{ij}-\phi^{n}_{ij}|\leq 0.0001$, then, the iterative substitution stops.

Because of the fact that, when one is doing a numerical value treatment of boundary conditions, the intercept error is $O(h)$, , , h is the grid length, its value in all of the calculations is $h=\pi/30>0.1$.

In cases where this type of convergence standard is employed, in calculations in which $Re=20$, the number of iterative substitutions on the average in calculations of ϕ_{ij} at each instant is approximately 20. The effects of error on the results of calculation are small, and calculations can be carried out with ease. When t is increased, there is no clear increase in the number of iterative substitutions for each instant.

IV. Calculation Results and Discussion

This article has made calculations involving a symmetrical Joukowsky airfoil with thickness 25.8% and has dealt with problems of flow-forms around objects in viscous gases when $Re=20$ and with angles of attack which were respectively 0 degrees and 42 degrees. The airfoil, at time $t=0$, is suddenly launched into motion from a dead stop. After that, it goes into straight line movement at uniform speed. Relatively speaking, we have done nothing more than calculate problems in the flow forms of non-steady state, viscous gases as they flow around airfoils. The results of the calculations have been printed out by computer. These flow diagrams are given in Fig. 1 through Fig. 4. The pressure distribution curves are as given in Fig. 5. The lift coefficient and drag coefficient curves are drawn out on the basis of calculation results and are given in Fig. 6 and Fig. 7 respectively. Due to the fact that, at present, it is difficult to

198

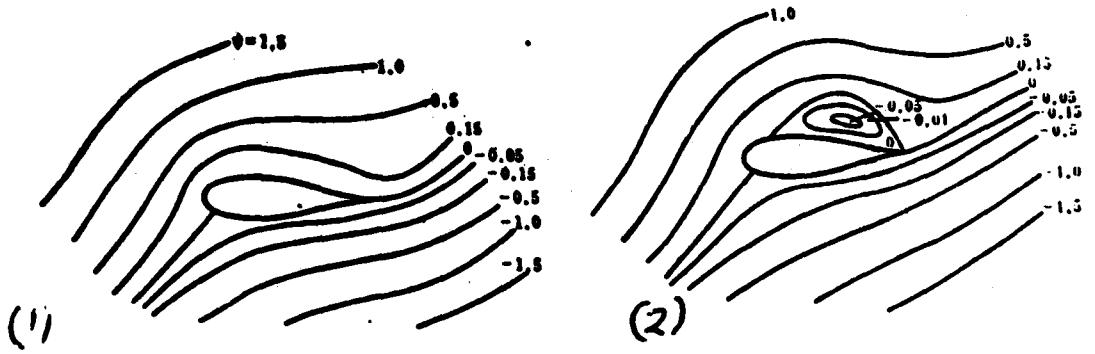

Fig. 1 Flow Diagram $Re=20,\ \alpha=42°,\ T=1.3$

Fig. 2 Flow Diagram $Re=20,\ \alpha=42°,\ T=4$

find direct comparisons to apply to experimental results or numerical value calculation results which come from differing situations. It

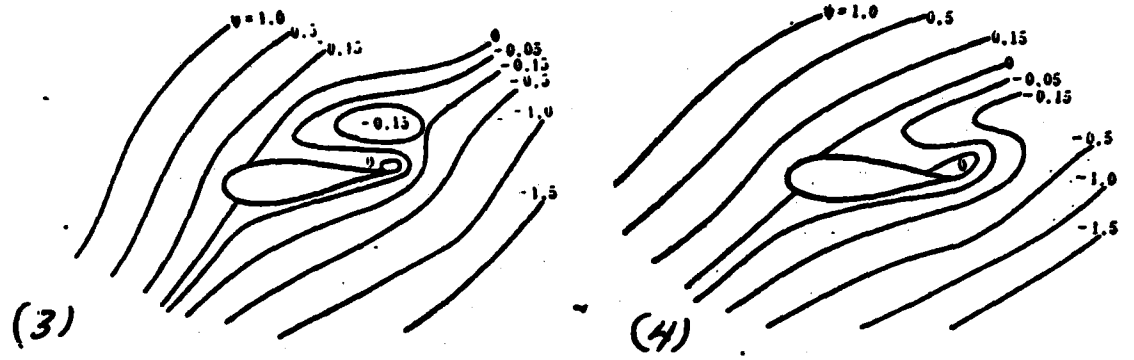

Fig. 3 Flow Diagram $Re=20,\ \alpha=42°,\ T=7$

Fig. 4 Flow Diagram $Re=20,\ \alpha=42°,\ T=10$

is only with the viscous flow diagrams for flows around long and slender elliptical columns in reference [2] that we carried out comparisons. These demonstrated that the calculations were basically reasonable.

199

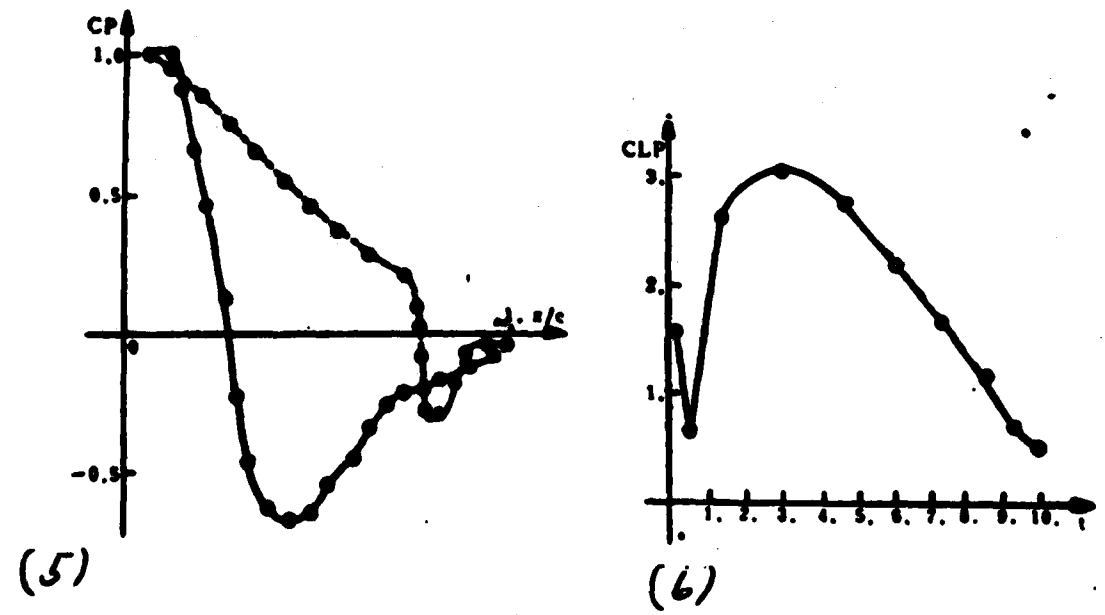

Fig. 5 Pressure Distribution $Re=20, \alpha=42°, T=7$ ● CP (Upper Wing Surface) ○ CP (Lower Wing Surface) $Re=20,\ \alpha=42°$

Fig. 6 Lift Coefficients

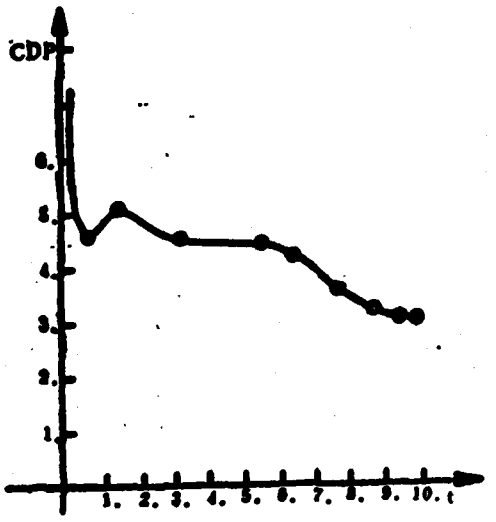

Fig. 7 Drag Coefficients $Re=20, \alpha=42°$

REFERENCES

[1] Wu, J.C., et al., AGARD Paper Cp No. 227 Unsteady Aerodynamics.
[2] Lugt, H.J., et al., *J. Fluid Mech.*, 65, Part 4, 711—734(1974).
[3] Mehta, Unmeel B., et al., *J. Fluid Mech.*, 67, Part 2, 227—256 (1975).
[4] Wu, J.C., *AIAA J.*, 14, 8 (1976). 19.1(1981).
[5] Schmall, Robert A., et al., *AIAA J.*, 12, 11 (1974).
[6] Wu, J. C., *AIAA J.*, 19, 4 (1981).

A NUMERICAL METHOD OF UNSTEADY FLOW FOR SOLVING NAVIER-STOKES EQUATION ———PAST A JOUKOWSKY AIRFOIL WITH ANGLE OF ATTACK

Du Dirong Li Jin
(Northwestern Polytechnical University)

Abstract

The present paper is the numerical solution of the unsteady incompressible viscous flow over Joukowsky airfoil by Navier-stokes equation with angle of attack of 0° and 42°. The thickness ratio of the symmetrical airfoil is 25.8%. Nondimensional time interval is from t=0 to t=10. Numerical results of interest, such as stream function distribution, surface pressure distribution, lift and drag coefficients are computed.

DISTRIBUTION LIST

DISTRIBUTION DIRECT TO RECIPIENT

ORGANIZATION	MICROFICHE
A205 DMAHTC	1
A210 DMAAC	1
B344 DIA/RTS-2C	9
C043 USAMIIA	1
C500 TRADOC	1
C509 BALLISTIC RES LAB	1
C510 R&T LABS/AVRADCOM	1
C513 ARRADCOM	1
C535 AVRADCOM/TSARCOM	1
C539 TRASANA	1
C591 FSTC	4
C619 MIA REDSTONE	1
D008 NISC	1
E053 HQ USAF/INET	1
E404 AEDC/DOF	1
E408 AFWL	1
E410 AD/IND	1
E429 SD/IND	1
P005 DOE/ISA/DDI	1
P050 CIA/OCR/ADD/SD	2
AFIT/LDE	1
FTD	
CCN	1
NIA/PHS	1
LLNL/Code L-389	1
NASA/NST-44	1
NSA/1213/TDL	2
ASD/FTD/NIA	1

END

12-87

DTIC